ELASTIC ELECTRON-DEUTERON SCATTERING MEASUREMENTS AND THE NEUTRON CHARGE FORM FACTOR AT VERY LOW MOMENTUM TRANSFERS

Robert Leavy Topping

NAVAL POSTGRADUATE SCHOOL
Monterey, California

THESIS

ELASTIC ELECTRON-DEUTERON SCATTERING MEASUREMENTS AND THE NEUTRON CHARGE FORM FACTOR AT VERY LOW MOMENTUM TRANSFERS

by

Robert Leavy Topping

Thesis Advisor: J.N. Dyer

December 1972

Approved for public release; distribution unlimited.

Elastic Electron-Deuteron Scattering Measurements and the Neutron Charge Form Factor at Very Low Momentum Transfers

by

Robert Leavy Topping
Commander, United States Navy
B.S., United States Naval Academy, 1958
M.S., United States Naval Postgraduate School, 1964

Submitted in partial fulfillment of the
requirements for the degree of

DOCTOR OF PHILOSOPHY

from the
NAVAL POSTGRADUATE SCHOOL
December 1972

ABSTRACT

Seventy-five measurements of the differential elastic electron-deuteron scattering cross section were made for values of q^2 ranging from 0.05 to 0.35 fm^{-2} at the NPS LINAC with electron scattering angles of 60° to 120°. The charge radius of the deuteron was determined to be $r_{E_d} = 1.9641 \pm 0.0074$ fm. Values of the neutron charge form factors were calculated using Lomon-Feshbach Models 1, 5, and 15 and relativistic corrections to the deuteron wave functions. Lomon-Feshbach Model 15 gave $\frac{d}{dq^2} G_{E_n}(0) = 0.0200 \pm 0.0058\ fm^2$, in closest agreement with the value of $\frac{d}{dq^2} G_{E_n}(0)$ determined by thermal neutron work. A Rosenbluth plot of the data at $q^2 = 0.2$ shows good agreement with theory.

TABLES OF CONTENTS

LIST OF TABLES

TABLE

LIST OF FIGURES

FIGURE

ACKNOWLEDGMENTS

It is a pleasure to thank those who have contributed so much to the completion of this work. First and foremost to Professor John N. Dyer, my thesis advisor, I want to express my sincere appreciation for his encouragement, his energetic assistance during those long hours of taking and analyzing data, and his unfailing support throughout this work.

Professor X.K. Maruyama most generously contributed his time, valuable theoretical and experimental insights, the basis of the radiation correction program, and a great deal of encouragement for which I am most grateful.

I also owe a debt of gratitude to Professor E.B. Dally whose expertise in the theory and experimental procedures of this field provided very useful guidance and whose successes in obtaining LINAC equipment from SLAC was essential to the completion of this work.

My sincere appreciation goes to Professor F.R. Buskirk for his most useful introduction to the theory of electron scattering as well as for his efforts, after his return from sabbatical, in keeping the LINAC operating for the final data runs.

To Mr. H. McFarland and Mr. D. Snyder go my sincere thanks for their generous contributions of their time, technical skills and hard work to keep the LINAC running.

Mr. M. O'Dea and Mr. R. Moeller responsively and inovatively provided many mechanical components of the experimental equipment for which I am very appreciative.

I am indebted to Mrs. P.C. Zeleny who provided much valuable programming assistance and to Professor W.B. Zeleny for his assistance on several theoretical subjects.

Professor E.L. Lomon of the Massachusetts Institute of Technology kindly provided the Deuteron Structure Factors given in Appendix C for which I am most grateful.

Finally, I would like to thank my wife, Lois, for her continuing support and understanding throughout graduate school.

I. INTRODUCTION

A. OUTLINE OF THE EXPERIMENT AND INTRODUCTION OF FORM FACTORS

The primary purpose of this work was to measure the charge form factor of the neutron, $G_{E_n}(q^2)$, at low values of q^2 (the square of the Lorentz invariant four-momentum transfer from the scattered electron to the neutron) in order to resolve differences among several earlier experiments [1,2,3,4].

Secondly, by comparing the G_{E_n} obtained with the use of several different deuteron wave functions to the G_{E_n} predicted by accurate thermal neutron experiments, one can select the S state and D state combinations of the deuteron wave functions that are in best agreement with experiment.

Thirdly, measurements of the deuteron cross section at low values of q^2 permit the rms charge radius of the deuteron to be determined accurately.

These three objectives were achieved by measuring the elastic electron - deuteron differential scattering cross section. The elastic electron - proton cross section was measured in order to normalize the measured deuteron cross section. The electron beam was produced by the Naval Postgraduate School linear accelerator (LINAC).

Since the primary purpose was the measurement of the charge form factor, it is useful to consider briefly here what a form factor is. In Section II a more detailed explanation will be given. The cross section, $\frac{d\sigma}{d\Omega}$, for a relativistic electron scattering from a nucleus that has zero spin and magnetic

moment and consists only of a point charge has been calculated by Mott [5]. The experimental cross section is related to the so-called Mott cross section by

$$\left(\frac{d\sigma}{d\Omega}\right)_{\text{Exp}} = \left(\frac{d\sigma}{d\Omega}\right)_{\text{Mott}} G^2(q^2) \qquad \text{(I-1)}$$

where G is the form factor. If the nucleus has no structure, i.e., it is a point, $G = 1$ at all values of q^2. If it has structure, $G = 1$ for q^2 equal to zero and G is less than one for q^2 greater than zero. A reason why $G(q^2)$ is called the form factor [3] is seen when the cross section for elastic scattering of an electron from a nucleus of charge Ze with finite extent is written [6] as

$$\left(\frac{d\sigma}{d\Omega}\right)_{\text{Exp}} = \left(\frac{d\sigma}{d\Omega}\right)_{\text{Mott}} \left[\int \frac{\rho(r)\, e^{i\vec{q}\cdot\vec{r}} d^3r}{Ze}\right]^2 , \qquad \text{(I-2)}$$

where $\rho(r)$ is the nuclear charge distribution and $c\hbar\vec{q}$ is the three-momentum transferred to the nucleus. The term in brackets is the form factor G and is the Fourier transform of the charge distribution. If one calculates the theoretical cross section for elastic scattering, it is seen that the charge distribution involves the product of the initial wave function of the scatterer at rest in the laboratory frame and the final wave function of the scatterer after it has absorbed the recoil momentum $c\hbar\vec{q}$. In Section II it will be shown that a relativistic correction to the deuteron wave function is required because of its recoil velocity. This is a small (a few percent) but important correction in this work.

If we consider elastic scattering of an electron from an infinitely massive (that is, a nucleus which does not recoil) nucleus of charge Ze Equation I-2 will correctly describe the scattering; $\rho(r)$ is then the static charge distribution. However, for light nuclei where recoil is important, such as deuterium and hydrogen which were used as targets in this work, the intuitive concept of the form factor as the Fourier transform of the charge distribution is not unambiguous. For example, if the charge distribution of the proton were spherical in one frame of reference then in another frame the Lorentz contraction of the distribution would cause it to be nonspherical. To describe form factors in a way more useful in theoretical work, they are considered as invariant functions of the four-momentum q rather than the three-momentum $c\hbar\vec{q}$, where $\hbar^2c^2q^2 = \hbar^2c^2\vec{q}^2 - (E_i-E_f)^2$ and E_i and E_f are the initial and final energies. When the recoil is small then $q^2 \approx \vec{q}^2$ and the concept of the form factor as the Fourier transform of the charge distribution has usefulness. As will be seen in Section II the invariant form factors have other theoretical meanings in terms of strong interaction dynamics.

There is another complication. Particles and nuclei may have magnetic moment distributions as well as charge distributions. These distributions may or may not have the same form as the charge distributions. Thus, a particle or nucleus that has a magnetic moment (but no quadrupole or higher moments) will have to be described by two independent form factors. The decomposition into electric and magnetic

distributions depends upon the frame of reference. For example, the elastic scattering of an electron from a massive nucleus with charge Ze and no magnetic moment will be correctly described in the laboratory frame by Equation I-2 if the nucleus is at rest in the laboratory frame. If, however, the calculation is performed in the electron's frame of reference then the moving nucleus will also have a magnetic field and thus an apparent magnetic moment. In this work we are ultimately interested in the electric form factor of the neutron. A particularly useful frame, the Breit or "brickwall frame", separates the electromagnetic interaction of the nucleons into two form factors, G_E, the electric form factor, and G_M, the magnetic form factor. Sachs <u>et</u> <u>al</u> [7,8] showed that these are particularly useful form factors since G_E and G_M can be expressed as the Fourier transforms of the spatial distributions of charge and magnetization in the Breit frame. The Breit frame is the frame in which $q^2 = \vec{q}^{\,2}$ [7], i.e., that has $E_i = E_f$ and that has the absolute value of the momentum of the incoming nucleon the same as the absolute value of the momentum of the outgoing nucleon and oppositely directed [9].

Consider the electric form factor of a nucleon in the Breit frame,

$$G_E(q^2) = \int_0^\infty \rho(r) \frac{e^{i\vec{q}\cdot\vec{r}} d^3r}{e} ,$$

which for a spherically symmetric particle may be written as

$$G_E(q^2) = \frac{4\pi}{eq} \int_0^\infty \sin(qr) r \, \rho(r) dr.$$

For small values of q^2 the sine may be expanded to give:

$$G_E(q^2) = G_E(0) - \frac{1}{6} q^2 r^2_{rms} , \qquad \text{(I-3)}$$

where r_{rms} is the root mean square radius of the charge distribution. A similar expansion may be made for the magnetic distribution to obtain the magnetic r_{rms}. The proton and neutron each have different form factors. Thus, four form factors are required to describe them: G_{E_p}, G_{E_n}, G_{M_p}, and G_{M_n}. The r_{rms} obtained by using Equation I-3 is determined in the Breit frame, but since Equation I-3 is only good at low values of q^2, the r_{rms} value determined is generally quoted as the nucleon's charge radius.

B. METHOD OF OBTAINING THE NEUTRON ELECTRIC FORM FACTOR, G_{E_N}

The process of obtaining G_{E_n} from the measured elastic electron-deuteron cross section will be outlined here and discussed in detail in Section II. First, the elastic electron-proton cross section was measured at a given scattering angle and scattered energy using hydrogen gas as a target. The hydrogen was then replaced with deuterium gas and the elastic electron-deuteron cross section was measured at the same scattering angle and with the same scattered energy. The incident electron energy was adjusted to give this condition. All geometries, beam currents, gas pressures, and operating procedures were kept as constant as possible while both the proton and the deuteron data were taken. In fact, the LINAC was operated continuously from the time an experiment started until it was completed with both cross sections

measured. The time required for such a "run" varied from about 15 to 40 hours.

Because absolute cross sections cannot be measured here owing to systematic uncertainties, the ratio of the cross sections, σ^d/σ^p, was formed. In this ratio, many systematic uncertainties cancel since the cross sections are measured under the same conditions. The absolute proton cross section has been measured in previous experiments [10,11,12], and these data have been fit by deVries [10] to formulas from which the cross section can be calculated. When the experimental ratio above is multiplied by the absolute proton cross section, the absolute deuteron cross section is obtained.

Several steps are required to extract G_{E_n} from this cross section. The experimental cross section is first divided by the Mott cross section of the deuteron to obtain the deuteron form factor, G_d. G_d accounts for all the structure in the deuteron, i.e., the electric and magnetic distributions within the neutron and proton as well as the convection of charge due to their motion within the deuteron and the magnetic moment caused by this convection of charge. Following Jankus [13], the deuteron was treated as though its two constituent particles, the neutron and proton, were point particles. The distribution of charge predicted by the deuteron wave function is then contained in a term called the deuteron charge structure factor, which depends only on q^2 and the wave function of the deuteron ground state. E.L. Lomon [14] has provided three selected sets of values, from his larger group of sets of values, for these deuteron charge structure

factors. Each of these is based on a different deuteron wave function obtained from nucleon-nucleon data [15].

Drickey and Hand [3] experimentally verified a proportionality between the magnetic form factor of the deuteron and its charge form factor, called a "scaling law". That relationship was used to remove that part of the deuteron form factor caused by the intrinsic magnetic moments of the proton and the neutron as well as that part of the deuteron magnetic moment caused by the convection of charge.

At this point only the extended charge distribution of the proton has not been accounted for in the extraction process. This distribution is accounted for by the proton electric form factor derived from deVries' data (see Appendix A). The neutron electric form factor, G_{E_n}, has thus been extracted from the deuteron cross section.

The above procedure is justified since the deuteron is a weakly bound structure, i.e., the proton and the neutron spend most of the time outside the range of nuclear forces and one can adequately describe the charge and current distribution within each nucleon as if they were free [13].

Early in this work, before the gas target system was operating, efforts were made to measure G_{E_n} by a process similar to that described above but using polyethylene targets of CH_2 and CD_2 to obtain the cross sections. There were several problems with that work but the most important limitation was the scattering from carbon which complicated the data reduction. The solid target data which were obtained were not as reproducible as the gas target data and are not included in this work.

C. RESULTS OF PREVIOUS EXPERIMENTS AND OF THIS WORK

In this work the neutron charge form factor, G_{E_n}, was measured for values of q^2 ranging from 0.05 to 0.35 fm^{-2}. The slope of G_{E_n} versus q^2 was obtained by a linear least squares fit to the data.

The slope in the limit that $q^2 \rightarrow 0$ has been measured in many experiments [16,17,18] which measured the interaction of thermal neutrons with atomic electrons. The most accurate and most recent measurement of this kind is that of Krohn and Ringo [4], who obtained

$$\frac{d}{dq^2} G_{E_n}(0) = 0.0193 \pm 0.0004 \ \mathrm{fm}^2. \qquad \text{(I-4)}$$

This is probably that best determined of all nucleon form factor parameters [19]. Drickey and Hand [3] measured G_{E_n} by measuring the ratio of the elastic electron-deuteron cross section to the elastic electron-proton cross section using liquid hydrogen and deuterium for targets and found that $G_{E_n} = 0.00 \pm 0.01$ over a range of q^2 from 0.3 to 2.2 fm^{-2}. That is, they found

$$\frac{d}{dq^2} G_{E_n} \approx 0,$$

which is in disagreement with the thermal neutron measurements.

Casper and Gross [20] developed relativistic corrections to electron-deuteron scattering and reanalyzed the data of Drickey and Hand. Using deuteron wave functions derived from the Feshbach-Lomon nucleon-nucleon model they found that the data of Drickey and Hand indicated

$$\frac{d}{dq^2} G_{E_n}(0) = 0.0153 \pm 0.0067 \ \mathrm{fm}^2,$$

which was consistent with the thermal neutron slope. Bumiller, et al. [21,2] extended the elastic electron-deuteron scattering data to q^2 of $0.10 \leq q^2 \leq 0.8$ fm^{-2}, using CH_2, CD_2, and C targets and substantiated the conclusions of Casper and Gross by obtaining a slope of 0.0179 ± 0.0036. This quoted error of ± 0.0036 is incorrect. It should have been quoted as ± 0.0089. Using the same equipment as Bumiller, Mader [1] continued the elastic electron-deuteron scattering work but used a gas target to avoid the carbon subtraction procedures which were necessary with the solid targets used by Bumiller et al. Although Mader's data are as accurate as Refs. 21 and 2, his measurements showed that $\frac{d}{dq^2} G_{E_n} \approx 0$ over a range of $0.05 \leq q^2 \leq 0.60$ fm^{-2}. In this work we have resolved this discrepancy by measuring the G_{E_n} slope to be

$$\frac{d}{dq^2} G_{E_n}(0) = 0.0200 \pm 0.0058 \text{ fm}^2,$$

which then compares favorably to the value of 0.0193 ± 0.0004 fm^2 as measured directly by the neutron-electron scattering experiments.

II. THEORY

A. ELASTIC ELECTRON-PROTON SCATTERING FROM A POINT PROTON

Although it has been proved [22] that the proton is not a point particle, it is convenient initially to solve for the cross section for elastic electron-proton scattering from a point proton.

The initial assumptions are: 1) the proton has a point charge and a point Dirac magnetic moment, 2) the one virtual photon exchange adequately describes the scattering process, and 3) the electron is a point particle. The Feynman diagram describing this process is

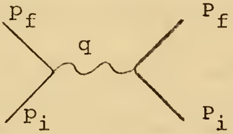

where p_i, p_f and P_i and P_f are the incident and final electron and proton four-momenta respectively and $c\hbar q$ is the four-momentum transferred in the scattering process, i.e.,

$$\hbar^2c^2q^2 = (p_i - p_f)^2 = \{(\vec{p}_i - \vec{p}_f)^2 - (E_i - E_f)^2\} = (P_i - P_f)^2.$$

In order to obtain the cross section for this elastic scattering process we make use of S-matrix formulism. The S-matrix is a matrix connecting the initial and final states of the process shown above. The electromagnetic interaction responsible for electron scattering may be treated by perturbation theory. The first approximation of the S-matrix is given by an integral over the interaction Hamiltonian,

$$S = 1 - i \int dt\, H_i(t),$$

where $H_i(t)$ may be written as a three dimensional integral over a Hamiltonian density $\tilde{H}_i(\vec{r},t)$

$$H_i(t) = \int d^3r\, \tilde{H}_i(\vec{r},t).$$

Since the electrons can be described by a second quantized Dirac field and the proton's electromagnetic field may be described by a vector potential, the interaction Hamiltonian density can then be written as

$$\tilde{H}_i(x) = - j^e_\mu(x) A_\mu(x),$$

where x is the four dimensional space time vector. The four-current of the electron can be written in terms of the four component state vector and Dirac matrices as

$$J^e_\mu(x) = - ie\, \overline{\Psi}_f(x)\, \gamma_\mu \Psi_i(x), \text{ with } \overline{\Psi}(x) = \Psi^+ \gamma_4.$$

The matrix element of this scattering, H_{fi}, is then

$$H_{fi} = - ie \int \overline{\Psi}_f(x) \gamma_\mu \Psi_i(x) A_\mu(x) d^3r \qquad \text{(II-1)}$$

giving the interaction of the electron current (from its initial state to its final state) with the electromagnetic field of the proton. By making use of the first Born approximation, the electromagnetic field due to the proton's transition current from the initial to the final plane wave state can be obtained by solving the inhomogeneous wave equation

$$\left(\nabla^2 - \frac{1}{c^2} \frac{\partial^2}{\partial t^2}\right) A_\mu(x) = -4\pi <f|J^N_\mu|i>$$

where the expectation value of the proton's current operator is the transition current creating the potential $A_\mu(x)$. The solution is

$$A_\mu(x) = \frac{4\pi}{q^2} ie\, \overline{\varphi}_f(x)\gamma_\mu\varphi_i(x),$$

where $\varphi(x)$ is the state vector of the proton. Substituting this result into Equation II-1 the matrix element is

$$H_{fi} = -\,4\pi e^2 \int \overline{\Psi}_f(x)\gamma_\mu\Psi_i(x)\, \frac{1}{q^2}\, \overline{\varphi}_f(x)\gamma_\mu\varphi_i(x)\, d^3x. \qquad \text{(II-2)}$$

Because of the use of initial and final state plane waves, the integration over space results in the delta-function $\delta(\vec{p}_f + \vec{P}_f - \vec{p}_i - \vec{P}_i)$, expressing momentum conservation. It is interesting to note that the $1/q^2$ term can be considered to be with either source current. Thus the proton may be considered as being scattered from the electron's field or the electron may be considered to be scattered from the field of the proton as it was above.

The cross section may now be obtained by calculating

$$\frac{d\sigma}{d\Omega} = \sum_{\substack{\text{final}\\ \text{states}}} \frac{\omega_{fi}}{\text{flux}} \qquad \text{(II-3)}$$

and averaging over the initial spin states, where

$$\omega_{fi} = \frac{2\pi}{\hbar} \left|H_{fi}\right| \delta(E_f - E_i)$$

and the flux is the incoming flux of electrons. The sum over final states is really an integral over all possible proton momenta and over that range of electron momenta which are within the solid angle of the detector. These integrations over momentum space and the averaging over the initial spins

and summing over the final spin states are tedious but then completed Equation II-3 yields

$$\left.\frac{d\sigma}{d\Omega}\right)_{\substack{\text{Dirac}\\ \text{proton}}} = \left(\frac{1}{4}\,\frac{e^4}{E_i^2}\,\frac{\cos^2\theta/2}{\sin^4\theta/2}\right)\left(1+\frac{q^2}{2m_p^2c^4}\tan^2\frac{\theta}{2}\right)\left(\frac{1}{1+\dfrac{2E_i\sin^2\theta/2}{m_pc^2}}\right), \quad \text{(II-4)}$$

where E_i is the energy of the incident electron and θ is the angle through which it is scattered. Both are measured in the system where the proton is initially at rest and

$$c^2\hbar^2q^2 = 4E_iE'_f\sin^2\theta/2$$

E_f is the final electron energy given by

$$E_f = \frac{E_i}{1+\dfrac{2E_i}{mc^2}\sin^2\theta/2} .$$

In the limit that m_ec^2/E approaches zero the first enclosed term on the right of Equation II-4 was calculated by Mott [5] in 1929, using the Dirac equation, to be the cross section of an electron scattered from a coulomb potential; in the case of a proton that physically means that the proton is a point charge and that it has zero spin and an infinite mass, i.e., it doesn't recoil. Let us call that the historical Mott cross section. The final enclosed term on the right is the recoil term which accounts for both the kinematics of the recoil and the fields associated with the accelerating proton. When the historical Mott cross section is multiplied by this recoil term it is generally called the Mott cross

section. That nomenclature is followed in this work. The $\tan^2\theta/2$ part of the second enclosed term accounts for the scattering contributed by the Dirac magnetic moment of the proton while the 1 in that term accounts for the point charge scattering. Equation II-4 thus provides the cross section for an electron scattering from a point proton with a point Dirac magnetic moment. However, there are two corrections which must be made to Equation II-4 in order that the theorectically predicted cross section of a proton agrees with measurements.

The first thing which is known to be wrong with Equation II-4 is that the magnetic moment of the proton is not equal to one nuclear magneton as is predicted by the Dirac equation, but is measured to be $\mu_p = + 2.79275 \pm 0.0003$ nuclear magnetons. Also the prediction of the Dirac equation of zero magnetic moment for the neutron compares badly with the measured neutron magnetic moment of $\mu_\eta = -1.9135 \pm 0.0003$ nuclear magnetons.

Pauli [23] has shown that the Dirac equation for a charged particle interacting with an electromagnetic field can be modified so as to represent a particle with an arbitrary magnetic moment by addding the operator

$$-\left(\frac{i\mathcal{K}}{\hbar c}\right)\gamma_\mu\gamma_\nu\left(\frac{\partial A_\mu}{\partial x_\nu} - \frac{\partial A_\nu}{\partial x_\mu}\right)$$

to the equation. Foldy [24] has verified that such a term satifies the restrictions of being Lorentz covariant and gauge invariant and has shown that the general interaction terms form an infinite series involving arbitrarily high derivitives

of the electromagnetic potential evaluated at the position of the particle. The series of coefficients of these terms can be interpreted as a series of moments of the charge and current distributions associated with the particle. We will return to this expansion later in this section.

Because the four potential, A_μ, can be regarded as the potential produced by the electron, the Pauli term can be shown to reduce to

$$\frac{\mathcal{K}_p}{2m_c^2}\,\sigma_{\mu\nu}\,(p_{i_\nu} - p_{f_\nu})$$

which is added to the γ_μ term of the nuclear current. Here $\mathcal{K}_p = 2.79 - 1.0 = 1.79$ is the anomalous magnetic moment of the proton in units of nuclear magnetons and

$$\sigma_{\mu\nu} = -\frac{i}{2}(\gamma_\mu\gamma_\nu - \gamma_\nu\gamma_\mu).$$

When the Pauli term is inserted into the matrix element of Equation II-2, the cross section for a point Dirac particle with its normal point magnetic moment and now also its anomalous point magnetic moment is obtained:

$$\left(\frac{d\sigma}{d\Omega}\right)_{\substack{\text{point}\\ \text{proton}}} = \left(\frac{d\sigma}{d\Omega}\right)_{\text{Mott}} \left\{1 + \frac{q^2}{4m^2c^4}\left[2(1+\mathcal{K}_p)^2\tan^2\left(\frac{\theta}{2}\right) + \mathcal{K}_p^2\right]\right\},$$

where

$$\left(\frac{d\sigma}{d\Omega}\right)_{\text{Mott}} = \left(\frac{e^4}{4E^2}\,\frac{\cos^2\theta/2}{\sin^4\theta/2}\right)\left(\frac{1}{1+\dfrac{2E\sin^2\theta/2}{m_pc^2}}\right).$$

The second change which must be included in the description of scattering from a real proton will now be considered. In 1955 Hofstadter and McAllister [22] measured the cross section of the proton and showed that the structure of a proton is more complicated than a point charge and point magnetic moment; the proton scattered as though it had a charge and magnetic moment "cloud" spread out to an rms radius of about 0.7 fm. Subsequent work (1960-61) on the proton at Stanford [25,11] showed that the magnetic moment associated with the Pauli term had a softer or more spread out distribution with an rms radius of about 1 fm, while the distribution of the charge had an rms radius of about 0.8 fm. These rms radii were calculated on the basis of Equation I-3 by assigning proton form factors $F_{1p}(q^2)$ to the Dirac charge and magnetic moment distribution and $F_{2p}(q^2)$ to the Pauli magnetic moment distribution. The addition of the anomalous magnetic moment to the interaction and now the provision permitting the Dirac and Pauli components to have spatial extent changes the proton contribution in the matrix element of Equation II-2 from

$$\overline{\varphi}_f(x)\gamma_\mu\varphi_i(x)$$

to

$$\overline{\varphi}_f\left(F_{1p}(q^2)\gamma_\mu + \frac{\mathcal{K}_p}{2mc^2}\,\sigma_{\mu\nu}(p_{i\nu}-p_{f\nu})F_{2p}(q^2)\right)\varphi_i .$$

The elastic electron-proton cross section with this modified current matrix element has been calculated by Rosenbluth [26] to be

$$\frac{d\sigma}{d\Omega} = \left(\frac{d\sigma}{d\Omega}\right)_{\text{Mott}}\left[F_{1p}^2 + \frac{q^2}{4m^2c^4}\left[2\left(F_{1p} + \mathcal{K}_p F_{2p}\right)^2 \tan^2\left(\frac{\theta}{2}\right) + \mathcal{K}_p^2 F_{2p}^2\right]\right. \qquad \text{(II-5)}$$

and is called the Rosenbluth cross section.

B. NEUTRON FORM FACTORS

The neutron has zero total charge. Both the electron and neutron have magnetic moments, however, and thus they can interact through the magnetic dipole-dipole interaction. Also, an incident electron has a magnetic field associated with it because of its charge and this will interact with magnetic moment of the neutron. These interactions are well understood and must be accounted for in the calculation of the electron neutron scattering formula.

There remains a third interaction which is generally called the neutron-electron interaction in the literature. This interaction is expected to be both spin and velocity independent if there is a separation of electrical charge in the neutron. Thus an electron, or any charged particle, penetrating the extended charge distribution of the neutron will be subjected to electrostatic forces. These may arise from two sources: 1), the intrinsic charge separation in the neutron analogous to the spreading out of charge in the Dirac proton and evidenced by the form factor F_{1n} analogous to F_{1p} of the proton, and 2), the anomalous magnetic moment of the neutron, described by a form factor F_{2n}, analogous to F_{2p} for the proton, if the anomalous magnetic moment has a spatial extent. Foldy [27,28] has shown that since the neutron satisfies the Dirac equation, and since it possesses an anomalous magnetic moment, then some charge separation is to be expected. He compared the amount of charge separation predicted because of the neutron's anomalous magnetic moment with that charge separation inferred by the very accurate thermal

neutron-electron measurements of the neutron's attractive potential for the electron made by several groups [16,17,29,30]. The predicted and inferred charge separations agreed within experimental error, implying that the so-called intrinsic or Dirac separation is not present. Since this requirement for charge separation within the neutron simply because it has an anomalous magnetic moment is not intuitive, this will be examined in more detail below, as will the results of the experiments that measured the neutron's attractive potential.

Several methods of measuring the attractive potential have been used. Only the first [16] of these is outlined here. If one measures the coherent scattering of neutrons by spinless (in order to remove effects due to magnetic interactions) atoms containing a nucleus and Z electrons, then the coherent scattering amplitude for neutrons whose wavelength is long compared to the size of the atom will be the algebraic sum of the scattering amplitudes due to the nucleus and the Z electrons. By decreasing the neutron wavelength until it is comparable to the size of the electronic cloud of the atom, destructive interference between the scattering from the individual electrons within the cloud of electrons can be achieved and the total coherent scattering cross section can be made to approach that of the nucleus alone. By separating these scattering effects, one obtains the so-called neutron-electron interaction. The result of the thermal neutron-electron experiments is expressed as the volume integral of the potential of the neutron-electron interaction. Plots of

the neutron (and the proton for comparison purposes) charge density and the interaction potential are given in Figure II-1 [31].

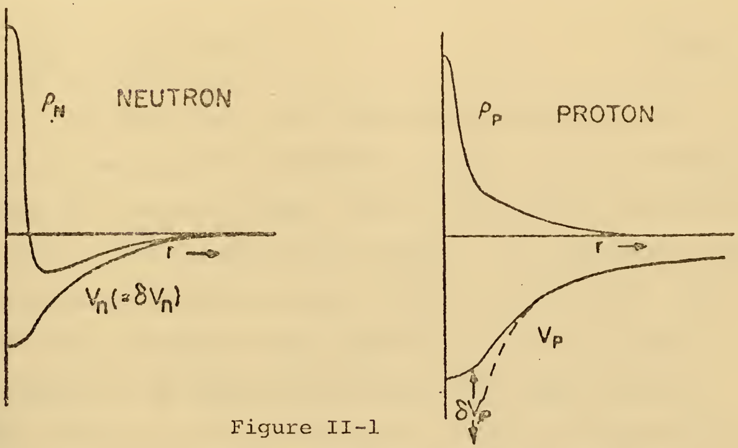

Figure II-1

Neutron and Proton Charge Densities and Interation Potentials Between These Particles and an Electron

The neutron-electron potential is denoted as δV_n; that is, it is the difference between what the neutron potential would be if it had no charge distribution and what it would be if it had a positive center and a negative outer region. This concept of a positive center and a negative outer region is justified by the results of the thermal neutron-electron scattering experiments and is also consistent with meson theory. The volume integral of this charge distribution does not permit an independent determination of the depth and volume of the potential. It does however permit the determination of the r^2_{rms} of the charge distribution by the following calculation.

Let

$$r^2_{rms} = \int r^2 \rho(r)\, d^3r$$

and then use Poisson's equation to obtain

$$r^2_{rms} = \frac{6}{4\pi e^2} \int \delta V d^3r. \qquad \text{(II-6)}$$

However, following Fermi, all experiments have reported results in the form of a potential V_o which was the average V_o which the electron sensed. This required that some average radius of this potential be adopted. By convention, that radius is the classical electron radius (2.81794 fm), which implies that classically the bound electrons in the atom were assumed to be interacting almost uniformly over the neutron, because as will be seen, the neutrons largest r_{rms} is less than 1 fm. That is, the electrons are not just sensing the outer charge layer as might be implied by the classical picture of a point electron of low momentum penetrating only the outer shell of the neutron charge distribution. This is perhaps best seen from the virtual photon scattering picture. The wavelength of the virtual photon is very long compared to the neutron diameter and the electromagnetic fields will be effectively constant at any time over the extent of the neutron with the greatest difference in these fields occurring between the extreme edges of the neutron. Thus, while it is the charge distribution near the edges of the neutron which show the deviation of the neutron from a particle with zero charge density everywhere, it is the average charge density, and through Poisson's equation the

average potential within the neutron, that is measured in these thermal neutron experiments. Using this average potential the volume integral of the interaction potential is then written

$$\int_0^{r_e} Vd^3r = V_o \int_0^{r_e} 4\pi r^2 dr = \frac{4}{3}\pi r_e^3 V_o = \frac{4}{3}\pi \frac{V_o e^2}{mc^2} r_e^2 \qquad \text{(II-7)}$$

where r_e is the classical electron radius.

Since Equations II-6 and II-7 are simply different ways of performing the volume integral they must be equal, therefore we have:

$$r_{rms}^2 = \frac{2V_o}{mc^2}(r_e^2)$$

thus

$$r_{rms}^2 = \frac{2V_o}{mc^2}\left(\frac{e^2}{mc^2}\right)^2$$

where V_o is put in the conventional units of million electron volts. Then

$$r_{rms}^2 = 31.078\ V_o\ (\mathrm{fm})^2 \ . \qquad \text{(II-8)}$$

The presently accepted value of V_o is [4]:

$$V_o = 3720 \pm 90 \text{ electron volts} \ . \qquad \text{(II-9)}$$

This value of V_o when substituted into Equation II-8 gives r_{rms}^2 charge of neutron = $-$ (0.34 fm)^2, the negative sign showing, since the charge on the outer shell is weighted by r^2 more heavily than the inner shell, that there is a charge separation in the neutron, and that the outer regions of the neutron are negative.

It was stated above that the two facts that the neutron satisfies the Dirac equation and that it has an anomalous magnetic moment are sufficient to account completely for the measured value of the potential V_o [27,31,32]. Let us now see why that statement is correct.

The relativistic Hamiltonian for a neutron with the anomalous magnetic moment as attributed by Pauli can be written as

$$H = \beta M + \vec{\alpha}\cdot\vec{P} - \mathcal{K}_n (e/2m)[\beta\vec{\sigma}\cdot\vec{H} - i\beta\vec{\alpha}\cdot\vec{E}]$$

where $\mathcal{K}_n$ is the anomalous (and total) magnetic moment of the neutron measured in nuclear magnetons. This can be reduced to the corresponding nonrelativistic Hamiltonian by the method of Foldy and Wouthuysen [33] which yields

$$H = \beta M + \beta p^2/2M - \mathcal{K}_n\left(\frac{e}{4M^2}\right)\beta \text{ div } \vec{E}$$

$$+ \mathcal{K}_n\left(\frac{e}{4M^2}\right)\beta\vec{\sigma}\cdot[\vec{P} \times \vec{E} - \vec{E} \times \vec{P}]$$

with terms of order greater than $(1/M)^2$ being neglected. For the coulomb field of a point electron located at $\vec{x}_e$ the above Hamiltonian becomes

$$H = \beta M + (\beta p^2/2M) + 4\pi\mathcal{K}_n (e^2\beta/4M^2)\,\delta(\vec{x}-\vec{x}_e) + \ldots$$

where the term containing the delta function is in the form of the electron-neutron interaction. Equating the volume integral of the neutron-electron interaction potential to this term one has [27]

$$V_o = \pi\mathcal{K}_n (e^2/M^2)[(4\pi/3)(r_e^3)]^{-1} = -3900 \text{ eV}.$$

This compares very well with the experimental result given in Equation II-9. Since the neutron charge distribution can be completely accounted for by its anomalous magnetic moment this means that there is, within experimental errors, no Dirac particle intrinsic charge distribution unless relativistic contributions fortuitously cancel this Dirac intrinsic charge distribution.

The distribution of the neutron anomalous magnetic moment was measured by Yearian and Hofstadter and Bumiller [34,35] in 1958. They used Rosenbluth's proton cross section as given in Equation II-5 with modifications to obtain the neutron cross section. Based principally on the thermal neutron work discussed above, they set $F_{1n} = 0$ to describe the neutron's lack of intrinsic charge and magnetic moment distribution and allowed F_{2n} to describe its anomalous moment. The neutron cross section was then

$$\frac{d\sigma}{d\Omega} = \left(\frac{d\sigma}{d\Omega}\right)_{\text{Mott}} F_{2n}^2 \, \mathcal{K}_n^2 \, \frac{q^2}{4M^2}\left[2\tan^2\frac{\theta}{2} + 1\right].$$

Electrons were scattered from a deuterium gas target at sufficiently high energies and large angles to enhance the magnetic scattering from the nucleons. By using the rather good approximation for inelastic scattering from a deuteron, i.e., $\sigma_d^{IN} = \sigma_p + \sigma_\eta$, they were able to obtain the r_{rms} of the anomalous magnetic moment of the neutron and concluded that it was between 0.8 and 0.9 Fermi.

C. CHARGE, MAGNETIC AND ISOTOPIC FORM FACTORS

Thus far the four form factors used to describe the distributions of charge and magnetic moment of the Dirac particle and the Pauli moment have been introduced in the historical manner in which they evolved. They may be summarized as follows:

F_{1p} is the form factor associated with the distribution of charge of the Dirac proton and also with the distribution of the intrinsic (Dirac) magnetic moment. In the static ($q^2 = 0$) limit $F_{1p}(0) = 1$.

F_{2p} is the form factor associated with the anomalous (Pauli) magnetic moment distribution of the proton. In the static limit $F_{2p}(0) = \mathcal{K}_p = 1.79$.

F_{1n} is the form factor associated with the distribution of charge of the Dirac neutron and also with the distribution of the intrinsic (Dirac) magnetic moment of the neutron. In the static limit $F_{1n}(0) = 0$.

F_{2n} is the form factor associated with the anomalous (Pauli) magnetic moment distribution of the neutron. In the static limit $F_{2n}(0) = \mathcal{K}_n = 1.91$.

It has been shown above that the anomalous (Pauli) magnetic moment of the neutron causes some charge distribution within the neutron. Therefore the form factor F_{2n} not only tells what the anomalous magnetic moment distribution is, but tells something about the charge distribution.

The work of Yennie, _et al_. (1957 [31], Ernst _et al_. (1960) [8] and Hand _et al_. (1963)[19] introduced linear combinations

of the four Dirac and Pauli form factors for both theoretical and experimental reasons. These combinations were the following:

$$G_{E_p} = F_{1p} - \frac{q^2}{4m^2c^2}\mathcal{K}_p F_{2p}$$

$$G_{m_p} = F_{1p} + \mathcal{K}_p F_{2p}$$

$$G_{E_n} = F_{1n} - \frac{q^2}{4m^2c^2}\mathcal{K}_n F_{2n}$$

$$G_{m_n} = F_{1n} + \mathcal{K}_n F_{2n}.$$

In Ref. 19 it is pointed out that these linear combinations correspond to zero, G_E, and one, G_m, unit of angular momentum transferred along the direction of the virtual photon exchanged in the scattering process. Reference [8] added more physical content to these linear combinations of F_1 and F_2 by showing that the rms radii of and charge and magnetic moment spatial distribution are derived from Equation I-3 by

$$\left[6 \frac{d}{dq^2} G_E\right]^{\frac{1}{2}} \quad \text{and} \quad \left[6 \frac{d}{dq^2} G_m\right]^{\frac{1}{2}}$$

at $q^2 = 0$. For this reason the descriptive names for G_E and G_M are the "charge" and "magnetic" form factors. Additionally, Ref. 19 points out that the cross terms of the charge and magnetic form factors do not interfere with each other in the Rosenbluth cross section when it is written in terms of G_E and G_M, while the Dirac and Pauli terms are mixed into the Rosenbluth cross section as products of each other, as can been seen by examining Formula II-5. Written in terms of G_E and G_M, the Rosenbluth cross section for the proton becomes

$$\frac{d\sigma}{d\Omega} = \left(\frac{d\sigma}{d\Omega}\right)_{\text{Mott}} \left[\frac{G^2_{Ep}}{1+\frac{q^2}{4m_p^2}} + \frac{q^2}{4m_p^2} \left(\frac{1}{1+\frac{q^2}{4m_p^2}} + 2\tan^2 \theta/2 \right) G^2_{M_p} \right] \quad \text{(II-10)}$$

with an analogous equation for the neutron cross section. G_E and G_M are obtained experimentally by measuring the cross section at at least two different scattering angles, at the same q^2. From the intercept of a plot of G^2 versus the coefficient of $G^2_{M_p}$ one obtains G_{E_p} and from the slope one obtains G_{M_p}. The static ($q^2 = 0$) values of these charge and magnetic form factors are:

$$\begin{aligned} G_{E_p}\,(q^2 = 0) &= 1 \\ G_{M_p}\,(q^2 = 0) &= 2.79 \qquad \text{(II-11)} \\ G_{E_n}\,(q^2 = 0) &= 0 \\ G_{M_n}\,(q^2 = 0) &= -\,1.91. \end{aligned}$$

We now consider what the slope of G_{E_n} tells about the charge distribution of the neutron by studying the primary scattering event of interest in this work, the e-d scattering. This process may be described by the Feynman diagram

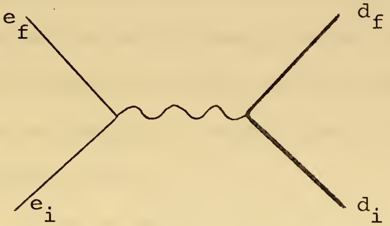

where e_i and e_f are the incident and scattered electron states, d_i and d_f are the target and recoiling deuteron states and q is the four-momentum transfer. The deuteron has a diameter of about 4 fm; in this work, with electron energies of about 35 to 100 MeV, the virtual photons had wavelengths in the range of 10 to 30 fm. With these long wavelengths compared to the extent of the deuteron and neutron, only the outer charge distributions are measured. It is important to note that the thermal neutron experiments [18,4,16,17] give a positive slope for $\frac{d}{dq^2} G_{E_n}'$ as do two of the e-d experiments [20,21]. This means that the quantity $-\frac{1}{6} r_{rms}^2$ is positive, i.e., that the outer part of the neutron is negative. This is so because the square of the rms radius is obtained from the expression

$$r_{rms}^2 = \int_0^\infty r^2 (4\pi r^2 \rho(r) dr)$$

where the total charge of the neutron $= \int_0^\infty 4\pi r^2 \rho(r) dr = 0$; thus a negative r_{rms}^2 shows that the charge density, $\rho(r)$, of the neutron must be more negative at larger radii. Historically, theoretical attempts have been made to explain nucleon charge distributions in terms of a third set of nucleon form factors which are called the isotopic form factors. These isotopic form factors are useful because the structure of nucleons is determined by the strong interaction and calculations can be arranged in such a way that one can take advantage of the conservation of isospin. As the form of the nuclear electric current operator [36]

$$J_\mu(x) = e\bar{\varphi}(x)\gamma_\mu \frac{1+\tau_3}{2} \varphi(x)$$

shows, the current has mixed transformation properties under rotations in isospin space; part of it transforms as a scalar and part as a third component of an isovector. As a consequence of these mixed transformation properties, the proton and neutron current elements may be expressed in terms of an isovector and isoscalar current, i.e.,

$$J_\mu^P(x) = J_\mu^S(x) + J_\mu^V(x) \quad \text{and}$$

$$J_\mu^N(x) = J_\mu^S(x) - J_\mu^V(x).$$

The electric and magnetic isotopic form factors then enter the cross section calculation as the coefficients of the scalar and vector current operators in the matrix element. The isotopic form factors, where the superscript denotes scalar or vector, are:

$$\begin{aligned}
G_E^S &= \tfrac{1}{2}\left[G_{E_p} + G_{E_n}\right] \xrightarrow[q^2 \to 0]{} \tfrac{1}{2} \\
G_E^V &= \tfrac{1}{2}\left[G_{E_p} - G_{E_n}\right] \xrightarrow[q^2 \to 0]{} \tfrac{1}{2} \\
G_M^S &= \tfrac{1}{2}\left[G_{M_p} + G_{M_n}\right] \xrightarrow[q^2 \to 0]{} \tfrac{1}{2}\,(\mu_p+\mu_n) \\
G_M^V &= \tfrac{1}{2}\left[G_{M_p} - G_{M_n}\right] \xrightarrow[q^2 \to 0]{} \tfrac{1}{2}\,(\mu_p-\mu_n)
\end{aligned} \qquad \text{(II-12)}$$

There have been attempts to give the isotopic form factors further meaning. While these attempts have not been completely successful, it is useful to consider them briefly. A state of n π mesons, produced by a photon, must have zero total charge and be odd under charge conjugation. Based on this, Drell and Zachariasen [37] have shown that only an even number of pions

contribute to the isotopic vector form factor and that only an odd number of pions can contribute to the isotopic scalar form factors. They also have shown that charge conjugation does not permit a single pion to be produced since the photon is odd under charge conjugation and the π^o, the only π which conserves charge, is even under charge conjugation. The possible intermediate states then include:

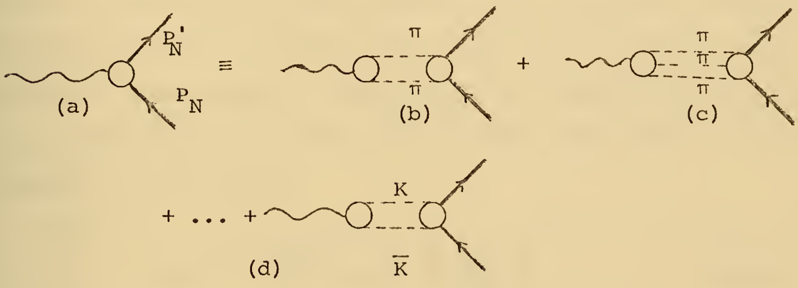

Figure II-2

Possible Intermediate Photon-Proton States

In the diagram in Figure II-2 the possible existence of pion-pion forces were disregarded; but we know that there are resonances in the two-pion and three-pion systems, and we expect that such resonances may have an effect on the electromagnetic structure of the nucleons. Chew _et al_. [38] and Nambu [39] have shown that such propagators as depicted in Figure II-2 (b) and (c) do in fact contribute to the form factors in such a way that they have poles at the masses of the ρ_o, ω_o and φ_o. The rho (isospin = 1, spin = 1) contributes to the isovector and the omega and phi (isospin = 0, spin = 1)

contribute to the isoscalar form factors. On the assumption that virtual clouds of mutually strongly interacting bound pions are responsible for the electromagnetic properties, these clouds show up as resonances in dispersion theoretical expressions for the form factors, for instance

$$G_E^S(q^2) = \frac{1}{\pi}\int_m^\infty \frac{g(q'^2)\,dq'^2}{q'^2-q^2} \qquad \text{(II-13)}$$

where m corresponds to the threshold for resonance creation. Furthermore, if one assumes that these vector mesons (spin =1) appear as sharp peaks in the spectra of weight functions $g(q'^2)$, i.e., neglecting the widths (ρ(100 MeV), ω(10 MeV), φ(3 MeV), Equation II-13 becomes

$$G_E^S(q^2) = \frac{1}{2}\left[\left(1-S_{el}\right)+\frac{S_{el}}{1+\frac{q^2}{M_S^2}}\right], \qquad \text{(II-14)}$$

which is the form factor expression which Clementel and Villi [40] have proposed, where S_{el} is a constant. The term $1-S_{el}$ represents the possibility of high mass resonances, i.e., it represents those resonances which have such high masses that their poles may be replaced by constants. M_S is the mass of the scalar resonances. There is one term for each resonance. Similar expressions for G_E^V, G_M^S and G_M^V were likewise developed and were used by deVries [10] to fit proton and neutron data. This fit is discussed in Appendix A and provided the normalization for the proton data obtained in this work.

Earlier in Section II it was observed that the outer regions of the neutron have been measured to be negative in the thermal neutron work. There are several theoretical reasons to believe that the outer regions should be negative [32,38]. Among these is the fact that the anomalous magnetic moment is almost entirely a vector in isotopic spin space, i.e., the anomalous moments of the neutron and proton are nearly equal in magnitude with opposite signs. Additionally since the isovector meson, the rho, is the least massive of the rho, omega, phi mesons, the uncertainty principle as well as the Yukawa potential indicate that the outer regions will be dominated by the rho meson.

D. METHOD OF EXTRACTING THE PROTON ELECTRIC FORM FACTOR FROM THE PROTON CROSS SECTION

The Rosenbluth cross section for the proton (Eq. II-10) can be written as:

$$\left(\frac{d\sigma}{d\Omega}\right)_{\text{proton}} = \left(\frac{d\sigma}{d\Omega}\right)_{\text{Mott}} \left[\frac{G^2_{E_p}}{1+\tau} + \frac{\tau}{1+\tau} G^2_{M_p} + 2\tau G^2_{M_p} \tan^2 \frac{\theta}{2}\right], \qquad \text{(II-15)}$$

where $\tau = q^2/4M_p^2$. This can be simplified by using the scaling law proposed by Lehmann <u>et</u> <u>al</u>. [41] and others [19], which states that

$$G_{E_p} = \frac{G_{M_p}}{\mu_p} . \qquad \text{(II-15a)}$$

Schumacher has shown that we should not expect isoscalar form factors to equal isovector form factors [42], and that a set of scaling laws which relate the form factors G_{M_p} and G_{M_n} to G_{E_p} and G_{E_n} are

$$G_{M_p} = \mu_p G_{E_p} + \mu_n G_{E_n}$$

and

$$G_{M_n} = \mu_n G_{E_p} + \mu_p G_{E_n} .$$

For our experiments, magnetic scattering generally accounted for only a percent or two of the total scattering in most runs and at most 10% of the scattering in a few runs; thus the difference in these two scaling laws, which was at most a 1.0% difference at $0.35q^2$, then made a difference in the cross section of less than a nominal 0.01% up to at most a 0.05%. Thus the conventional scaling law was used to reduce the calculations. When the magnetic contribution is accounted for by using the scaling relationship, Equation II-15a, Equation II-15 reduces to

$$\frac{d\sigma^p}{d\Omega} = \sigma_M^p(\theta) \frac{G_{E_p}^2}{1+\tau} \left[1+ \tau\mu_p^2+(1+\tau)(2\tau)\mu_p^2\tan^2 \frac{\theta}{2}\right], \qquad \text{(II-16)}$$

where

$$\left.\frac{d\sigma^p}{d\Omega}\right|_{\text{Mott}} \equiv \sigma_M^p(\theta) .$$

Because the last two terms in the bracket are due to the magnetic form factors it is convenient to group them together by defining

$$C_p = \tau\mu_p^2 + 2\tau\mu_p^2(1+\tau)\tan^2 \frac{\theta}{2} . \qquad \text{(II-17)}$$

Because the proton cross section can be written as

$$\frac{d\sigma^p}{d\Omega} = \sigma_M^p(\theta)G_p^2, \qquad \text{(II-18)}$$

where G_p is the proton form factor, we can obtain the proton electric form factor by combining II-16, II-17, and II-18 as

$$G_{E_p}^2 = G_p^2 \frac{(1+\tau)}{(1+C_p)} = K_M^p G_p^2 = K_M^p \frac{\frac{d\sigma^p}{d\Omega}}{\sigma_M^p(\theta)} , \qquad \text{(II-19)}$$

where

$$K_M^p = \frac{(1+\tau)}{(1+C_p)}$$

is defined as the proton magnetic correction term. Thus by measuring the proton cross section and dividing it by $\sigma_M^p(\theta)$ and then multiplying this quotient by K_M^p one extracts the square of the proton electric form factor.

E. THE DEUTERON GROUND STATE

Before the elastic electron-deuteron calculation is studied it is useful to consider the ground state of the deuteron. This is particularly true in this case of elastic scattering because the deuteron is in its ground state both before and after the scattering event. It is an experimental fact that the deuteron has but one bound state and that is the ground state. Since the discovery of the deuteron in 1932 many of its characteristics have been measured and provide useful guidance in interpreting the electron deuteron scattering data. Some of the more important are discussed below.

1) The neutron and proton are bound together by an energy of 2.2256 ± 0.0015 MeV.

2) The angular momentum is $1\hbar$, and the parity is even.

3) The magnetic dipole moment is $\mu_d = 0.857393 \pm 0.00003$ nuclear magnetons.

4) The electric quadrupole moment is 0.00282 ± 0.00002.

5) The root-mean-square electromagnetic radius of the deuteron is 1.96 ± 0.02F.

6) The deuteron potential has a repulsive core with an rms radius of about 0.4F.

7) The mass of the deuteron is 1875.585 MeV.

Elementary calculations solve for the deuteron wave function in a square well neutron proton potential using the measured binding energy. The solution shows that the neutron and proton spend most of the time outside of the square well potential. The ground state is mostly a 1S state, i.e., an $\ell = 0$ state, which is indicated not only from general energy considerations [43], but from the fact that the algebraic sum of the proton and neutron magnetic moments nearly equals the deuteron magnetic moment. This indicates that the intrinsic spins of these particles are aligned and that there is no orbital angular momentum. If the nuclear force were spin independent, one should expect to observe a singlet state, $^1S_0$ with the same energy. However, no bound state with J = 0 has been found in the deuteron. This indicates that the neutron-proton force is stronger when the spins are parallel than when they are antiparallel; however, this does not mean that the antiparallel or singlet force is zero. In fact, the singlet force is almost strong enough to produce a bound state.

Although the above description of the deuteron is accurate to first approximation, a better description is possible. First, one notes that the algebraic sum of the proton and neutron magnetic moment is 0.87925 ± 0.0004 while the measured magnetic moment of the deuteron is 0.857393 ± 0.00003 nm. This difference, about 2½%, is larger than the experimental error. The second problem with the description given above is that a pure S state implies that the quadrupole moment is zero since the wave function is spherically symmetric, while the

deuteron in fact has a positive quadrupole moment. The only other state in which two particles give the same angular momentum and parity is the $^3D_1$ state ($\ell = 2$, $S = 1$, $J = 1$). The conclusion is that the total wave function of the deuteron must have the form $\Psi = a_S\Psi_S + a_D\Psi_D$ where the subscripts indicate S state and D state and the coefficients satisfy $a_S^2 + a_D^2 = 1$ in order to normalize the total wave function. The exact value of a_D that produces a quadrupole moment in agreement with the experimental value depends on the radial part of the function Ψ_D, which in turn depends upon the details of the radial dependence of the neutron-proton potential. Values of the D state probability, $P_D = a_D^2$, in the range of 3 to 7% have been obtained from calculations using different potentials [44]. A mixed deuteron ground state with $a_D^2 \approx 4\%$ produces an electric quadrupole moment and a magnetic dipole moment, both in qualitative agreement with observations. It is one of the objects of this work to help determine which wave function best fits these values and from this determine more properties of the nuclear potential. Different wave functions which are considered in this work have different percentages of D state. However it is possible to keep the same percentage of D state and to change the quadrupole moment by changing the range of the tensor potential. This potential cannot be spherical as that produces a pure S state. The positive quadrupole moment indicates that the two nucleons prefer to line up with their spin vectors along the same line rather than side by side. The tensor potential which is a function of the angle between the spin vector of the neutron

and the proton and the radius vector r separating them accounts for this preferential alignment of spins and is a potential which must be added to the dominant spherical potential.

Several textbooks [43,45,46] cover in detail all the concepts that were briefly discussed above. Having summarized the deuteron ground state we now consider in detail the elastic electron deuteron scattering process.

F. ELASTIC ELECTRON-DEUTERON SCATTERING

Jankus [13] in 1956 derived the cross section for elastic electron-deuteron scattering in the first Born approximation. In his calculation the nucleons were represented by point charges and point magnetic moments. The electron was considered extremely relativisitic, but the deuteron was treated nonrelativistically.

While the nucleons have spin one half and two form factors, the deuteron, with spin 1, has three form factors. This is consistent with the work of Glaser and Jaksic [47] and others [48] which predicts that the cross section for scattering a relativistic electron from a potential of spin J will contain 2J + 1 form factors.

Jankus's result, written in the more current terms [49], and including form factors for the proton and neutron, i.e., permitting Jankus's point nucleons to have extent, is

$$\frac{d\sigma^d}{d\Omega} = \sigma_M^d(\theta)\left\{G_0^2(q^2)+ \frac{8}{9}\eta^2 G_2^2(q^2)+ \frac{2}{3}\eta G_1^2(q^2)\left[1+2(1+\eta)\tan^2\frac{\theta}{2}\right]\right\}, \quad \text{(II-20)}$$

where $\eta=q^2/4M_d$ and $G_0(q^2)$, $G_1(q^2)$ and $G_2(q^2)$ are the charge, quadrupole and magnetic moment form factors of the deuteron.

These are given by

$$G_0 = (G_{E_p} + G_{E_n})C_E, \qquad \text{(II-21)}$$

where

$$C_E = \int_0^\infty \left[u^2(r) + w^2(r)\right] j_0(q\,\tfrac{r}{2})\,dr \qquad \text{(II-22)}$$

for the charge from factor;

$$G_2 = (G_{E_p} + G_{E_n})C_Q, \qquad \text{(II-23)}$$

where

$$C_Q = \frac{3}{\sqrt{2}\eta}\int_0^\infty \left[u(r)w(r) - \frac{w^2(r)}{2\sqrt{2}}\right] j_2(q\,\tfrac{r}{2})\,dr \qquad \text{(II-24)}$$

for the quadrupole form factor, and

$$G_1 = 2\,\frac{M_d}{M_p}\left\{\left(G_{M_p} + G_{M_n}\right)C_S + \left(G_{E_p} + G_{E_n}\right)C_L\right\} \qquad \text{(II-25)}$$

for the magnetic form factor, where

$$C_S = \int_0^\infty \Big\{\left[u^2(r) - \frac{w^2(r)}{2}\right] j_0(q\tfrac{r}{2}) + \left[\frac{w(r)u(r)}{\sqrt{2}} + \frac{w^2(r)}{2}\right] j_2(q\,\tfrac{r}{2})\,dr \qquad \text{(II-26)}$$

and

$$C_L = \frac{3}{2}\int_0^\infty w^2(r)\left[j_0(q\,\tfrac{r}{2}) + j_2(q\,\tfrac{r}{2})\right]dr. \qquad \text{(II-27)}$$

$(G_{M_p} + G_{M_n})C_S$ determine the contribution of the intrinsic magnetic moments of the proton and the neutron to the cross section and $(G_{E_p} + G_{E_n})C_L$ determines the magnetic contribution of the convection of charge in the deuteron to the cross section.

Here M_p and M_d are the mass of the proton and deuteron respectively and u(r) is the S-state wave function and w(r)

is the D-state wave function normalized so that

$$\int_0^\infty \left[u^2(r) + w^2(r)\right] dr = 1 \qquad \text{(II-28)}$$

and $j_0(q\,\frac{r}{2})$ and $j_2(q\,\frac{r}{2})$ are spherical Bessel functions.

The static limits of the functions above are

$$G_0(0) = 1, \qquad G_2(0) = M_d^2 Q,$$

$$G_1(0) = \frac{M_d}{M_p}\left[\mu_p + \mu_n - \frac{3}{2} P_D(\mu_p + \mu_n - \tfrac{1}{2})\right],$$

$$\tfrac{1}{2}\left[G_{E_p}(0) + G_{E_n}(0)\right] = G_{E_S}(0) = \tfrac{1}{2}, \tfrac{1}{2}(G_{M_p}(0) + G_{M_n}(0)) = G_{M_S}(0) = \tfrac{1}{2}(\mu_p + \mu_n),$$

$$C_E(0) = 1, \; C_Q(0) = M_d^2 Q, \; C_S(0) = 1 - \frac{3}{2} P_D \qquad \text{(II-29)}$$

and

$$C_L(0) = \frac{3}{2} P_D,$$

Q is the quadrupole moment of the deuteron, μ_p and μ_n are the proton and neutron magnetic moments, and

$$P_D = \int_0^\infty w^2(r)\, dr$$

is the D-state probability of the deuteron.

Introducing the nucleon form factors to Jankus's results of course assumes that the nucleons are not distorted in the deuteron. The fact that these nucleons are so weakly bound that they spend a sizable portion of their time far apart makes this assumption of non-distortion plausible.

Gross [50] and Casper [20] have calculated relativistic corrections to the electron deuteron scattering problem. While these corrections could come primarily from relativistic

modifications of (a) the deuteron wave functions and (b) the nucleon current, the latter have been shown to be small by Gourdin [71] and also by Gross. The relativistic modifications of the deuteron wave function depend not just on the Lorentz-contraction factor, which is actually a contraction in two directions [31], but also on the fact that the equal-time wave function in the rest frame is not the same as the equal-time wave function in the moving frame [20]. Gross goes on to solve for the corrections to the deuteron wave function and then obtains workable expressions for the corrections in terms of u(r) and w(r). Gross's expression for G_0, G_1, and G_2 are then much more complicated than those of Equation II-21, II-23, and II-25. For example, Gross's complete result for the deuteron charge form factor is

$$C_E = \left(1 - q^2/32M_d^2\right)\int_0^\infty (u^2+w^2)\, j_0\left(q\,\frac{r}{2}\right) dr - \frac{q^2}{24M^2}\int_0^\infty (u^2 - uru' - uku + 7w^2 - w\,r\,w' - wkw)\left[j_0\left(q\,\frac{r}{2}\right) + j_2\left(q\,\frac{r}{2}\right)\right] dr + \frac{q^2}{16M_d^2}\int_0^\infty (uru' + wru' + wrw')\, j_0\left(q\,\frac{r}{2}\right) dr, \qquad \text{(II-30)}$$

where prime refers to differentiation with respect to r and $k = r^2\left[\frac{d^2}{dr^2} - \alpha\right]$, $\alpha = \sqrt{M\epsilon}$, and ϵ = deuteron binding energy.

The first integral is the usual Jankus nonrelativistic result.

Schumacher and Bethe [44] and Elias et al. [49] note that the relativistic corrections of Casper and Gross [20] to the deuteron form factors, to order $q^2/2M_p^2$, enter simply as a factor $(1 - \tau/2)^2$ on the right hand side of Equation II-20,

where $\tau = q^2/4M_p^2$. Equation II-20 can be further simplified for small q^2 by using the scaling law [42]

$$G_1 = \mu_d G_0 \frac{M_d}{M_p} \qquad \text{(II-31)}$$

which is not a law but an approximate fit to the data which can be derived theoretically from the nonrelativistic quark model and SU6. (SU6 also predicts $\mu_p/\mu_n = 1.5$ which is not quite true.)

By making the relativistic correction as noted by Schumacher above and using the scaling law, Equation II-20 becomes

$$\frac{d\sigma^d}{d\Omega} = \sigma_M^d(\theta)\left\{G_0^2(q^2) + \frac{8}{9}\eta^2 G_2^2(q^2) + \frac{2}{3}\mu_d^2 G_0^2 \tau\left[1+2(1+\eta)\tan^2\frac{\theta}{2}\right]\right\}(1-\frac{\tau}{2})^2. \qquad \text{(II-32)}$$

Rewriting this using Equation II-21 and dropping the quadrupole term as it is less than 5×10^{-4} at the highest value of q^2 reached in this experiment, we then have

$$\frac{d\sigma^d}{d\Omega} = \sigma_M^d(\theta)(G_{E_p} + G_{E_n})^2 C_E^2\left\{1 + \frac{2}{3}\mu_d^2 \tau(1+2(1+\eta)\tan^2\frac{\theta}{2})\right\}(1-\frac{\tau}{2})^2. \qquad \text{(II-33)}$$

If we define $C_d = \frac{2}{3}\tau\mu_d^2(1+2(1+\eta\ \tan^2\frac{\theta}{2}))$ (II-34)

and note that

$$\frac{d\sigma^d}{d\Omega} = \sigma_M^d(\theta) G_d^2, \qquad \text{(II-35)}$$

then

$$G_d^2 = (G_{E_p} + G_{E_n})^2 C_E^2 (1+C_d)(1-\frac{\tau}{2})^2. \qquad \text{(II-36)}$$

Additionally, if we define K_m^d as the deuteron magnetic and

relativistic correction we have:

$$K^{d}_{mr} = \left(\frac{1}{1+C_d}\right)\left(\frac{1}{1-\frac{\tau}{2}}\right)^{2} . \qquad \text{(II-37)}$$

We obtain the so-called deuteron electric form factor G_{E_d} from Equation II-36, i.e.,

$$G^{2}_{E_d} = (G_{E_p}+G_{E_n})^{2}C^{2}_{E} = \frac{G^{2}_{d}}{(1+C_d)(1-\frac{\tau}{2})^{2}} = G^{2}_{d}K^{d}_{mr} = K^{d}_{mr}\,\frac{\frac{d\sigma^{d}}{d\Omega}}{\sigma^{d}_{M}(\theta)} . \qquad \text{(II-38)}$$

With both the deuteron and proton electric form factors available we now obtain the neutron electric form factor by first forming the ratio of G_{E_d} to G_{E_p}, i.e.,

$$\frac{G_{E_d}(q^{2}_{d})}{G_{E_p}(q^{2}_{p})} = \frac{(G_{E_p}(q^{2}_{d}) + G_{E_n}(q^{2}_{d}))C_E}{G_{E_p}(q^{2}_{p})} , \qquad \text{(II-39)}$$

where the q^{2}_{d} and q^{2}_{p} indicate that the proton and neutron in the deuteron have received a four-momentum transfer different from that of the proton which was the nucleus of the hydrogen target. This was so in this experiment because the incident electron energy was such that the recoil electron from both hydrogen and deuterium targets had the same final energy. Thus the transmission efficiency of the spectrometer and the detector efficiencies were held constant for both targets, but the four-momentum transfer was slightly different. Since the proton electric form factor is available from deVries [10]b' fit we may scale the $G_{E_p}(q^{2}_{p})$ measured from hydrogen to the $G_{E_p}(q^{2}_{d})$ measured in deuterium. Thus the electric form factor

of the proton in the hydrogen that would be predicted from the hydrogen measurement, if the hydrogen had experienced the same four-momentum transfer as did the proton in the deuterium is given by

$$G_{E_p}(q_d^2) = G_{E_p}(q_p^2)\left\{\frac{G_{E_p}(q_d^2)}{G_{E_p}(q_p^2)}\right\}_{\text{deVries}} . \qquad \text{(II-40)}$$

Equation II-39 may be rewritten in terms of the measured quantities, the deuteron and proton cross sections, by using Equations II-19 and II-38. This gives

$$\frac{\left[G_{E_p}(q_d^2) + G_{E_n}(q_d^2)\right] C_E}{G_{E_p}(q_p^2)} = \left(\frac{K^d_{mr}\,\frac{d\sigma^d}{d\Omega}}{\sigma^d_m(\theta)}\right)^{\frac{1}{2}}\left(\frac{\sigma^p_m(\theta)}{K^p_m\,\frac{d\sigma^p}{d\Omega}}\right)^{\frac{1}{2}} . \qquad \text{(II-41)}$$

Now forming this ratio, i.e., Equation II-41, with the same four-momentum transfer for the proton in both the deuterium and hydrogen we have:

$$\frac{\left[G_{E_p}(q_d^2) + G_{E_n}(q_d^2)\right] C_E}{G_{E_p}(q_d^2)} = \left(\frac{\frac{d\sigma^d}{d\Omega}\;\sigma^p_m(\theta)\;K^d_{mr}}{\frac{d\sigma^p}{d\Omega}\;\sigma^d_m(\theta)\;K^p_m}\right)^{\frac{1}{2}}\left\{\frac{G_{E_p}(q_p^2)}{G_{E_p}(q_d^2)}\right\}_{\text{deVries}} , \qquad \text{(II-42)}$$

which gives

$$\frac{G_{E_n}(q_d^2)}{G_{E_p}(q_d^2)} = \left(R\,\frac{\sigma^p_m(\theta)}{\sigma^d_n(\theta)}\,\frac{K^d_{mr}}{K^p_m}\right)^{\frac{1}{2}}\left\{\frac{G_{E_p}(q_p^2)}{G_{E_p}(q_d^2)}\right\}_{\text{deVries}}\frac{1}{C_E} - 1, \qquad \text{(II-43)}$$

where R is the experimental ratio of the deuteron cross section to the proton cross section.

Note that $\sigma_m^p(\theta)$ and K_m^p were calculated at the incident energy of the electron on the hydrogen, which was higher than the energy of the electron on the deuteron, at which $\sigma_m^d(\theta)$ and K_{mr}^d were calculated.

The neutron electric form factor, $G_{E_n}(q_d^2)$, then is given by

$$G_{E_n}(q_d^2) = \left[\left(R\,\frac{\sigma_m^p(\theta)}{\sigma_m^d(\theta)}\,\frac{K_{mr}^d}{K_m^p}\right)^{\frac{1}{2}}\left\{\frac{G_{E_p}(q_p^2)}{G_{E_p}(q_d^2)}\right\}_{\text{deVries}}\frac{1}{C_E} - 1.0\right] G_{E_p}(q_d^2) \tag{II-44}$$

which may be rewritten as

$$G_{E_n}(q_d^2) = \left\{\frac{G_{E_d}}{G_{E_p}}\,\frac{1}{C_E} - 1.0\right\} G_{E_p}(q_d^2). \tag{II-44b}$$

$G_{E_n}(q_d^2)$ is the G_{E_n} which includes Gross's relativistic corrections. It appears at first to be quite different from those of Stewart and Mader because they used the nonrelativistic deuteron wave function to calculate G_{E_n} and then added the change in G_{E_n} which is due to this relativistic correction in the deuteron wave function to the nonrelativistically calculated G_{E_n}. They used Gross's equation 10 [20] in a form which is practically model independent within the range of q^2 considered here [2], i.e.,

$$(G_{E_n})_{\text{rel}} = G_{E_n} + \Delta G_{E_n} = G_{E_n} + q^2/8m_p^2 .$$

This can be shown to be very close to the correction of Schumacher used in this work by considering the following. Schumacher's relativistic correction enters as a factor $(1 - \tau/2)^2$ on the right hand side of Equation II-20. This

correction is carried forward to Equation II-43. If we form the nonrelativistic ratio of G_{E_n} to G_{E_p} we have

$$\left(\frac{G_{E_n}}{G_{E_p}}\right)_{\substack{\text{non}\\ \text{Rel}}} = \left(R\,\frac{\sigma^p_m(\theta)}{\sigma^d_m(\theta)}\,\frac{K^d_m}{K^p_m}\right)^{\frac{1}{2}} \left\{\frac{G_{E_p}(q_p^2)}{G_{E_p}(q_d^2)}\right\} \frac{1}{C_E} - 1. \qquad \text{(II-45)}$$

Define

$$K^d_{mr} = K^d_m \,\frac{1}{(1-\tau/2)^2} \;.$$

If K^d_{mr} were inserted in Equation II-44 in place of K^d_m we would have

$$\left(\frac{G_{E_n}}{G_{E_p}}\right)_{\text{Rel}} .$$

Since

$$\left(\frac{G_{E_n}}{G_{E_p}}\right)_{\text{Rel}} = \left(R\,\frac{\sigma^p_m(\theta)}{\sigma^d_m(\theta)}\,\frac{K^d_m}{K^p_m}\right)^{\frac{1}{2}} \left\{\frac{G_{E_p}(q_p^2)}{G_{E_p}(q_d^2)}\right\} \frac{1}{C_E(1-\tau/2)} - 1, \qquad \text{(II-46)}$$

then:

$$\left(\Delta\,\frac{G_{E_n}}{G_{E_p}}\right) = \left(\frac{G_{E_n}}{G_{E_p}}\right)_{\text{Rel}} - \left(\frac{G_{E_n}}{G_{E_p}}\right)_{\substack{\text{non}\\ \text{Rel}}} = \left(R\,\frac{\sigma^p_m(\theta)}{\sigma^d_m(\theta)}\,\frac{K^d_m}{K^p_m}\right)^{\frac{1}{2}} \left\{\frac{G_{E_p}(q_p^2)}{G_{E_p}(q_d^2)}\right\} \left(\frac{\tau}{2}\right) \frac{1}{C_E}$$

$$\text{(II-47)}$$

and

$$\Delta G_{E_n} = \left(R\,\frac{\sigma^p_m(\theta)}{\sigma^d_m(\theta)}\,\frac{K^d_m}{K^p_m}\right)^{\frac{1}{2}} \left\{\frac{G_{E_p}(q_p^2)}{G_{E_p}(q_d^2)}\right\} \frac{G_{E_p}(q_d^2)}{C_E}\;\frac{q^2}{8m_p^2}\,, \qquad \text{(II-48)}$$

where $\tau = q^2/4m_p^2$ has been written explicitly. Since the coefficient of $q^2/8m_p^2$ in Equation II-48 is experimentally within 2 percent of unity throughout this experiment, then we see that Schumacher's method and Stewart's and Mader's method are in good agreement.

G. THE ROSENBLUTH PLOT

Rosenbluth derived the cross section for electron-proton scattering based on the one photon exchange. Jankus made the same assumption in calculating the deuteron cross section. Examining Jankus's result, given in Equation II-20, and, reproduced below,

$$\frac{d\sigma^d}{d\Omega} = \left(\frac{d\sigma^d}{d\Omega}\right)_{Mott} \left\{G_0^2(q^3) + \frac{8}{9}\eta^2 G_2^3(q^2) + \frac{2}{3}\eta G_1^2(q^2)\,[1+2(1+\eta)\tan^2\frac{\theta}{2}]\right\}. \tag{II-48a}$$

which can be written as

$$\frac{d\sigma^d}{d\Omega} = \left(\frac{d\sigma^d}{d\Omega}\right)_{Mott} G_d^2 . \tag{II-48b}$$

it can be seen that if the deuteron cross section is measured at different angles but at a constant q^2, then a plot of G_d^2 versus $(1+2(1+\eta)\tan^2\frac{\theta}{2})$ should give a straight line with $G_0^2 + \frac{8}{9}\eta^2 G_2^2$ as the intercept and $\frac{2}{3}\eta G_1^2$ as the slope. Thus a linear plot of such data would indicate that the one photon process accurately describes the phenomena. Such a plot has been made in Section VB.

Equation II-48b cannot be used directly because that equation is presumed to give an absolute cross section. The absolute deuteron cross section is obtained through knowledge of the hydrogen cross section. Since deVries b' fit is the best fit to the proton absolute cross section, this is used to normalize the data. That is

$$\left(\frac{d\sigma^p}{d\Omega}\right)_{Absolute} \equiv \left(\frac{d\sigma^p}{d\Omega}\right)_{deVries} = N\left(\frac{d\sigma^p}{d\Omega}\right)_{LINAC} \tag{II-49}$$

where N is the normalization factor for a given point.

Therefore

$$N = \left(\frac{d\sigma^p}{d\Omega}\right)_{\text{deVries}} \Big/ \left(\frac{d\sigma^p}{d\Omega}\right)_{\text{NPS LINAC}} . \qquad \text{(II-50)}$$

Because the deuteron and proton cross sections were measured under the same experimental conditions, the absolute deuteron cross section is

$$\left(\frac{d\sigma^d}{d\Omega}\right)_{\text{Absolute}} = N \left(\frac{d\sigma^d}{d\Omega}\right)_{\text{NPS LINAC}} .$$

It follows that

$$\left(\frac{d\sigma^d}{d\Omega}\right)_{\text{Absolute}} = \left\{\left(\frac{d\sigma^p}{d\Omega}\right)_{\text{deVries}} \Big/ \left(\frac{d\sigma^p}{d\Omega}\right)\right\} \left(\frac{d\sigma^d}{d\Omega}\right)_{\text{LINAC}} .$$

In terms of the experimental ratio R, where

$$R = \left\{\left(\frac{d\sigma^d}{d\Omega}\right)_{\text{NPS LINAC}} \Big/ \left(\frac{d\sigma^p}{d\Omega}\right)_{\text{NPS LINAC}}\right\} ,$$

$$\left(\frac{d\sigma^d}{d\Omega}\right)_{\text{Absolute}} = \left(\frac{d\sigma^p}{d\Omega}\right)_{\text{deVries}} R.$$

But

$$\left(\frac{d\sigma^d}{d\Omega}\right)_{\text{Absolute}} = \left(\frac{d\sigma^d}{d\Omega}\right)_{\text{Mott}} G_d^2 ,$$

therefore

$$G_d^2 = \left\{\left(\frac{d\sigma^p}{d\Omega}\right)_{\text{deVries}} \Big/ \left(\frac{d\sigma^d}{d\Omega}\right)_{\text{Mott}}\right\} R_m , \qquad \text{(II-51)}$$

where $\left(\frac{d\sigma^p}{d\Omega}\right)_{\text{deVries}}$ and $\left(\frac{d\sigma^d}{d\Omega}\right)_{\text{Mott}}$ were calculated by programs TOPROTON and TOPDEUTR which are listed in Appendix E and the ratio R_m was the weighted mean given by Equation IV-20.

The statistical error in G_d was calculated from

$$S_{G_d} = \frac{\left\{ \left(\frac{d\sigma^p}{d\Omega}\right)_{\text{deVries}} \Big/ \left(\frac{d\sigma^d}{d\Omega}\right)_{\text{Mott}} \right\} S_{R_m}}{2G_d}$$

where S_{R_m} is calculated from Equation IV-21.

Several points were taken in order that the data could be checked for consistency on a Rosenbluth plot. The results are given in Section V-B.

III. EXPERIMENTAL EQUIPMENT AND PROCEDURES

A. THE NAVAL POSTGRADUATE SCHOOL LINEAR ACCELERATOR (LINAC)

The NPS LINAC is a 100 MeV accelerator technically similar to the Stanford University Mark III linear accelerator which is described by Chodorow _et al_. [51]. A detailed description of the NPS LINAC is given by Barnett and Cunneen [52] and a schematic floor plan is given in Figure III-1. The accelerator receives up to 22 megawatts of peak power from each of the three klystrons. The machine is pulsed at a rate of 60 pulses/sec, each pulse being about 1 microsecond in duration. Electrons are injected at 80 kev and can be accelerated to energies between 15 and 100 MeV with an average beam current of about 5 microamperes. The beam energy is selected by the beam deflection magnets. The magnetic field of these magnets is measured by an NMR probe. The beam is focused down to a diameter of about 2mm at the target by the quadrupole magnets. The spread in the beam energy is controlled by the slit settings.

B. THE SPECTROMETER AND COUNTING SYSTEM

The spectrometer is a 120°, 16 inch double-focusing magnetic spectrometer described in detail by Oberdier [44]. Ten detectors span a portion of the focal plane of the spectrometer, thus giving 10 counting channels for each spectrometer setting. Each detector (a NE102 plastic scintillator) is 7/16 inch wide and 1/16 inch thick. The 7/16 inch width

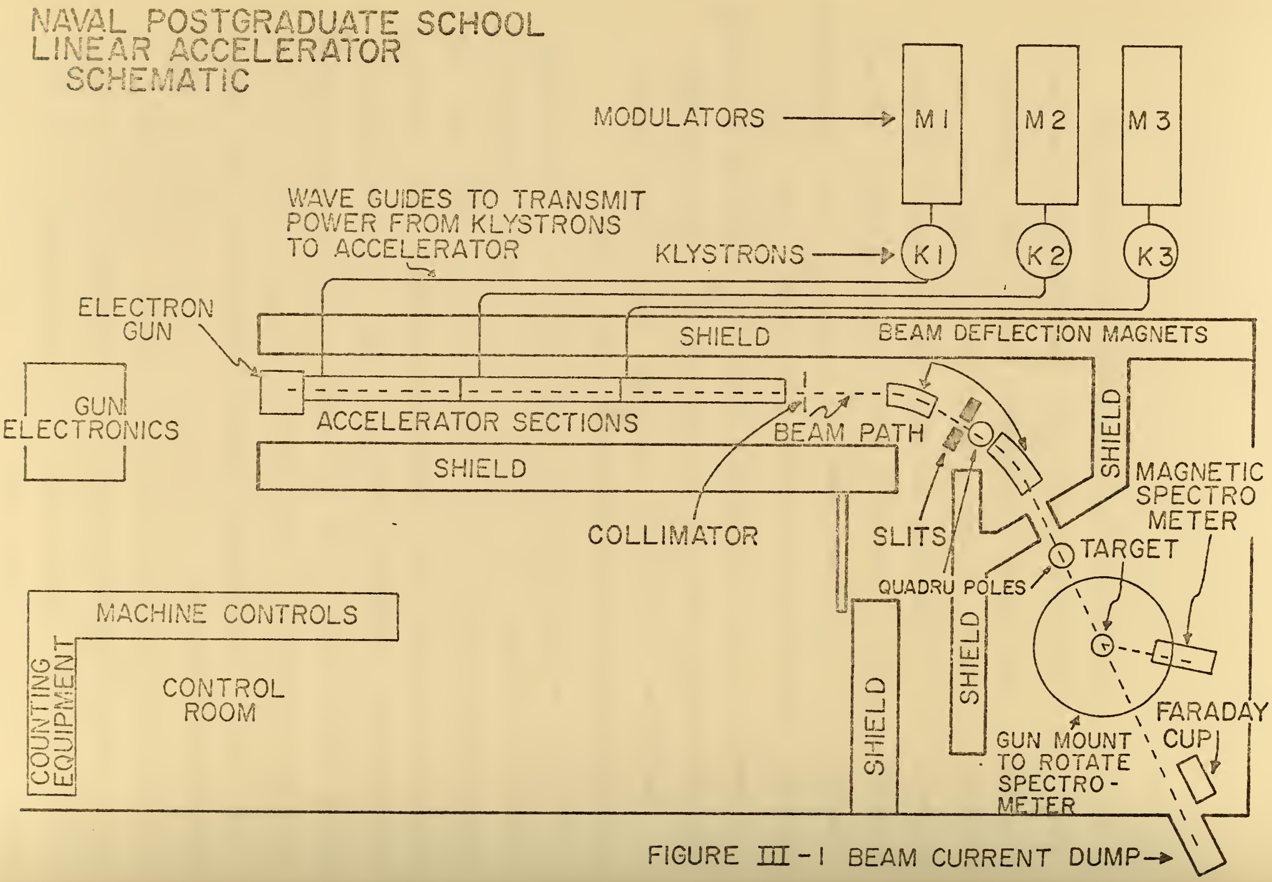
NAVAL POSTGRADUATE SCHOOL
LINEAR ACCELERATOR
SCHEMATIC
MODULATORS
M 1
M 2
M 3
WAVE GUIDES TO TRANSMIT POWER FROM KLYSTRONS TO ACCELERATOR
KLYSTRONS
K 1
K 2
K 3
ELECTRON GUN
SHIELD
BEAM DEFLECTION MAGNETS
GUN ELECTRONICS
ACCELERATOR SECTIONS
BEAM PATH
SHIELD
SHIELD
MAGNETIC SPECTRO METER
COLLIMATOR
SLITS
TARGET
QUADRU POLES
MACHINE CONTROLS
SHIELD
CONTROL ROOM
COUNTING EQUIPMENT
SHIELD
FARADAY CUP
GUN MOUNT TO ROTATE SPECTRO-METER
BEAM CURRENT DUMP

FIGURE III-1

allows a momentum spread $\Delta p/p$ of about 0.3% for each counter. Behind these ten detectors are two large detectors, both of which span the same portion of the focal plane of the spectrometer as do the 10 smaller scintillators. An electron passing through one of the ten scintillators produces a light pulse, which is collected by the photomultiplier tube, amplified and transmitted to the control room where it is discriminated, and is then sent to the scaler if both backing counters simultaneously registered outputs. This triple coincidence pulse to the scaler must also occur during the time that the master gating circuit is pulsing the scaler in order that the count will register. The gating circuit prevents background counts from registering between beam pulses. A block diagram of the counting system is given in Figure III-2.

The scalers in channels 4 through 7 are capable of recording periodic pulses up to about 150 M_{H_Z} while the other six channels of the ten channel ladder are connected to scalers that can record periodic pulses up to 20 M_{H_Z}. Only data in channels 4 through 7 were analyzed since these could accumulate data more rapidly. The count rate in these channels was held below 60 counts/second on all runs. Count rate correction data were obtained and were used to provide the count rate correction factor given in Equation (IV-11). The correction factor was linear out to about 100 counts/second, thus maintaining the counts below 60 counts/second was more than adequate.

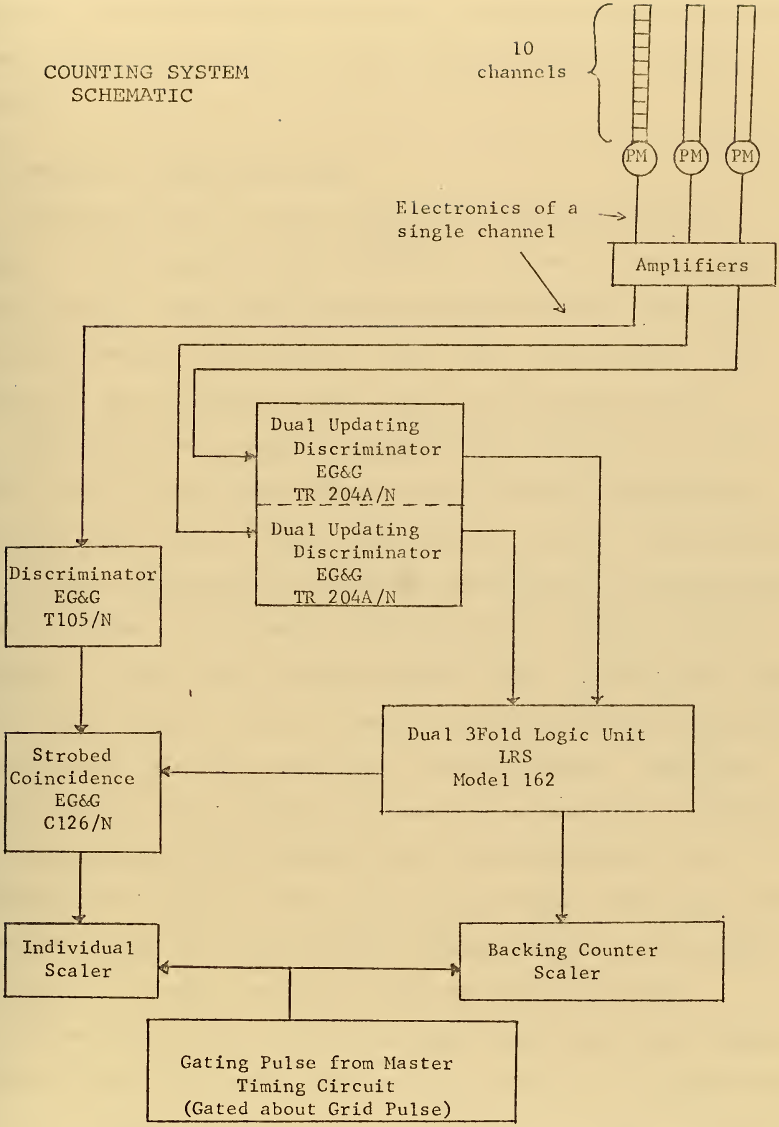
COUNTING SYSTEM SCHEMATIC
10 channels
PM
PM
PM
Electronics of a single channel
Amplifiers
Dual Updating Discriminator EG&G TR 204A/N
Dual Updating Discriminator EG&G TR 204A/N
Discriminator EG&G T105/N
Dual 3Fold Logic Unit LRS Model 162
Strobed Coincidence EG&G C126/N
Individual Scaler
Backing Counter Scaler
Gating Pulse from Master Timing Circuit (Gated about Grid Pulse)

Figure III-2

The gas target is covered in detail in Appendix D. Both H_2 and D_2 were maintained at liquid nitrogen temperature and at about 150 psig in order to have a high density of target nuclei.

C. METHOD OF OBTAINING DATA

Consider first the data which were obtained during a "run" to determine the ratio σ^d/σ^p at a given q^2 and scattering angle. The same data were taken for both deuterium and hydrogen and consisted of that which was recorded automatically and a lesser amount that was recorded manually.

That which was recorded automatically consisted of anywhere from 30 to 60 individual units of data, depending on the run. Each unit of data was called a "point" and consisted of the data accumulated at a given spectrometer setting while a given number of incident electrons passed through the gas target. In each run, the spectrometer was initially set such that the scattered elastic spectrum was well above channel 4. The first of the data points was recorded there. Then the energy of the spectrometer was lowered between 0.02 to 0.05 MeV, depending on the energy range the spectrometer was sweeping, and another data point was recorded. This process continued until the spectrometer setting was below the peak of channel 7. The last data point was then recorded.

After the selected amount of beam charge had been accumulated at each data point, the following data were automatically fed to a teletype machine that both printed a hard copy and punched a paper tape, a) the number of counts recorded in

each of the 10 channels, b) the number of counts in coincidence in the two backing counters, c) the time required to obtain the given charge, d) the incident energy of the electrons, e) the capacitance of the capacitor used to integrate the incident beam, f) the setting of the spectrometer in MeV, g) the maximum voltage permitted on the capacitor, and h) a number which, when divided by 30 (the full scale reading of the integrator), gave the fractional value of the maximum voltage at which the integration of the beam current stopped.

The data which were recorded manually included Secondary Emission Monitor (SEM) efficiencies and the gas pressure. The SEM efficiencies were taken just prior to the first data point, at the peak of each channel and after the last data point. The gas pressure was recorded at the start and finish of each liquid nitrogen "fill" (as defined in Appendix C), which generally occurred about once at each data point. The leakage current in the integration circuits was also recorded manually and was used to determine the ground loop errors, but was not used to calculate the cross section as it was always such a small correction.

The above data were always taken under conditions that were as identical as possible for both the deuteron and proton. That is, the experimental geometries, the accelerator beam current, the pressure of the target gases, the scattered electron energy, the detection and electronics systems and all other possible variables were maintained, as nearly as possible, the same.

Runs were made at values of q^2 that went from 0.025 fm^{-2} to 0.40 fm^{-2}. However, scattering from the target windows or a contaminant in the gas masked the data at 0.025 fm^{-2}, while high background levels and small cross sections made the data taken at 0.40 fm^{-2} unreliable. Thus the reproducible data reported here covered a region from 0.05 to 0.35 fm^{-2}. Within this range of q^2, forward angle scattering was preferentially selected to emphasize the electric interaction.

The most significant change in running conditions between the deuteron and proton was the change in beam energy made so that the scattered electrons would have the same energy in both cases. This insured that the transmission of electrons through the spectrometer and the efficiencies of the detectors would be the same while taking D_2 and H_2 data. This also meant that the q^2 for hydrogen was slightly different than for deuterium. This difference was accounted for in Equation II-42.

The spectrometer was saturated by increasing the current in the coils to a setting corresponding to 100 MeV before data were taken in either H_2 or D_2 in order to insure that the same hysteresis loop could be obtained on both spectrums. The energy defining slits were generally set to give a full width at half maximum to beam energy ratio of about 0.4%. The count rate was held below 60 counts per second during all runs. The number of counts recorded varied from as much as 170,000 to as few as 10,000 in a single channel. The number of counts obtained depended primarily upon the size of the cross section.

An empty target measurement was made at the last spectrometer setting as well as at several others throughout the energy range in which data had been taken. Usually those four or five readings indicated a "flat" background. Only at the lowest q^2 of 0.05 F^{-2} did any structure show itself in these empty target background measurements. Thus with all but the $q^2 = 0.05\ F^{-2}$ data runs, the full target background measurements taken at energies well above the peak of each channel were averaged and then projected at those same values throughout each channel's elastic peak. The $q^2 = 0.05\ F^{-2}$ data were handled differently because there was scattering from contaminants in the gases and the windows which complicated the background spectrum. In that case empty target background was taken at each and every spectrometer setting of both the hydrogen and deuterium. These empty target points were then scaled, point by point, to the full target background in order to obtain the full target background under each elastic peak.

A significant improvement in procedure over other work which had been done at this facility is the procedure that steps each detector completely across each elastic peak. Formerly, the data from all ten channels were used to construct one elastic peak by measuring the dispersion between detectors and the efficiency of all others with respect to a chosen reference detector. This calculation of the efficiencies introduced errors around 0.5% into the former method which were avoided here.

IV. DATA ANALYSIS

A. GENERAL METHOD OF DATA REDUCTION

The treatment of the experimental data (see Section III-D) is described here. The first step was to change the form of the data from punched paper tape to computer card data. This was accomplished by a program that required the data in paper tape form to be read into an on-line teletype which was connected to the NPS IBM 360. This program caused the data to be punched out on computer cards. Because of a peculiarity in the data readout system of the accelerator, decimal points were punched as colons. A small program was written which took the punched deck mentioned above as input data and replaced all colons with decimal points in a second punched deck. This deck was then interpreted and checked with the printed teletype output. Hydrogen and deuterium data were separated and were used as input to FORTRAN programs TOP#FORM where # ran from channel 4 through 7. The TOP#FORM program is listed in Appendix D. TOP#FORM was written primarily to calculate the cross section measured by a particular channel, but it was also used to provide count rate corrected data and to normalize all points to a standard incident charge, since the automatic termination of the integration at each spectrometer setting did not always stop at the same value. TOP#FORM then prints out these count rate corrected, charge normalized counts for each spectrometer setting. This part of TOP#FORM was used to plot these so-called corrected counts. For that plotting run other input

data which are necessary to calculate a cross section, such as radiation corrections, pressure, etc. were given dummy values. These count rate corrected and normalized counts for all four detectors for both the deuterium and the hydrogen were then plotted and the position of each peak and the shape of the scattered spectrum was determined by visually fitting a smooth curve through the points. A typical plot of such data is given in Figures IV-1a and IV-1b. The difference in energy between each peak and the final spectrometer energy at which data were taken was then measured because the radiation corrections depend upon ΔE, and this value was put into the FORTRAN program TOPRADCR which is listed in Appendix E. Additionally, the peak energy (which is used as the final energy of the electron) as well as the pressure of the hydrogen and deuterium are entered as input data to TOPRADCR. TOPRADCR has the virial coefficients of hydrogen and deuterium and the composition and thicknesses of the gas target windows stored as constants. These constants and the run data mentioned above permit TOPRADCR to calculate the density of the gas for each channel and the Schwinger, bremsstrahlung and Landau radiation corrections. The rationale behind the radiation correction calculations is given in Section IV-C. The average background was calculated for each channel by adding all counts recorded prior to the start of the rise in each channel and dividing by the number of spectrometer settings which recorded these counts.

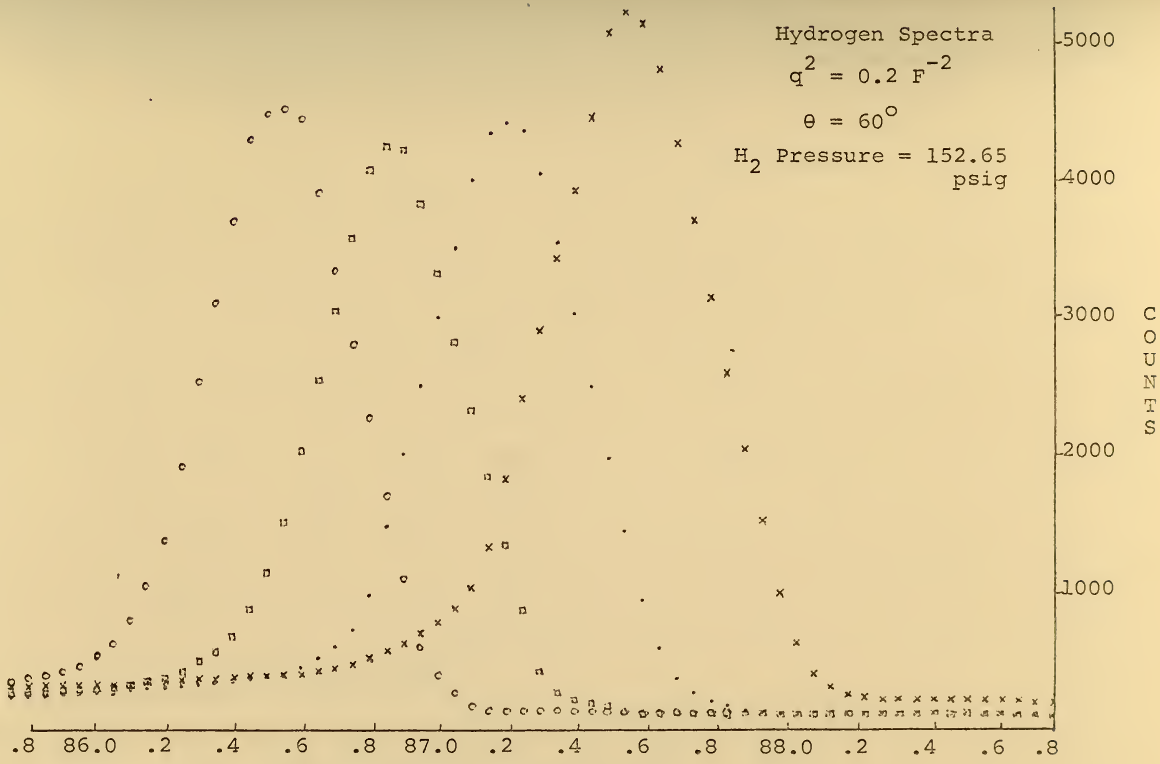
Hydrogen Spectra
$q^2 = 0.2\ F^{-2}$
$\theta = 60^\circ$
H_2 Pressure = 152.65 psig
5000
4000
3000
2000
1000
COUNTS
.8
86.0
.2
.4
.6
.8
87.0
.2
.4
.6
.8
88.0
.2
.4
.6
.8
Spectrometer Energy (MeV)

Figure IV-1a.

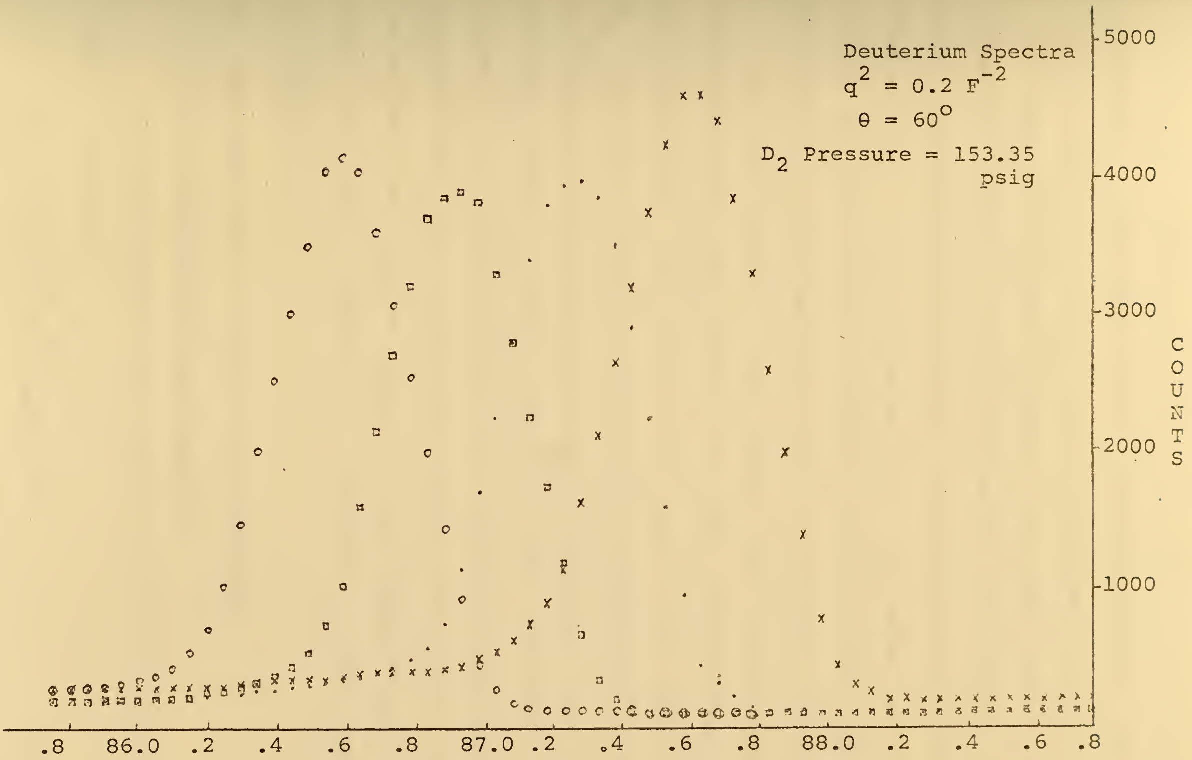

Figure IV-1b. Spectrometer Energy (MeV)

With these calculations done, the Schwinger correction, the product of the Bethe and the Landau corrections, the gas density, the SEM efficiency and the background counts for each channel were typed on computer cards and entered with the appropriate hydrogen or deuterium deck as the data for TOP#FORM which then calculated the elastic cross section and the statistical error in that cross section. The method of calculating the cross section is given in Section IV-B. The method of calculating the statistical error is derived in Section IV-D.

Four cross section ratios (one for each channel) were formed from the cross sections, and then a weighted mean ratio was calculated. The electric form factor of the neutron, G_{E_n}, was then calculated by using this weighted mean ratio, R_m, and the appropriate cross sections and magnetic corrections and form factors as shown in Equations IV-14 and IV-15. The values of the proton electric form factors and the proton and deuteron Mott cross sections and magnetic corrections were calculated from computer programs called TOPROTON and TOPDEUTR which are listed in Appendix E. Values of D_c were from data in Appendix C.

B. THE CALCULATION OF ELASTIC CROSS SECTIONS

1. The Experimental Cross Section

The experimental cross sections have been calculated from the expression

$$\sigma_{Exp} = \frac{N_{sc}\,\mathcal{H}_s\,\mathcal{H}_b\,\mathcal{H}_I}{N_{in}\,\eta_t\,\Delta\Omega}\ \mathrm{cm}^2\mathrm{ster}^{-1} \qquad \text{(IV-1)}$$

where

N_{sc} is the number of scattered electrons counted in a particular channel,

N_{in} is the number of incident electrons,

η_t is the number of target atoms per cm^2,

$\Delta\Omega$ is the solid angle defined by the spectrometer slits, and

$\mathcal{K}_s$, $\mathcal{K}_b$ and $\mathcal{K}_I$ are radiative corrections (see Section IV-B).

η_t is given by

$$\eta_t = \frac{\rho\ t\ N_a}{A \cos \varphi}, \qquad \text{(IV-2)}$$

where

ρ is the density of the target (gm/cm^2),

t is the thickness of the target (cm),

N_a is Avogadro's number,

A is the atomic weight of the target gas,

and

φ is the angle between the normal to a plane solid target and incident beam of electrons. In the gas target analysis φ is set equal to zero as the angle φ is not defined, i.e., rotation of the gas target still presents the same number of target atoms per square centimeter.

N_{in} is determined by

$$N_{in} = \frac{Q}{e} = \frac{CV}{e\varepsilon_{SEM}} \qquad \text{(IV-3)}$$

where

Q = total charge of incident electrons

e = electron charge of 1.60210×10^{-9} coulombs

c = capacitance of integrator in farads,

v = voltage of integrator in volts,

and

ϵ = efficiency of SEM.

Equation IV-1 is appropriately used to calculate absolute cross section, but it was used in this experiment even though absolute cross sections were not measured. This is a correct procedure because, in this experiment, the ratio of the cross sections of the deuteron and proton was formed and the systematic errors effectively concelled as all data were taken under almost the same conditions for both the proton and the deuteron.

N_{sc}, the total number of scattered electrons, is obtained by integration. Consider Figure (IV-2), where the number of detected electrons in a particular counting channel is plotted against the spectrometer energy.

Let E_i be a spectrometer setting

and

N_i the number of counts recorded in this channel at that spectrometer setting.

Then

$$N_{sc} = \frac{\text{area under scattering peak (in Counts - MeV)}}{\delta E} \qquad \text{(IV-4)}$$

where

δE = the energy width of an individual detector.

This is because each detector has a finite dimension and therefore counts all electrons in the spread ΔE. Thus

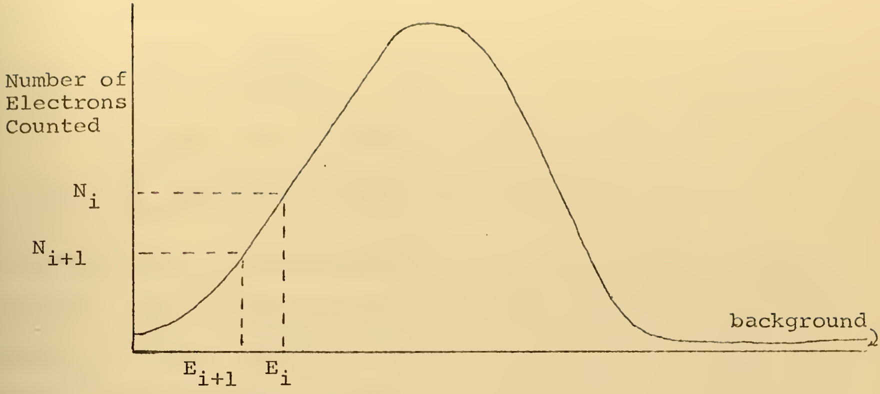

Figure IV-2. Spectrum of Counts in a Single Detector

in obtaining N_{sc} we have:

$$N_{sc} = \int_{E_i}^{E_f} \frac{dN}{dE}\, dE \text{ where } \frac{dN}{dE} \text{ is the number of} \qquad \text{(IV-5)}$$

counts per interval of energy. This integral is numerically approximated by the sum

$$N_{sc} = \sum_{i=1}^{n-1} \frac{\frac{1}{2}(N_i + N_{i+1})(E_i - E_{i+1})}{\delta E} \; . \qquad \text{(IV-6)}$$

The energy width δE is obtained in terms of E_i by using the dispersion relation for the spectrometer optics,

$$\frac{\delta E}{E} = \frac{\omega}{Dr_o} \qquad \text{(IV-7)}$$

where D has been experimentally determined to be 3.92 [53], r_o is the mean radius of the spectrometer, 16 inches, and 'ω' is the width of each detector (NE102 plastic scintillators) which is 7/32 inches.

Therefore

$$\frac{\delta E}{E_i} = \frac{7/32''}{3.92(16'')} = 0.0034877 \ . \qquad \text{(IV-8)}$$

Putting these together, we have

$$N_{sc} = \sum_{i=1}^{n-1} \tfrac{1}{2}[N_i+N_{i+1}](E_i-E_{i+1})/0.0034877\ E_i .$$

The energy E_i in the denominator is the spectrometer energy setting. This setting is very near the center energy of the band of electron energies which the spectrometer detects when set to the reading E_i. However, the energy of the electrons which hit counter 10 will be higher than any other detected electrons and the energy of the electrons which hit channel 1 will be the lowest in energy. In order to take into account the fact that each detector is recording electrons with different energies than the spectrometer setting E_i, several runs were made to determine both the absolute calibration of the spectrometer and the relative energy spacing of each of the four center channels. By comparing the calculated elastic peak energy with the spectrometer setting E_i, it was determined that the peak of channel number 5 was 0.17% higher than the energy setting of the spectrometer. Thus channel number 5 was chosen as the reference energy channel. By successively lowering the spectrometer setting from an energy above the elastic peak of channel number 4 through channel number 7, the dispersion of the magnet was measured. This procedure was done at LINAC energies of 17 MeV, 30 MeV, 60 MeV, and 90 MeV. The average dispersion of these measurements showed that the average energy of the electrons which counter η (where η is

4,5,6, or 7) detected was given by

$$E_\eta = E_i (1.0 + 0.0039\ (\eta-5)) \qquad \text{(IV-9)}$$

when the spectrometer is set at E_i.

Finally,

$$\frac{d\sigma}{d\Omega} = \sigma_{Exp} =$$

$$\frac{\left(\sum_{i=1}^{n-1} \tfrac{1}{2}\left[N_i+N_{i+1}\right]\left(E_i-E_{i+1}\right)\Big/ 0.0034877E_i(1.0+0.0039(\eta-5))\right)\mathcal{H}_s\mathcal{H}_b\mathcal{H}_I}{\left(\frac{CV}{e\,\epsilon_{SEM}}\right)\left(\frac{\rho\ t\ Na\ cm^{-2}}{A}\right)\left(1.831 \times 10^{-3}\ \text{steradians}\right)}$$

(IV-10)

where the solid angle, $\Delta\Omega$ is 1.831×10^{-3} steradians.

2. Corrections to the Observed Counts

a. Equation IV-9 would correctly measure an absolute cross section if:

i) N_i, the number of counts recorded on the scalars, was the actual number of electrons scattered, i.e., if the electronic system did not have a finite resolving time. Even though the scalars are capable of counting periodic pulses up to rates of 150 MHz, they lose counts when random (Poisson) pulses are counted at high rates. At 60 counts per second, which was the highest count rate which was permitted during this experiment, about 6% of the counts were lost.

ii) N_i consisted only of counts due to the scattering from the target gas and was not contaminated by background counts.

iii) The efficiency of the detectors were known.

b. The count rate correction was determined experimentally by scattering from an aluminum target at count rates up to 500 counts/sec. The number of counts detected was plotted as a function of the count rate. Up to about 100 counts/second the number of counts recorded decreased linearly with rate. A linear fit was made to the data in this region, and gave

$$N(\text{count rate corrected}) = \frac{N(\text{recorded})}{1-0.00097N/t} \qquad (\text{IV-11})$$

where N/t is the average count rate determined by dividing the recorded number of counts by the time of the integration.

c. The background was determined by counts obtained at energies greater than the elastic peak of either H_2 or D_2, whichever was the target at that time, for each of the four detectors. The average number of counts for each channel, in this region, was then determined and was used as the background. During each run an empty target background was also taken to insure that there was no rise or fall in this extrapolated average background under the elastic peak caused by some source other than the H_2 or D_2.

d. The efficiency of each detector was not determined because the object of this experiment was to obtain the ratio of the deuteron cross section to the hydrogen cross section. Because this ratio was determined for each of the four detectors separately, the efficiency of each detector cancelled and therefore is not included in the determination of the cross section.

e. An electrometer was used to measure the integrated incident beam current for each data point. The circuitry associated with the electrometer was set to stop the

integration and the counting system whenever a predetermined voltage across a capacitor charged by the current from a SEM was reached. The electrometer did not always stop at exactly the same voltage but varied sometimes by as much as a percent or two. Therefore both the hydrogen and the deuterium counts were normalized to a standard voltage ($V_{\text{Reference}}$) for each run. Thus, if V_{Actual} was the actual voltage at the end of the integration, then the number of counts recorded was corrected by

$$N(\text{corrected for voltage}) = N_{\text{Actual}}\,\frac{V_{\text{Reference}}}{V_{\text{Actual}}}\,. \tag{IV-12}$$

The cross section, after correcting for count rate, background and voltage cutoff is

$$\frac{d\sigma}{d\Omega} = \frac{\frac{1}{2}\sum_{i=1}^{n-1}\left(\left(\left\{\left[\frac{N_i\,\frac{V_{ref}}{V_{act}}}{(1-0.00097\text{Rate}_i)} - \text{BKG}\right] + \left[\frac{N_{i+1}\,\frac{V_{ref}}{V_{act}}}{(1-0.00097\text{Rate}_{i=1})} - \text{BKG}\right]\right\}\right)}{\left(\frac{CV}{e\epsilon_{SEM}}\right)\left(\frac{\rho\ t\ Na\ cm^{-2}}{A}\right)\left(1.831 \times 10^{-3}\ \text{steradians}\right)}\,.$$

$$\frac{(E_i-E_{i+1})\mathcal{H}_s\mathcal{H}_b\mathcal{H}_I}{0.0034877(1.0+0039(\eta-5))E_i}\Bigg). \tag{IV-13}$$

C. RADIATION CORRECTION CALCULATIONS

The proton cross section was derived by Rosenbluth [26] with the assumption that a single virtual photon is exchanged in the scattering process as shown in Figure IV-3.

The deuteron cross section, as derived by Jankus [13] in the impulse approximation, also assumes that one virtual photon is exchanged as shown in Figure IV-4.

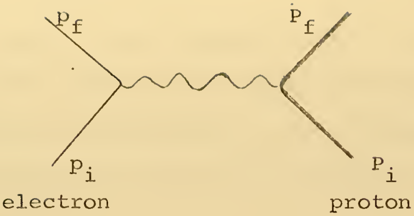

Feynman Diagram of Rosenbluth Calculation

Figure IV-3

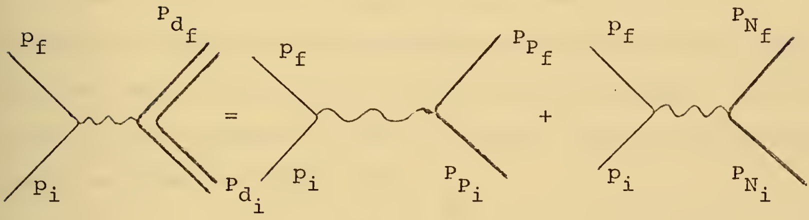

Feynman Diagram of Impulse Approximation

Figure IV-4

Unfortunately, when one does an electron scattering experiment these processes are not the only ones which occur, and the experimenter must take into account competing processes in order to be able to compare experiment and theory. In fact the experimental scattered energy spectrum which is measured contains the effects of three such competing processes which must be accounted for before one can obtain the cross sections for processes as shown in Figures IV-3 or IV-4.

These competing processes are:

1) Photon emission and absorption while the electron is in the field of the scattering nucleus of interest. The correction to the cross section due to this process was first calculated by Schwinger [54] and is commonly called the Schwinger Correction.

2) Bremsstrahlung emission in the target before or after the nuclear scattering of interest.

3) Excitation and ionization of material in the target.

Each of the above processes causes the energy of a scattered delectron to be less than it would be if the only process which occurred was the one photon exchange. Thus, a radiative tail appears on the low energy side of the elastic peak, as shown in Figure IV-5.

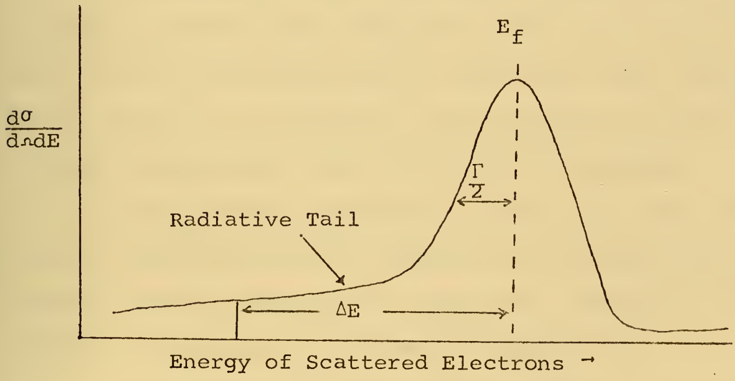

Elastic Peak with Radiation Tail

Figure IV-5

To obtain a cross section for the nuclear scattering event of interest, the experimenter would have to continue down the radiative tail to zero energy in order to capture those scattered electrons which have some probability of losing all their energy in the three processes listed above. In practice, the measurement is stopped at ΔE below the elastic peak (see Figure IV-5). The value of ΔE is generally of the order of at least four half-widths ($\Gamma/2$)[55]. Thus fewer electrons are detected and the experimental cross section is less than it should be. Since each of the three processes mentioned above contributes to the radiative tail, corrections must be made to account for the undetected electrons with energy less than $E_f - \Delta E$.

1. Schwinger Correction

The largest of the corrections is that which accounts for photon emission and absorption while the electron is in the field of that nucleus which causes the large angle scattering which is of interest. This correction to the cross section was generally about 15% in this experiment.

The Schwinger correction accounts for many interactions which may occur in addition to the one virtual photon exchange shown in Figures IV-3 and IV-4. Several of these possible interactions are shown in Figure IV-6.

In processes (a) and (b) real photons are emitted before and after the nuclear scattering. Processes (c), (d), and (e) are called vertex renormalization terms and (f) is the vacuum polarization term. Improved radiative corrections to electron-proton scattering have been calculated by Tsai [56]

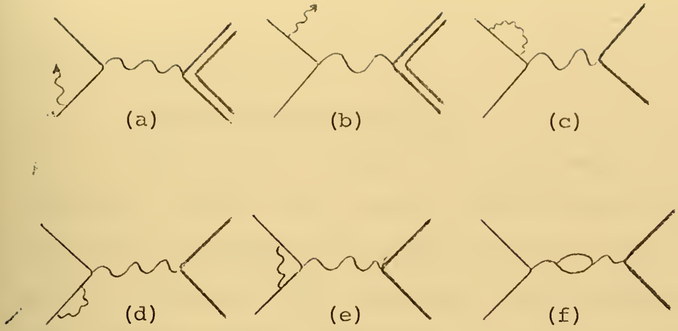

Feynman Diagrams of Schwinger Correction Interactions

Figure IV-6

and by Meister and Yennie [57] and include the effects of proton recoil. Numerical evaluation of the Schwinger corrections in this work used the results given in the review article by Maximon [58].

$$\mathcal{K}_s = e^{\delta_s} = e^{\left[\frac{2\alpha}{\pi}\left(\ln\frac{(E_iE_f)^{\frac{1}{2}}}{\Delta E}\right)\left(\ln q^2/m^2 - 1\right)\right]} \times$$

$$\left\{1 + \frac{2\alpha}{\pi}\left[\frac{13}{12}\left(\ln q^2/m^2 - 1\right) - \frac{1}{4}\ln^2\frac{E_i}{E_f} - \frac{17}{36} - \frac{1}{2}\left(\frac{\pi^2}{6} - L_2\left(\cos^2\frac{\theta}{2}\right)\right)\right]\right\}$$

where E_i and E_f are the electron energies prior to and after scattering, α is the fine structure constant, m is the electron mass, q^2 is the four-momentum transfer, and

$$L_2(x) = -\int_0^x \frac{\log(1-t)}{t}\,dt$$

is the Spence function.

2. Bremsstrahlung Correction

When passing through the target material, the electrons also radiate away energy through radiative collisions with atomic electrons and nuclei other than the target nucleus of interest. The energy loss due to bremsstrahlung has been studied by Bethe and Heitler [59], who calculated the cross section $\Phi(E_o)$ and the average energy loss due to this process. By approximating this cross section Heitler [60] and Bethe and Ashkin [61] obtain:

$$-\frac{dE_o}{dx} = E_o X_o$$

where X_o is the radiation length, which is the distance over which the electron has its energy reduced by a factor 1/e. In this experiment, the expression given by Butcher and Messel [62] has been used to calculate the radiation length X_o:

$$X_o = \frac{A}{4\alpha N_o\, r_e^2 z(z+0.8)\rho\, \ln(183z^{-1/3})}\ \text{cm}$$

where N_o is Avogadro's number and r_e is the classical electron radius, ρ is the density in gm/cm^3 and A is in grams/mole.

The target, which consisted of the hydrogen or deuterium gas, was in a pressure vessel which had 0.001 inch steel windows for the incident and scattered beam. For the bremsstrahlung correction, and also the Landau corrections, the target was treated as a homogeneous molecular compound of

steel and either H_2 or D_2 which consisted roughly of $Fe_1 H_{26}$, or $Fe_1 D_{26}$, where the "molecular formula" was calculated for each gas pressure. This formula accounts for the 1 mil windows and the 2 inches of target gas at 150 psig and 77°K. Following Butcher and Messel the radiation length for such a compound target was calculated from

$$\frac{1}{X_o} = \left(\frac{1}{\sum_i \eta_i A_i}\right)\left(\sum_i \frac{\eta_i A_i}{X_o^i}\right) .$$

In the actual FORTRAN programs the X_o were multiplied by the average density of this compound to give X_o in gm/cm^2.

Bethe and Heitler [59] also give the probability that an electron traversing t radiation lengths will have an energy loss less than α times its initial energy (aside from the ionization loss and the scattering from the nucleus of interest). That probability is

$$P_{(\alpha)} = \frac{\alpha^{(t/\ln 2)}}{\Gamma(1+ t/\ln 2)} \cdot$$

Hofstadter has integrated this and calculated the correction factor to the observed cross section; this bremsstrahlung correction factor may be written as [6]

$$\mathcal{K}_B = \exp\left(\frac{T}{X_o \ln 2}\right)\log\left(\frac{E}{\Delta E}\right) ,$$

where T is the thickness of the target, including the two steel 0.001 inch windows as well as the gas, in gm/cm^2, and E is the geometric mean electron energy while going through the target. K_B was about 1.02 in this experiment.

3. Ionization Correction

As the electrons in the beam pass through the target they also lose energy by excitation and ionization in the gas and in the gas target windows. Landau [63] first calculated both the average energy a monoenergetic beam would lose, and the spread, or straggling, of the energy distribution of the beam after passing through a thin target. From this distribution it is possible to calculate the fraction of electrons which are not detected because data is taken only down to $E_o - \Delta E$. Figure IV-7 shows a theoretical spectrum of monoenergetic incident electrons after passing through a layer of material. Γ is the full-width at half-maximum. Q_{prob} is the most probable energy loss due to ionization and E_{INC} is the incident energy, and $N(E)$ is the number of electrons detected at energy E.

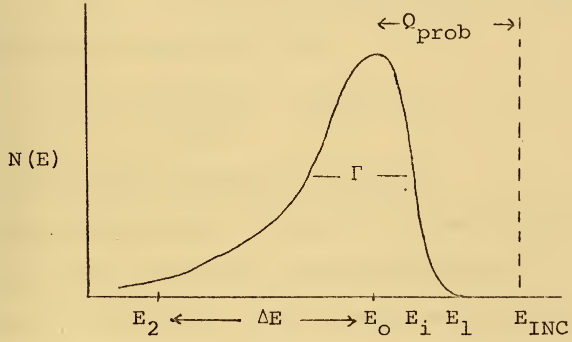

Effect of Ionization on Spectrum of Monoenergetic Incident Beam

Figure IV-7

Following Landau's [63] method, but using the general notation of Breuer [64], one can calculate the fraction, $\Psi(\Delta E)$, of the beam one does not detect (because of ionization losses) if data taking stops ΔE below the peak in Figure IV-7 as

$$\Psi(\Delta E) = \int_0^{E_2} N(E)\,dE \Big/ \int_0^{E_{inc}} N(E)\,dE \,.$$

Landau [63] gave a graph of $\Psi(\Delta E)$ but he also derived an approximation for $\Psi(\Delta E)$, as have others [65], which has been used in this work:

$$\Psi(\Delta E) = \frac{1}{\omega} ,$$

where the value of ω as provided by Bŏrsch-Supan [66] is

$$\omega = \lambda\left(1- \frac{\ell n\ \lambda + A}{\lambda + 1}\right)$$

where $A = \gamma - 1 = -0.4228...$,

γ is Eulers constant,

$\lambda = \frac{\Delta E}{\xi} - 0.05$ (is an approximation to the λ as defined by Landau and Bergstrom [67],

$\xi = 0.154 \dfrac{\Sigma\ \eta_i z_i}{\Sigma\ \eta_i A_i}\ T$ MeV, and

T = target thickness is gm/cm^2.

η_i is the number of atoms of element (i) per molecule of the target which here was considered to be a homogenous mixture of the 0.001 steel windows and the gas in the target vessel, and z_i and A_i are the atomic number and atomic weight of element (i).

The ionization correction is given by

$$\mathcal{K}_i = (1- \Psi(\Delta E))^{-1}$$

In this experiment $\mathcal{K}_i$ was less than 1.01, i.e., the Landau ionization correction was less than one percent.

D. ERROR ANALYSIS

1. Systematic Errors

Because this experiment measured the ratio of the deuteron to the proton cross section, many systematic errors in each of these cross sections, such as solid angle, scattering angle, SEM efficiency, target thickness, and counting rate corrections were effectively cancelled when the ratio of the two cross sections were formed. This follows because the data for both cross sections were taken during one continuous LINAC running period with the geometries the same and the beam characteristics, excluding the incident energy, as nearly identical as possible.

A systematic error which does not cancel in this ratio experiment is that which can arise because of possible impurities in the hydrogen and deuterium gases. The supplier of the target gases advertized 99.5% pure deuterium and 99.995% pure hydrogen. However, after closer investigation it was discovered that their analytic equipment can only detect 0.3% or more contamination of D_2 in H_2 or H_2 in D_2. All the data taken in this experiment used only one bottle of deuterium and one of hydrogen, thus all data were taken with the same amount of possible contaminant. If there were a difference in the contamination of H_2 or D_2 this difference would have caused a non zero intercept of the plot of G_{E_n} versus q^2. For example, a 0.3% contamination of D_2 and a

0.0% contamination of H_2 would have lowered the intercept by about 0.0015.

Whenever empty target background was compared to the background above the peak, the deuterium background always had the same spectrum distribution in both the empty and full cases. However, at lower q^2 (particularly $q^2 = 0.05$) the hydrogen spectrum above the hydrogen peak clearly showed a contaminant in the gas which, if it were a low atomic number contaminant would have been a few percent, but if it were a high atomic number contaminant it would have been less than a few tenths of a percent. The closeness of the intercept of G_{E_n} versus q^2 to zero (we report 0.0000 ± 0.0012 for LF model 15) indicates that the H_2 and D2 contaminants were, in fact, almost equal. The following figure shows the difference between the H_2 and D_2 spectra. The elastic peaks in these cases would be at about 1000 counts.

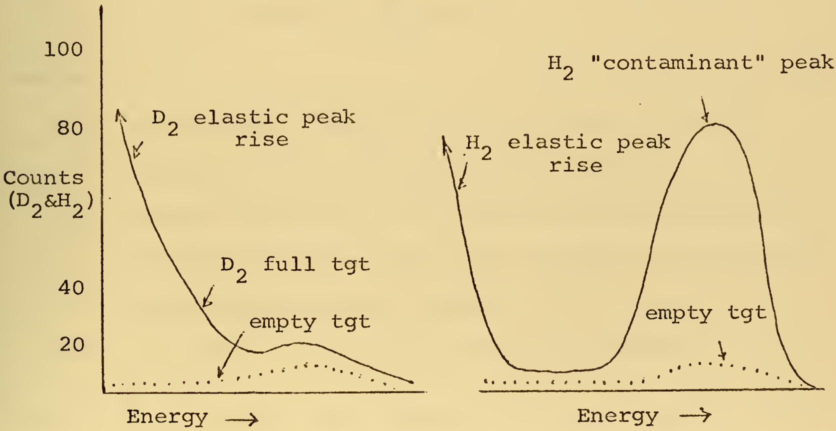

2. Random Errors

The random errors in this ratio experiment, besides the statistical (Poisson) counting errors, came from errors in determining the density of the gas in the target, variations in the SEM efficiency during a run, energy shifts of the incident beam, leakage currents in the beam current integrators, and very small errors in the radiation corrections resulting from errors in determining ΔE.

The statistical error for each cross section, due to the Poisson distribution of the number of electrons scattered for a given number of incident electrons, was calculated by a subroutine in the same program that calculated the cross section and included the statistical errors made in determining the background subtraction. To determine the fractional error in the cross section caused by these statistical fluctuations, the cross section, X, may be written as

$$X = \text{Constant} \cdot \sum_{k=1}^{M} (N_k - B)$$

where

N_k = Total counts (count rate and voltage corrected) obtained at the k^{th} spectrometer setting,

B = Average background to be subtracted (determined at energies above the peak) and assumed to be the same for each spectrometer setting, and

M = The number of settings of the spectrometer.

Let $N = \sum_{k=1}^{M} N_k$ be the total number of counts, then:

$$X = \text{Constant} \cdot (N - M \cdot B).$$

The variance of the cross section is

$$\sigma_x^2 = \left(\frac{\partial x}{\partial N}\right)^2 \sigma_N^2 + \left(\frac{\partial x}{\partial B}\right)^2 \sigma_B^2$$

which gives

$$\sigma_x^2 = (\text{Constant})^2 (N+M^2\sigma_B^2)$$

where σ_B^2 is the variance in the average background and $\sigma_N^2 = N$.

Let $B_T = \sum_{i=1}^{J} B_i$ (where B_i = background at i^{th} setting) and J is the number of spectrometer settings above the peak at which background was taken.

Since $B = \frac{\Sigma B_i}{J}$ then $\sigma_B^2 = \frac{1}{J^2} \sum^{J} \sigma_{B_i}^2 = \frac{1}{J^2} \sum^{J} B_i = \frac{1}{J^2} B_T = \frac{B}{J}$.

Thus

$$\sigma_x^2 = (\text{Constant})^2 [N+M^2 \frac{B}{J}]$$

and the fractional standard deviation of the cross section is

$$\frac{\sigma_x}{x} = \left\{\frac{N+M^2B/J}{[N-MB]^2}\right\}^{\frac{1}{2}}$$

which can also be expressed as

$$\frac{\sigma_x^2}{x^2} = \frac{1}{N_o} + \frac{MB(1+ M/J)}{N_o^2}$$

where N_o = N-MB and the first term gives the variance due to the true counts and the second gives the variance resulting from the background.

The errors in the measured cross sections caused by errors in determining the density of the gas in the target varied slightly from run to run, but were always less than about 0.1%. The pressure dropped while liquid nitrogen was being pumped and then rose again and stayed steady until the

next nitrogen fill, but the variations were almost identical in the hydrogen and the deuterium, and were about 0.3% of the measured pressure. In calculations, the average pressure at the start of the nitrogen fill or at the completion of the fill was the pressure actually used, depending on which was more constant. In calculating the gas density, of course, if the pressure at the start (completion) of the fill was used for hydrogen, then the pressure at the start (completion) of the fill was also used for deuterium.

Generally, six SEM efficiencies were measured during a data run on each gas; one was taken at the start of the run, one at each of the four peaks, and one at the completion of data taking. At each point, four or more measurements were made, and the fractional standard deviation of a single measurement was usually less than 0.2%, giving a fractional standard deviation of the mean of the SEM readings of less than 0.08% for the six readings.

Because of problems such as variations in line voltage, the beam energy was not constant and thus the scattered energy also would change slightly from time to time throughout a run. The result of these changes was a shift of counts from one channel to another of the counting ladder. This was most noticeable when data were being taken along the steep slopes of elastic peaks; often a low count in one channel would be accompanied by a high count in an adjacent channel. The obvious method of reducing these shifts was to close the energy defining slits more, but this increased the background and thus the ratio of real counts to background became

less - giving larger errors on the measured cross sections. Nevertheless, the experimenter could not always unambiguously estimate how many counts were added or subtracted from a given elastic peak due to energy shifts.

An examination of many runs shows that there was no apparent energy shift problem in those runs where the cross section was large and the slits could be closed and still maintain a good peak to background ratio. In other runs where the slits were opened wider, it appeared that a variation of as much as a percent could have occurred at several points in an elastic peak. Adjacent data points and general elastic peak shapes were used to smooth out these large fluctuations. It is estimated that in the poorer runs these energy shifts could have caused an error in the average measured cross section ratio of as much as 0.2%.

There were slight leakage currents in the circuits used to measure and integrate the beam current. These currents were reduced by improving the insulation of various components and by cleaning all sensitive elements. The leakage currents on the SEM and the faraday cup, along with all the circuits used to accumulate the currents, were measured and found to be almost trivial. These measurements were repeated during each run and remained very constant. If the electron beam was perfectly constant during all parts of a given run, the leakage current would introduce no errors. Usually the electron current was held constant to within 20%; this would cause an error in the ratio of the cross sections of about 0.02%.

Finally, there is the error in measuring the exact position of the peak of the elastic spectrum from the plotted data. The amount of this error varies with such things as beam stability, energy, and the widths of the slits but generally was about 0.01 MeV. This error causes an error in the measurement of ΔE which in turn causes an error in the Schwinger, bremsstrahlung, and ionization corrections. The error in the measured cross section due to this ΔE error for all three radiation corrections was of the order of 0.05%. The error in ΔE also causes an uncertainty in the final energy value at which one terminates the integration of the elastic spectrum. This error caused about a 0.03% error in the measured cross section.

Combining all the above errors except the statistical errors and the energy shift errors (since these two vary so much from run to run), it is seen that the total fractional error in the measured cross section is about 0.14%. In addition to this, the statistical errors in the cross sections varied from an average of less than about 0.2% to a maximum of about 0.4% for a few runs, while the energy shift errors varied from apparently zero through an average of less than 0.1% with about 4 runs possibly having errors as large as 0.2%. A summary of the errors discussed above is given in Table IV-1.

The average error in the cross section ratio due to all random errors except the statistical error, $S_{\text{Avg.Others}}$, has been calculated from the values of the average cross section errors in Table IV-1 to be 0.24%. The total error of the weighted mean ratio R was then formed from

$$S^2_{\text{Total}} = S^2_{\text{Stat.}} + S^2_{\text{Avg.Others}} \,. \qquad \text{(IV-1)}$$

TABLE IV-1

Random Errors in Cross Section Data

Errors	Average Values of Errors
Statistical	0.3%
Gas Density	0.1%
SEM Efficiency	0.08%
Energy Shifts	0.10%
Leakage Currents	0.014%
ΔE Measurement (Radiation Corrections)	0.05%
ΔE Measurement (Integration)	0.03%

Two significant sources of error were avoided in this work that were present in previous work [2]. The use of a gas target in place of a polyethylene target and the independent determination of the cross section ratios by each channel permitted these improvements. The gas target scatters electrons from the target nuclei all along the beam path, but only those nuclei which satisfy the scattering geometry, i.e., those which will scatter and recoil through both a collimator which is about 6 inches from the gas target and the spectrometer slits which are 16 inches from the target, can enter the spectrometer. Thus if the experimenter first scatters from hydrogen, maintains the exact geometry, and then fills the target with deuterium and scatters from it, he does not have to calculate the target thickness in order to obtain a perfectly

accurate ratio of cross sections - if target thickness were the only possible error in the cross section determination. This is not the case if he used a solid target which is thinner than the collimated entrance width to the spectrometer. Stewart [2], who used a thin polyethylene target to measure the deuteron and proton cross sections, estimated the target thickness error as 0.5%. A second significant error which was avoided in this work was the error experienced in determining the relative efficiencies of each of the ten channels. This error was quite informally established to be 0.5% in Ref. 2. In this present work each detector scanned the complete elastic spectra and the ratio of the deuteron cross section to the proton cross section was formed separately for the individual detectors. This eliminated any detector efficiency errors which would have arisen had the method of Ref. 2 been used.

Having established what errors were made in the measured cross sections, one can determine how these errors propagated into the value of G_{E_n}. Let the standard deviation of a cross section be denoted by S_p and S_d for the proton and deuteron. Let $R = \sigma^d/\sigma^p$ where

σ^d = experimental cross section of the deuteron and

σ^p = experimental cross section of the proton.

G_{E_n} is determined from

$$G_{E_n} = \left(\frac{G_{E_d}}{G_{E_p}} \frac{1}{D_C} - 1.0 \right) G_{E_p} \qquad \text{(IV-14)}$$

and G_{E_d}/G_{E_p} is determined from

$$\left(\frac{G_{E_d}}{G_{E_p}}\right)^2 = R \frac{\sigma^p_{Mott}}{\sigma^d_{Mott}} \frac{K^d_{mr}}{K^p_m} \frac{G^2_{E_p}(q^2_p)}{G^2_{E_p}(q^2_d)} . \tag{IV-15}$$

Solving first for the fractional error in R due to the errors in both cross sections we have [42]:

$$\frac{S^2_R}{R^2} = \frac{S^2_d}{(\sigma^d)^2} , + \frac{S^2_p}{(\sigma^p)^2} \tag{IV-16}$$

where S_R is the standard deviation of the ratio R.

The error in the ratio of $\frac{G_{E_d}}{G_{E_p}}$ is determined from Equation IV-15, thus the standard fractional deviation of the ratio G_{E_d}/G_{E_p}, denoted by $S^{\%}_{G_{E_d}/G_{E_p}}$, is

$$S^{\%}_{G_{E_d}/G_{E_p}} = \frac{1}{2} \frac{S_R}{R} . \tag{IV-17}$$

From Equation IV-14 we determine the variance in G_{E_n} to be:

$$S^2_{G_{E_n}} = \left(S^{\%}_{G_{E_d}}\right)\left(\frac{G_{E_d}}{G_{E_p}}\right)^2\left(\frac{G_{E_p}(q^2_d)}{D_C}\right)^2 \tag{IV-18}$$

and using Equation IV-15, the standard deviation in the neutron electric form factor is

$$S_{G_{E_n}} = \frac{1}{2} S_R \left(\frac{1}{R} \frac{\sigma^p_{Mott}}{\sigma^d_{Mott}} \frac{K^d_{mr}}{K^p_m}\right)^{\frac{1}{2}} \frac{G_{E_p}(\bar{q}^2_p)}{D_C} . \tag{IV-19}$$

Up to this point in the error analysis only the errors in one channel have been discussed, i.e., S_R is the

error in R due to errors in the deuteron and proton cross sections for any given channel. Letting R_i be the ratio measured by channel i and S_{Ri} its standard deviation, then the weighted mean of all four channels, R_m, for any given run is obtained by calculating

$$R_m = \frac{\sum_{i=4}^{7} \left(\frac{R_i}{S_{R_i}^2} \right)}{\sum_{i=4}^{7} \left(\frac{1}{S_{R_i}^2} \right)} \qquad \text{(IV-20)}$$

and the standard deviation of this weighted mean ratio is

$$S_{R_m}^2 = \frac{1}{\sum_{i=4}^{7} \left(\frac{1}{S_{R_i}^2} \right)} \quad . \qquad \text{(IV-21)}$$

R_m and S_{R_m} are the experimental values of the ratio and of the standard deviation of that ratio quoted in Table V-I for each run and are the values used to determine all derived quantities for each run in this work, e.g., G_{E_n}, $S_{G_{E_n}}$, G_d^2 and all others.

E. REJECTION OF DATA

Twenty one runs are reported in this work. In each run the cross section ratio, R, was measured for each of the four channels, giving a total of 84 measurements of R. However, nine of these 84 measurements have not been included in the data analysis because of clear indicators that each had large systematic errors.

The data given in Table V-I for $q^2 = 0.05$ at $\theta = 60^\circ$ does not include the data of channel 5 since the "contamination" background subtaction method discussed in Section III-B for the $q^2 = 0.05$ data did not work well for that channel.

Energy shifts caused clear irregularities in four runs. For this reason the following were not included in the data reported in Table V-I: channel 5 in the second $q^2 = 0.10$ run, channel 6 in the first $q^2 = 0.2$ run, channel 7 in the second $q^2 = 0.2$, $\theta = 90^\circ$ run, and channels 4, 5, and 6 in the second $q^2 = 0.2$, $\theta = 60^\circ$ run.

The inability to establish reliable backgrounds caused the rejection of the data of channel 4 in both $q^2 = 0.35$ runs.

V. EXPERIMENTAL RESULTS

A. NEUTRON CHARGE FORM FACTORS

The data from 21 runs are reported here. Each run consisted of four measurements of R, the ratio of the elastic electron-deuteron cross section to the elastic electron-proton cross section. Of these 84 measurements of R, 9 are not included in the reported data for reasons given in Section IV-E.

Table V-I gives the q^2 transferred to the deuteron, the scattering angle θ, the incident energies of the electron incident on the proton, E_{i_p}, and deuteron, E_{i_d}, the experimental ratio R_m and the standard deviation of the ratio R as determined by the total error (defined in Section IV-D) and the statistical (Poisson) error for that run. Also given are quantities which were determined by calculations. These quantities are explained in Section II. Using the experimental results and the calculated quantities given in Table V-I, the ratio of the deuteron electric form factor to the proton electric form factor has been derived and is listed in the right hand column.

The neutron electric form factor G_{E_n} was obtained by using Equation II-43 in the following form

$$G_{E_n}(q_d^2) = \left[\left(R \, \frac{\sigma_m^p(\theta) \; K_{mr}^d}{\sigma_m^d(\theta) \; K_m^p} \right)^{\frac{1}{2}} \left\{ \frac{G_{E_p}(q_p^2)}{G_{E_p}(q_d^2)} \right\} \frac{1}{C_E} - 1 \right] G_{E_p}(q_d^2) .$$

The deuteron charge form factor C_E listed in Appendix C and the G_{E_d}/G_{E_p} and $G_{E_p}(q_d^2)$ values given in Table V-I were used to solve for G_{E_n}. The value of C_E depends upon the deuteron wave function as well as q^2. Three sets of the 21 values of G_{E_n} have been calculated for Lomon-Feshbach models #1, #5, and #15.

The best estimate of the error in each of these 21 values of G_{E_n}, for each LF model, is the error obtained using S_{Total} from Equation IV-1. The best estimate of the value of $\frac{d}{dq^2} G_{E_n}$ reported for each of the three models was obtained from these sets of G_{E_n} weighted by S_{Total}. For comparison, $\frac{d}{dq^2} G_{E_n}$ was also calculated from the G_{E_n} data weighted by its statistical error only, and also with equal weighting given to each G_{E_n} to provide an insight into the sensitivity of the result to weighting of the data.

After calculating each G_{E_n} and its S_{Total} an average G_{E_n} and its S_{Total} at each q^2 was calculated. A plot of the average G_{E_n} (with its S_{Total}) versus q^2 is provided for each of the three models. For LF model 15 the value of each G_{E_n} and its S_{Total} is also given.

For the 21 runs reported, all values of G_{E_n} were calculated from the FORTRAN programs listed in Appendix E. In addition, in order to check these programs in 15 runs, the values of G_{E_n} were also calculated on a Wang Model 700 calculator using programs not written by the author. These Wang calculations used the same raw data, but used different calculations and independent smoothing of the elastic peaks to determine G_{E_n}. The values of G_{E_n} determined by each of

TABLE V-I (Measured Ratio G_{E_d}/G_{E_p})

q_d^2 (f_m^{-2})	Θ	$\frac{E_{i_p}\ (\mathrm{MeV})}{E_{i_d}\ (\mathrm{MeV})}$	Exp. Ratio $R = \frac{\sigma^d_{Exp}}{\sigma^p_{Exp}}$	Std. Dev. of R Total and (Statistical)	Mag. Corr. (K) $\frac{K_{deuteron}}{K_{proton}}$	$\frac{G_{E_p}(q_p^2)}{G_{E_p}(q_d^2)}$	$\frac{\sigma^p_{mott}}{\sigma^d_{mott}}$	$\frac{G_{E_d}}{G_{E_p}} \pm$ Total and (Statistical) Error
0.05	75°	37.02 36.50	0.9724	0.0038 (0.0030)	0.99997 0.99114	0.99396 0.99404	0.16837 0.17578	0.9693 ± 0.0019 (0.0015)
	60°	44.80 44.43	0.9654	0.0046 (0.0040)	1.0000 .99338	0.99400 0.99404	0.30269 0.31356	0.9685 ± 0.0023 (0.0020)
0.10	75°	52.89 51.80	0.9390	0.0042 (0.0035)	0.99993 0.98230	0.98789 0.98815	0.81525 0.86757	0.9475 ± 0.0021 (0.0018)
	75°	52.89 51.80	0.9331	0.0034 (0.0024)	0.99993 0.98230	0.98789 0.98815	0.81525 0.86757	0.9445 ± 0.0017 (0.0012)
	75°	52.89 51.80	0.9262	0.0046 (0.0038)	0.99993 0.98230	0.98789 0.98815	0.81525 0.86757	0.9410 ± 0.0023 (0.0019)
	75°	52.89 51.80	0.9221	0.0040 (0.0031)	0.99993 0.98230	0.98789 0.98815	0.81525 0.86757	0.9389 ± 0.0020 (0.0016)
0.2	120°	54.24 51.99	0.8068	0.0118 (0.0106)	0.99466 0.89020	0.97555 0.97653	0.72058 0.81829	0.8901 ± 0.0053 (0.0048)

0.2	120°	54.30 52.05	0.8280	0.0102 (0.0099)	0.99465 0.88999	0.97550 0.97653	0.71893 0.81637	0.9018 ± 0.0046 (0.0045)
	120°	54.30 52.05	0.8057	0.0082 (0.0079)	0.99465 0.88999	0.97550 0.97653	0.71893 0.81637	0.8896 ± 0.0036 (0.0035)
	75°	75.77 73.57	0.8402	0.0049 (0.0042)	0.99985 0.96493	0.97582 0.97653	0.39041 0.42650	0.8921 ± 0.0022 (0.0019)
	90°	65.72 63.50	0.8294	0.0049 (0.0042)	0.99896 0.95129	0.97582 0.97653	0.22434 0.24871	0.8871 ± 0.0022 (0.0019)
	90°	65.72 63.50	0.8365	0.0052 (0.0046)	0.99896 0.95129	0.97569 0.97653	0.22434 0.24871	0.8894 ± 0.0023 (0.0020)
	60°	91.52 89.34	0.8204	0.0051 (0.0045)	1.0000 0.97359	0.97595 0.97653	0.70815 0.76120	0.8849 ± 0.0023 (0.0020)
	60°	91.52 89.34	0.8275	0.0076 (0.0072)	1.0000 0.97359	0.97595 0.97653	0.70815 0.76120	0.8887 ± 0.0034 (0.0032)
0.25	75°	85.16 82.39	0.7987	0.0056 (0.0051)	0.99982 0.95641	0.96982 0.97082	0.30690 0.33890	0.8687 ± 0.0024 (0.0022)
0.30	90°	81.43 78.05	0.7718	0.0057 (0.0052)	0.99845 0.92817	0.96365 0.96516	0.14386 0.16338	0.8537 ± 0.0024 (0.0022)
	90°	81.43 78.05	0.7529	0.0060 (0.0055)	0.99845 0.92817	0.96365 0.96516	0.14386 0.16338	0.8432 ± 0.0025 (0.0023)

0.30	90°	81.43 78.05	0.7558	0.0070 (0.0066)	0.99845 0.92817	0.96365 0.96516	0.14386 0.16338	0.8448 ± 0.0030 (0.0028)
	75°	90.39 90.39	0.6973	0.0049 (0.0043)	0.99978 0.95135	0.96625 0.96516	0.27138 0.28073	0.8426 ± 0.0021 (0.0018)
0.35	90°	88.41 84.43	0.7192	0.0054 (0.0048)	0.99819 0.91695	0.95767 0.95955	0.12122 0.13916	0.8242 ± 0.0022 (0.0020)
	90°	84.43 84.43	0.6596	0.0056 (0.0051)	0.998191 0.923404	0.96112 0.95955	0.13341 0.13916	0.8281 ± 0.0023 (0.0021)

these methods showed very good agreement, well within the statistical errors. This agreement is convincing evidence that the computer programs used in the data reduction did not contain errors which could bias the conclusions reported in this paper. The ratio R reported in Table V-I is the average R for those 15 runs.

The average value of G_{E_n} at each q^2, using Lomon-Feshbach Model #1, is given in Table V-II.

The average value of G_{E_n} at each q^2, using Lomon-Feshbach Model #5, is given in Table V-III.

The value of G_{E_n} calculated from L-F Model 15 and its $S_{G_{E_n}}$ for each of the 21 runs is given in Table V-IV.

The average value of G_{E_n} at each q^2, using Lomon-Feshbach Model #15 is given in Table V-V.

B. ROSENBLUTH PLOT

At $q^2 = 0.2$ deuteron and hydrogen data were taken at 60, 75, 90, and 120 degrees in order that a Rosenbluth Plot could be constructed. The theoretical interpretation of the Rosenbluth Plot is discussed in Section II-G. Table V-VI gives the experimental data and the derived quantities used as data for the Rosenbluth plot given in Figure V-5.

C. CHARGE RADIUS OF THE DEUTERON

The deuteron charge rms radius was calculated by Method II given by Schumacher and Bethe [44]. They have provided the charge radius of the deuteron from several deuteron wave functions. L-F #1 and L-F #5 have a charge radius of 1.971 fm

TABLE V-II

Average G_{E_n} at Each q^2 Using Lomon-Feshbach Model #1

q^2 (fm^{-2})	C_E (LF#1)	G_{E_n}	$S_{G_{E_n}}$ (Total)
0.05	0.96881	0.0002	0.0015
0.10	0.93967	0.0036	0.0011
0.20	0.88667	0.0028	0.0011
0.25	0.86247	0.0070	0.0027
0.30	0.83961	0.0073	0.0014
0.35	0.81796	0.0095	0.0019

A linear fit to the data in Table V-II gives:

$$G_{E_n} = (-0.0003 \pm 0.0012) + (0.0245 \pm 0.0059)q^2, \qquad \text{(V-1)}$$

while a linear fit of G_{E_n} weighted by the statistical $S_{G_{E_n}}$ only gives:

$$G_{E_n} = (0.0001 \pm 0.0010) + (0.0231 \pm 0.0049)q^2, \qquad \text{(V-2)}$$

and the 21 points, if equally weighted, give

$$G_{E_n} = (-0.0004 \pm 0.0016) + (0.0263 \pm 0.0072)q^2 \qquad \text{(V-3)}$$

A plot of the data in Table V-II is given in Figure V-1.

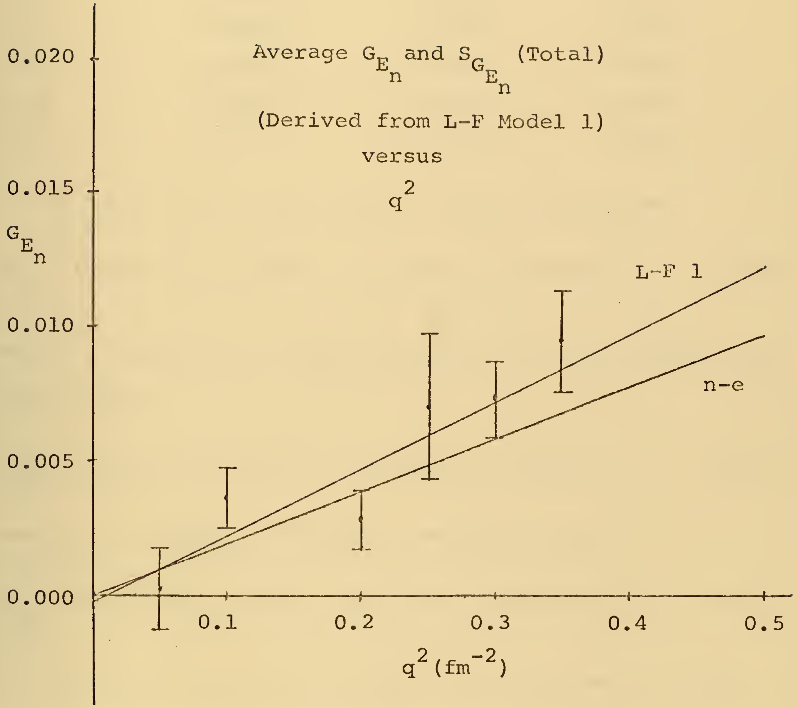
Average G_{E_n} and $S_{G_{E_n}}$ (Total)
(Derived from L-F Model 1)
versus
q^2
0.020
0.015
G_{E_n}
0.010
0.005
0.000
0.1
0.2
0.3
0.4
0.5
$q^2\,(\mathrm{fm}^{-2})$
L-F 1
n-e

Figure V-I

TABLE V-III

Average G_{E_n} at Each q^2 using Lomon-Feshbach Model #5

q^2 (fm^{-2})	C_E (LF#5)	G_{E_n}	$S_{G_{E_n}}$ (Total)
0.05	0.96881	0.0002	0.0015
0.10	0.93966	0.0036	0.0011
0.20	0.88665	0.0028	0.0011
0.25	0.86244	0.0070	0.0027
0.30	0.83956	0.0074	0.0014
0.35	0.81790	0.0096	0.0019

A linear fit to the data in Table V-III gives:

$$G_{E_n} = (-0.0003 \pm 0.0012) + (0.0249 \pm 0.0059)q^2 \qquad \text{(V-4)}$$

While a linear fit of G_{E_n} weighted by the statistical $S_{G_{E_n}}$ only gives:

$$G_{E_n} = (0.0001 \pm 0.0010) + (0.0234 \pm 0.0049)q^2 \qquad \text{(V-5)}$$

and the 21 points, if equally weighted, give

$$G_{E_n} = (-0.0003 \pm 0.0016) + (0.0266 \pm 0.0072)q^2. \qquad \text{(V-6)}$$

A plot of the data in Table V-III is given in Figure V-2.

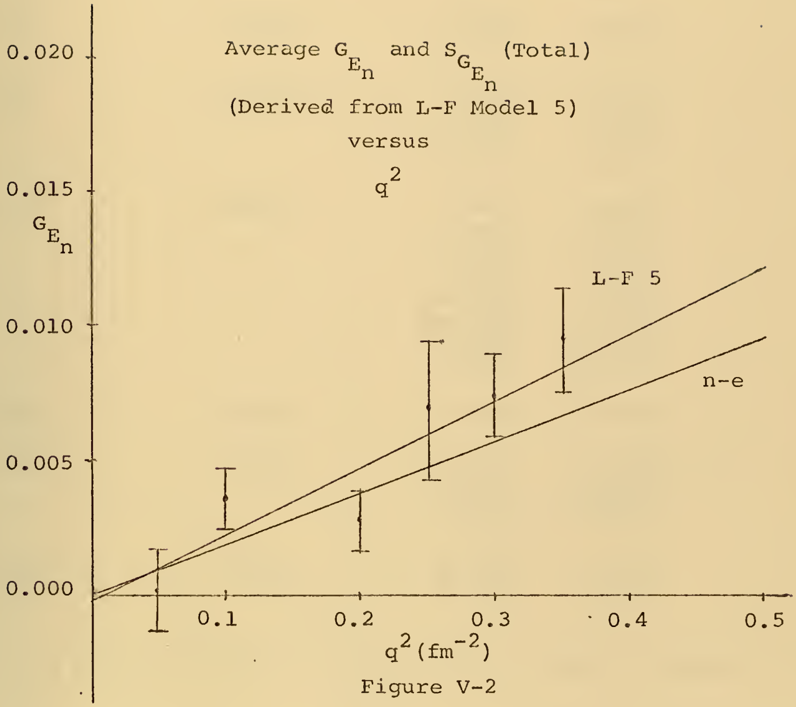

0.020
0.015
0.010
0.005
0.000
G_{E_n}
Average G_{E_n} and $S_{G_{E_n}}$ (Total)
(Derived from L-F Model 5)
versus
q^2
L-F 5
n-e
0.1
0.2
0.3
0.4
0.5
$q^2 (fm^{-2})$

Figure V-2

TABLE V-IV

G_{E_n} and $S_{G_{E_n}}$ (Total) for Each of the 21 Runs

Calculated from Lomon-Feshbach Model #15

q^2 (fm^{-2})	C_E (LF#15)	G_{E_n}	$S_{G_{E_n}}$ (Total)
0.05	0.96899	0.0003	0.0019
		-0.0005	0.0023
0.10	0.94002	0.0079	0.0021
		0.0047	0.0017
		0.0011	0.0024
		-0.0012	0.0021
0.20	0.88731	0.0031	0.0058
		0.0159	0.0051
		0.0025	0.0040
		0.0053	0.0024
		-0.0002	0.0024
		0.0023	0.0025
		-0.0026	0.0025
		0.0015	0.0037
0.25	0.86324	0.0061	0.0031
0.30	0.84049	0.0152	0.0028
		0.0031	0.0029
		0.0050	0.0034
		0.0024	0.0024
0.35	0.81895	0.0062	0.0026
		0.0107	0.0027

A plot of the data in Table V-IV is given in Figure V-3.

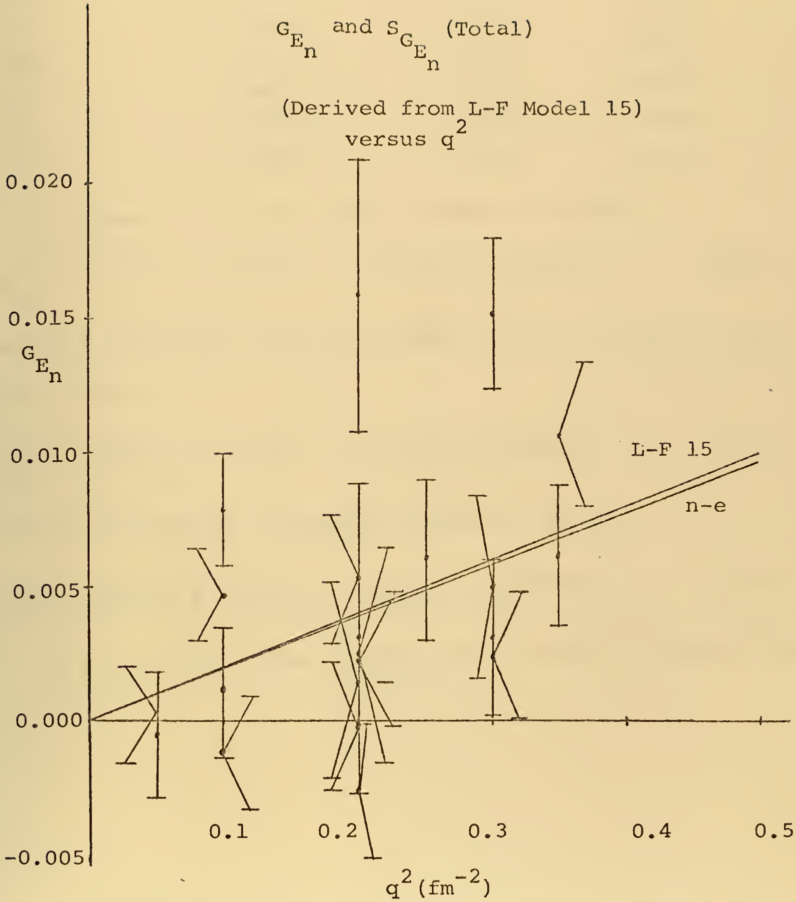
G_En and S_GEn (Total)
(Derived from L-F Model 15)
versus q^2
0.020
0.015
G_En
0.010
0.005
0.000
-0.005
L-F 15
n-e
0.1
0.2
0.3
0.4
0.5
q^2 (fm^-2)

Figure V-3

TABLE V-V

Average G_{E_n} at Each q^2 Using Lomon-Feshbach Model #15

q^2 (fm^{-2})	C_E(LF#15)	G_{E_n}	$S_{G_{E_n}}$ (Total)
0.05	0.96899	0.0000	0.0015
0.10	0.94002	0.0034	0.0010
0.20	0.88731	0.0021	0.0011
0.25	0.86324	0.0061	0.0031
0.30	0.84049	0.0062	0.0014
0.35	0.81895	0.0084	0.0019

A linear fit to the data in Table V-V gives:

$$G_{E_n} = (-0.0000 \pm 0.0012) + (0.0200 \pm 0.0058)q^2 \qquad \text{(V-7)}$$

While a linear fit of G_{E_n} weighted by the statistical $S_{G_{E_n}}$ only gives:

$$G_{E_n} = (0.0000 \pm 0.0010) + (0.0194 \pm 0.0050)q^2 \qquad \text{(V-8)}$$

and the 21 points, if equally weighted, give:

$$G_{E_n} = (-0.0003 \pm 0.0016) + (0.0231 \pm 0.0072)q^2 \qquad \text{(V-9)}$$

A plot of the data in Table V-V is given in Figure V-4.

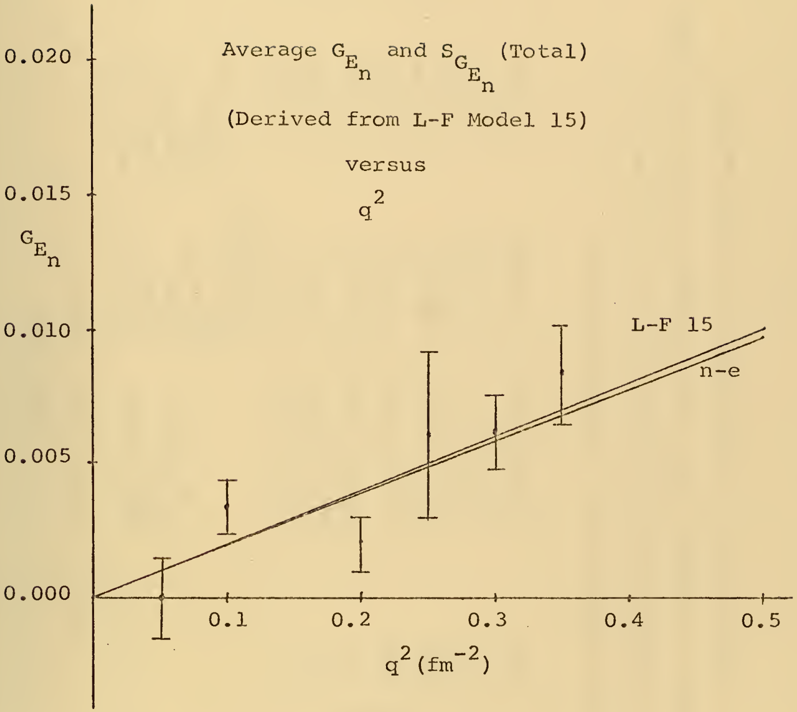Average G_{E_n} and $S_{G_{E_n}}$ (Total)
(Derived from L-F Model 15)
versus
q^2
0.020
0.015
G_{E_n}
0.010
0.005
0.000
L-F 15
n-e
0.1
0.2
0.3
0.4
0.5
q^2 (fm^{-2})

Figure V-4

TABLE V-VI

$G_d^2(0.2)$, Deuteron Form Factor Squared at $q^2 = 0.20$ fm^{-2}

Scattering Angle (degrees)	$1+2(1+\eta)\mathrm{tg}^2\theta/2$	Experimental Ratio R $\pm S_R$(Total)	deVries b' Proton Cross Section $\sigma^p_{\mathrm{deVries}}$ $(\times 10^{29})\,\mathrm{cm}^2$	Mott Cross Section of Deuteron σ^d_{Mott} $(\times 10^{29})\,\mathrm{cm}^2$	Deuteron Form Factor Squared G_d^2
60	1.667	0.8204±0.0051	0.69277	0.76120	0.7466±0.0045
60	1.667	0.8275±0.0076	0.69277	0.76120	0.7531±0.0070
75	2.178	0.8402±0.0049	0.38530	0.42650	0.7590±0.0044
90	3.0011	0.8294±0.0049	0.22449	0.24908	0.7475±0.0044
90	3.0011	0.8365±0.0052	0.22449	0.24908	0.7539±0.0046
120	7.0037	0.8068±0.0110	0.077026	0.081829	0.7594±0.0103
120	7.0037	0.8280±0.0102	0.076859	0.081637	0.7795±0.0096
120	7.0037	0.8057±0.0083	0.076859	0.081637	0.7585±0.0078

A linear fit to the data in Table V-VI showed that:

$$G_d^2(0.2) = (0.7460\pm0.0040)+(0.0026\pm0.0012)[1+2(1+\eta)\tan^2\theta/2]. \qquad (V\text{-}10)$$

While, if the second 120 degree run, which stands out from the other 7, is omitted,

$$G_d^2(0.2) = (0.7488\pm0.0043)+(0.0013\pm0.0013)[1+2(1+\eta)\tan^2\theta/2]. \qquad (V\text{-}11)$$

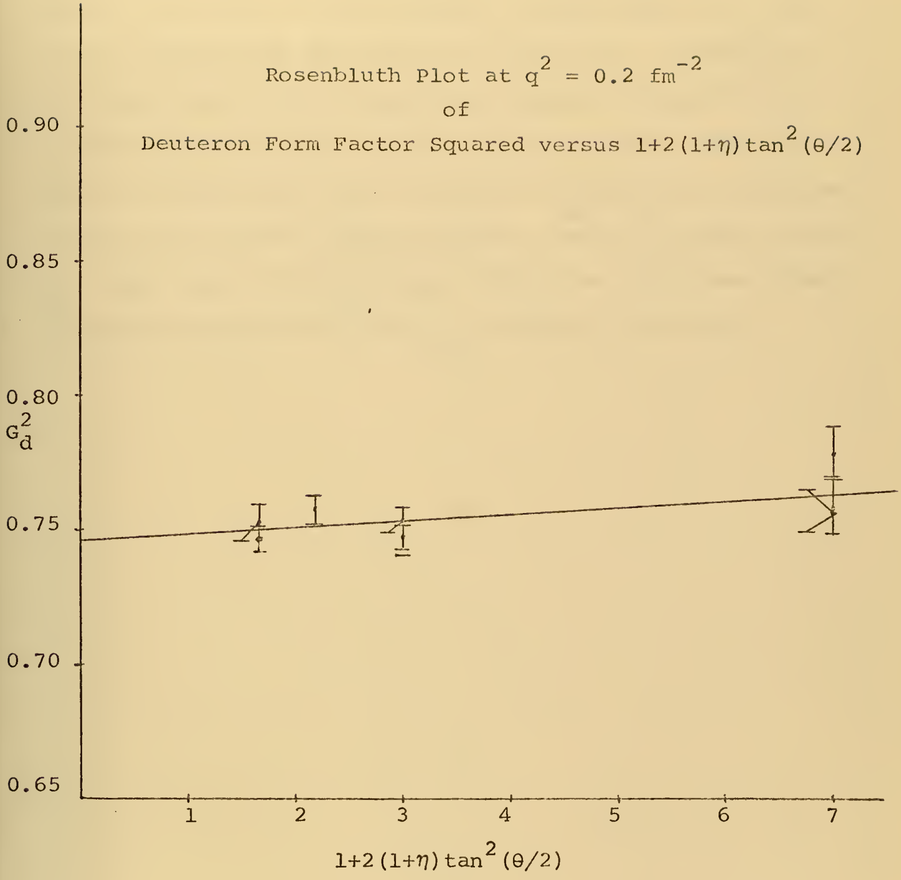
Rosenbluth Plot at $q^2 = 0.2$ fm^{-2}
of
Deuteron Form Factor Squared versus $1+2(1+\eta)\tan^2(\theta/2)$
0.90
0.85
0.80
G_d^2
0.75
0.70
0.65
1
2
3
4
5
6
7
$1+2(1+\eta)\tan^2(\theta/2)$

Figure V-5

while L-F #15 has $r_e = 1.965$ fm. The experimental $\frac{d}{dq^2} G_{E_n}(0)$ which were determined using L-F #1, 5, and 15 are plotted against the square of the deuteron charge radius, $r^2_{E_d}$, as given by Schumacher and Bethe, in Figure V-6. Schumacher notes that such a plot yields an excellent straight line for all models with the correct binding energy. The intersection of this line with the value of $\frac{d}{dq^2} G_{E_n}(0)$ determined by the very accurate neutron-electron scattering work yields $r^2_{E_d}$. The value of the deuteron charge rms radius was determined from Figure V-6 to be $r_{E_d} = 1.9641 \pm 0.0074$ fm.

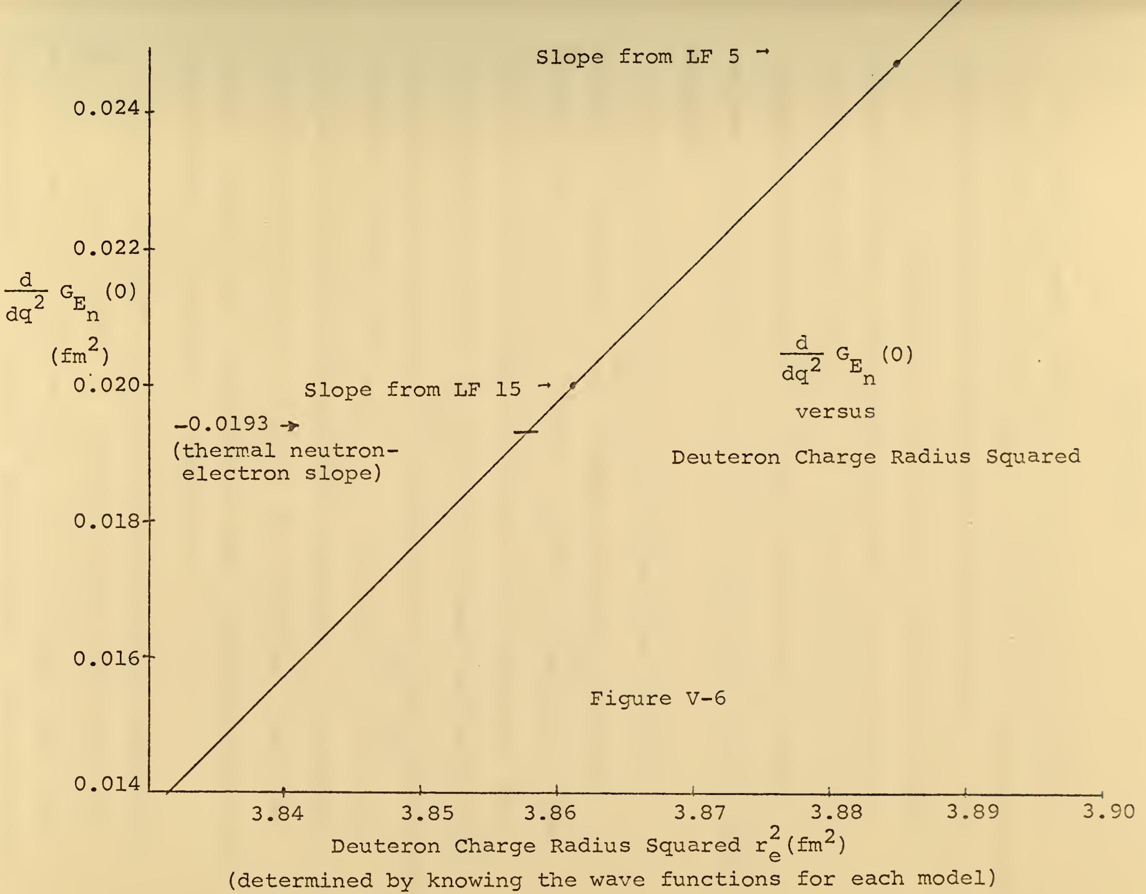

$\frac{d}{dq^2} G_{E_n}(0)$

versus

Deuteron Charge Radius Squared

Figure V-6

VI. CONCLUSIONS

From the 75 measurements of the ratio of the elastic electron-deuteron cross section to the elastic electron-proton cross section at low q^2 the following conclusions are drawn:

i) the discrepancy in the neutron charge form factor measured in several earlier experiments [1,2,3,4] was resolved. The value of $\frac{d}{dq^2} G_{E_n}(0)$ was determined to be in agreement with the thermal neutron results for all three deuteron wave functions (L-F 1,5,15) which were used to analyze the data.

ii) the value of $\frac{d}{dq^2} G_{E_n}(0)$ ranged from (0.0245 ± 0.0059) fm^2 when L-F 1 was used to extract G_{E_n} from the deuteron data, through (0.0249 ± 0.0059) fm^2 when L-F 5 was used, to (0.0200 ± 0.0058) fm^2 when L-F 15 was used. Thus L-F 15 produced a value of $\frac{d}{dq^2} G_{E_n}(0)$ in best agreement with the very accurate thermal neutron results of $\frac{d}{dq^2} G_{E_n}(0)=0.0193 \pm 0.0004$ fm^2 and was determined to be the model (of the three considered) which best describes the deuteron. The method of calculating the LF wave functions for different models and the more significant differences between the three models considered here is discussed in Appendix C.

iii) the charge radius of the deuteron was measured to be $r_{E_d} = 1.9641 \pm 0.0074$ fm. Prior to this result the most recent measurement [21] was $r_{E_d} = 1.95 \pm 0.02$ fm. The very accurate value of the reported charge radius of the deuteron was possible because all data were taken at or below

$q^2 = 0.35\ \mathrm{fm}^{-2}$ and thus it could all be used to determine the intercept and coefficient of the q^2 term in the equation

$$G_{E_n}(q^2) = G_{E_n}(0) - \frac{q^2}{6}\ r^2_{rms} \quad .$$

iv) as a check on the results of this experiment a Rosenbluth plot of all of the data taken at $q^2 = 0.2\ \mathrm{fm}^{-2}$ was produced in Figure V-5. The slope of this line is (0.0026 ± 0.0012). The theoretical slope of this line is $\frac{2}{3}\eta\ G_1^2$ (see Section II-G). Using the "scaling law" (Equation II-31) this slope becomes $\frac{2}{3}\eta(4_d G_0 \frac{M_d}{M_p})^2$ where $G_0 = (G_{E_p} + G_{E_n})C_E$. At $q^2 = 0.2$ the theoretical slope is equal to 0.000822. The experimental slope is about 1.5 σ_{Total} from this value. However, Table V-VI shows, as does Figure V-5, that the second 120° point has a significantly different value of G_d^2 than do the others. If this one point is dropped, a linear fit to the remaining 7 points gives a value of the slope of 0.0013 ± 0.0013 in good agreement with the theoretical slope. This shows that the one photon exchange is valid for the deuteron at this q^2.

APPENDIX A

DE VRIES B' FIT

De Vries *et al.* [10] analysed the proton cross section measurements of Bumiller *et al.* [11] which consisted of 58 data points, the 114 points of Janssens *et al.* [10], and the 6 points of Chen *et al.* [12] as well as the 71 deuteron cross section measurements which de Vries presented. These data were used to obtain the best fit to the three pole Clementel-Villi [40] model for the isotopic form factors given in Equations A-1. This de Vries fit is valid only in the low q^2 region.

$$G_E^S = 0.50 \left\{ \frac{S_{E_1}}{1 + \frac{q^2}{15.6}} + \frac{S_{E_2}}{1 + \frac{q^2}{26.6}} + (1 - S_{E_1} - S_{E_2}) \right\}$$

$$G_E^V = 0.50 \left\{ \frac{V_{E_1}}{1 + \frac{q^2}{M_\rho^2}} + (1 + V_{E_1}) \right\}$$

$$G_M^S = 0.44 \left\{ \frac{S_{M_1}}{1 + \frac{q^2}{15.6}} + \frac{S_{M_2}}{1 + \frac{q^2}{26.6}} + (1 - S_{M_1} - S_{M_2}) \right\}$$

$$G_M^V = 2.353 \left\{ \frac{V_{M_1}}{1 + \frac{q^2}{M_\rho^2}} + (1 - V_{M_1}) \right\} \qquad \text{(A-1)}$$

The proton form factors are

$$G_{E_p} = G_E^S + G_E^V$$

$$G_{M_p} = G_M^S + G_M^V$$

while the neutron form factors are

$$G_{E_n} = G_E^S - G_E^V$$

$$G_{M_n} = G_M^S - G_M^V .$$

De Vries started with this theoretical model given by Equations A-1 and computed cross sections which were then compared with the experimental data. The free parameters appearing in the model were adjusted so that a minimum in χ^2 was obtained.

The mass of the ρ meson was taken as a free parameter since the width of the resonance was so wide (100 MeV), but the seven other free parameters were reduced to six by applying the constraint

$$\left(\frac{d}{dq^2} G_{E_n}\right)_{q^2=0} = 0.021F^{-2}.$$

Data from the several experiments mentioned above were combined in several different combinations. A reduced chi-square was calculated for each of these. Combinations b and b' were recommended by the authors as the best fits. In this experiment the values of the free parameters given by the b' fit were used since Buchanan [68] has reanalyzed all known proton, neutron, and deuteron data and concluded that de Vries b' fit best describes the proton form factors. The

b' combination includes the data of Janssens *et al.*, de Vries *et al.*, and Chen *et al.*, and gives the following for the values of the parameters.

$S_{E_1} = 2.628$	$S_{M_1} = 4.193$
$S_{E_2} = -1.853$	$S_{M_2} = -3.435$
$V_{E_1} = 1.191$	$V_{M_1} = 1.064$
$M_\rho 2 = 8.463$	

APPENDIX B

THE VIRIAL COEFFICIENTS OF HYDROGEN AND DEUTERIUM

In this experiment the target gases were contained in a metal gas chamber that was in good thermal contact with a liquid nitrogen reservoir which was at atmospheric pressure. The chamber was filled from high pressure bottles of H_2 or D_2 through reducing and regulating valves to a gauge pressure of about 150 psig. The density of the gas in the target was then computed using the virial coefficients of H_2 and D_2 at $77.35^{o}K$ (liquid nitrogen temperature). Since the pressure was monitored continuously throughout a data run the virial expansion was calculated in terms of pressure coefficients.

Using the data of Michels and Goudeket [69] and the method given in the Handbook of Physics [70] the gas density was determined to be

$$\rho = \frac{PM}{RT}\left(\frac{1}{1+B'P+C'P^2}\right) \text{gm/cm}^3$$

where

$$B' = -0.189409 \times 10^{-3} \text{ in}^2/\text{lb}$$

$$C' = 0.1298969 \times 10^{-7} \text{ in}^4/\text{lb}^2 .$$

At 150 psig hydrogen had a density of 0.0036723 gm/cm^3 and deuterium 0.0073391 gm/cm^3.

During a run the pressure was recorded and was then used to calculate (in FORTRAN program TOPRADCR) the gas density which in turn was used in Equation IV-2 to obtain the number

of target atoms per cm^2 and in the bremsstrahlung and Landau radiation correction calculations as well as to partially determine the cross section in Equation IV-13.

The American Institute of Physics Handbook, Third Edition, which was published coincidently with the completion of the writing of this thesis, has virial coefficients different from those given in Reference 70. The data of Reference 70 was used for all calculations in this work. If the data of the AIPH, Third Edition, are used the primary results of this work will not be changed. That is, the slope of G_{E_n}, the radius of the deuteron and the slope of the Rosenbluth plot are unchanged. There will, however, be a difference in the intercepts of both $G_{E_n}(0)$ versus q^2 and of the Rosenbluth plot. This change in virial coefficients will cause the intercept of G_{E_n} to be raised to 0.0023, which might indicate that the "contaminent" in the H_2 discussed in Section IV-D is several tenths of a percent.

APPENDIX C

LOMON-FESHBACH DEUTERON ELECTRIC CHARGE STRUCTURE FACTORS

The deuteron electric charge structure factor, C_E, is defined as

$$C_E = \int \left[u^2(r) + v^2(r)\right] J_0 \left(\frac{q^r}{2}\right) dr$$

where u(r) and v(r) are respectively the deuteron S-and D-state wave functions normalized so that $C_E = 1$ when $q = 0$, J_0 is the spherical Bessel function of order zero, q is the four-momentum transferred and r is the separation between the neutron and proton. In order that one might extract the neutron form factor from data which give the shape of the deuteron one needs to have C_E, which means that one must have u(r) and v(r). These are determined from the nuclear model used. Lomon and Feshbach derived nuclear models from nucleon-nucleon data by fitting a boundary condition model interaction determined largely by field-theoretic forms [15]. Lomon and Feshbach use an energy independent boundary condition for the deuteron wave function,

$$F = r_o \left(\frac{1}{\Psi} \frac{\partial \Psi}{\partial r}\right),$$

where r_o is the range of the potential. This condition must be different in each angular momentum state [72]. E.L. Lomon [14] has provided values of C_E based upon three different nuclear models. These values of C_E are listed in Table C-I.

The three models which have been considered are called LF#1, LF#5 and LF#15 in agreement with Ref. 15. Model L-F #1 has a deuteron binding energy of 2.2242 MeV and 4.57 percent D-state; model L-F #5 has a binding energy of 2.2245 MeV and 5.202 percent D-state; model L-F #15 has a binding energy of 2.2236 MeV and 7.55 percent D-state.

TABLE C-I

LOMON-FESHBACH DEUTERON ELECTRIC CHARGE STRUCTURE FACTORS

q^2 (F^{-2})	C_E (LF#1)	C_E (LF#5)	C_E (LF#15)
0.025	0.98414	0.98413	0.98423
0.05	0.96881	0.96881	0.96899
0.10	0.93967	0.93966	0.94002
0.15	0.91235	0.91234	0.91285
0.20	0.88667	0.88665	0.88731
0.25	0.86247	0.86244	0.86324
0.30	0.83961	0.83956	0.84049
0.35	0.81796	0.81790	0.81895
0.40	0.79741	0.79735	0.79851
0.45	0.77789	0.77782	0.77907
0.50	0.75929	0.75921	0.76057
0.55	0.74156	0.74147	0.74291
0.60	0.72462	0.72452	0.72604
1.3	0.54649	0.54626	0.54854
2.0	0.43328	0.43293	0.43555
3.0	0.32637	0.32588	0.32867
4.0	0.25438	0.25378	0.25657

APPENDIX D

THE GAS TARGET SYSTEM

A schematic diagram of the gas target system as it was developed for this experiment is shown in Figure D-1. A detailed scale drawing of the gas target assembly is given by Savage [71]. In this section both the best and the poorest techniques which were used in this experiment to operate the gas target system are discussed and hopefully this will prevent others from following some unprofitable techniques.

As the linear accelerator was being turned on for a run the gas fill system was connected together between valves V7 and V8 and valves V1, V2 and V7 were opened. (Actually V7 and V8 were always open during all the runs done with the final technique.) The pressure gauge was checked to see that it read zero gauge pressure. Then valve V1 was closed and valves V3, V5 and V8 were opened. The forepump was turned on to evacuate the complete gas fill system up to valves V4 and V6 which are parts of the gas bottles. This pulled the system down to about 50 microns.

After the accelerator had been tuned for the correct energy a large (50 liter) liquid nitrogen dewar was connected to feed the liquid nitrogen reservoir. Temperature sensors were placed in this reservoir. These sensors were taped to a plastic rod and were arranged along this rod as shown in Figure D-1. Whenever the nitrogen level fell below the top

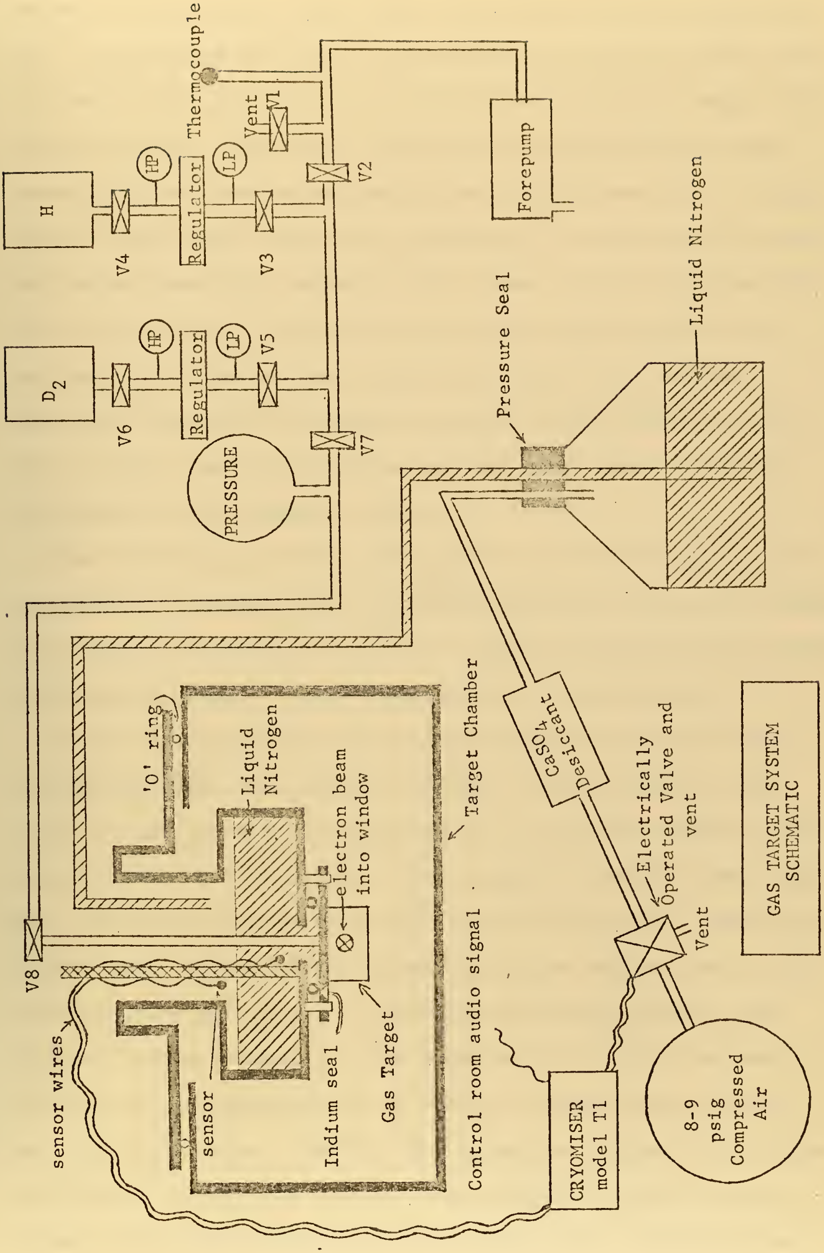
H
D_2
HP
LP
Regulator
HP
Regulator
LP
V1
V2
V3
V4
V5
V6
V7
V8
Vent
Thermocouple
Forepump
PRESSURE
Pressure Seal
Liquid Nitrogen
'O' ring
Liquid Nitrogen
electron beam into window
Target Chamber
Gas Target
Indium seal
sensor
sensor wires
Control room audio signal
CRYOMISER model T1
$CaSO_4$ Desiccant
Electrically Operated Valve and vent
Vent
8-9 psig Compressed Air
GAS TARGET SYSTEM SCHEMATIC

Figure D-I

sensor the Cryomiser would open the valve in the compressed air line forcing air into the dewar and, since the dewar had a pressure seal at the top, this forced liquid nitrogen into the gas target reservoir. Through trial and error it was found that one minute of pumping was satisfactory; if longer "fill" times were set on the Cryomiser it was found that the gas target assembly became so cold that it would harden the "O" ring seal and a serious vacuum leak would occur. A shorter fill time did not adequately fill the reservoir. The lower sensor would sound an alarm in the end station if the nitrogen level fell below it, and this audio alarm was reproduced in the control room.

In the early runs the gas target was allowed to cool for at least 15 minutes before the first gas was put in the target. In later runs, the gas was put in immediately after the liquid nitrogen was pumping; both methods were satisfactory.

After a vacuum of at least 50 microns was read on the thermocouple and the liquid nitrogen had started to pump, valve V2 was closed. A pressure of 50 microns insured that any contaminants in the gas fill system would add less than one contaminant molecule in 10^5 target molecules. Both regulators were turned to the closed position and valves V3 and V5 would also be closed. Valve V4 was then opened. The pressure gauge marked HP, for high pressure, read between 2000 to 200 psig depending of course on the amount of gas left in the bottle. The LP, low pressure, gauge should then read zero. If it did valve V3 was opened. Since the gas target had 1 mil stainless steel windows the regulator was

moved slowly and steadily in order that these windows would not be unnecessarily strained as the pressure increased from vacuum to about 150 psig. This pressure was read on both the LP gauge and on the much more accurate, larger gauge in Figure III-2 simply shown with the word pressure on its face. The regulator maintained the system very near the set pressure throughout all runs although there usually was some pressure drop for a short time while the gas and nitrogen systems reached equilibrium. A remote control TV camera was panned from the gas target to the large pressure gauge after the operator had insured that the beam was properly aligned through the gas target. The camera then generally remained on the large pressure gauge throughout the run. Since the gas pressure would drop whenever a nitrogen fill was progressing, the operator recorded the pressure of the gas at the start of the fill (i.e., when the audio warning went on in the control room) and he would also record the pressure at the end of the 1 minute fill (when the audio stopped).

After all the hydrogen data were taken valve V4 was closed and valves V2 and V5 were opened. Valve V2 was opened very slowly in order that the 1 mil stainless window would not be unloaded too quickly as it experienced the decrease from 150 psig. to vacuum. Valve V5 was opened at this time to ensure that no hydrogen leaked through it during the hydrogen fill. Again a vacuum of at least 50 microns was pulled on the entire system up to valves V4 and V6 (the regulators did not provide a vacuum barrier). After the system was down to at least 50 microns, valves V2, V3 and V5 were closed. The

regulator on the deuterium was checked to ensure that it was closed, thus there was no step-like rise in pressure on the gas target windows when valve V6 was opened. Again if the deuterium LP gauge read zero, valve V5 was opened and the deuterium regulator was turned slowly to reduce the strain on the 1 mil steel window. After reading about 150 psig. on the large gauge the system had some time to come to equilibrium as the operator re-tuned the accelerator. After checking the position and appearance of the beam on the target the remote TV camera was again put on the large pressure gauge and the gas pressure was again recorded at the start and finish of each nitrogen fill as the deuterium data were taken.

After taking the deuterium data valve V6 was closed and valves V2 and V3 were opened and the system was again pulled to at least a 50 micron vacuum. Then the accelerator beam was sent through the empty target in order to obtain empty target background at several spectrometer settings over the range of data taken on that run.

After the accelerator was secured the forepump and the cryomiser were also turned off and valve V1 was opened. This let the gas system down to air and condensed some gases, e.g. water vapor in the gas target. The gas target was not left at vacuum because it was believed that the 1 mil windows would fail if the target chamber should have had a vacuum failure. Very early in these experiments valve V8 was then closed in order that excess water would not condense in the gas target, but as the liquid nitrogen evaporated during the night the 1 mil windows were blown out - presumably due to

high vapor pressure within the gas target. The later technique was to disassemble the fill line at valve V8. This protected the target from a mishap as described above should someone have accidently closed V8 or even V1.

Finally the compressed air line was separated and was vented directly into the liquid nitrogen reservoir directly above the gas target. This accelerated the rate of evaporation of the liquid nitrogen and generally would have all the nitrogen, and more importantly, all the water which condensed during this evaporation removed from the reservoir within 12 hours. It was found that if the experimenter starts to fill the reservoir with liquid nitrogen for another run before the condensed water from the last run is completely evaporated, then he will most probably cause the indium seal between the gas target and the reservoir to fail severely - in fact in two experiments the target chamber went to air and only the quick closing automatic valve at the collimator saved the electron gun.

It should be mentioned that the gas target with valve V8 closed will not leak any detectable amount of gas during at least a 10 hour period. In the early part of this work valve V8 was closed after the initial filling of the target with gas, but the pressure at the end of the run generally did not reproduce the initial pressure - it was generally higher. These pressure variations were of the order of one percent - too much of a variation to permit the accuracy of measurement required for these experiments. Thus the open target method

described above was used with continuous monitoring of the pressure throughout the run, i.e. by recording the pressure at the start and finish of each nitrogen fill.

APPENDIX E

COMPUTER PROGRAMS USED IN DATA REDUCTION

The following FORTRAN programs were used to calculate quantities explained elsewhere in this work.

TOPRADCR calculated the Schwinger, bremsstrahlung and ionization (Landau) radiation corrections as well as the density of the deuterium and hydrogen.

TOP#FORM calculated the experimental cross section for each channel. The sample listed is the program for channel number 5 (i.e. η =5). It was also used to obtain the smoothed data which was plotted to define the elastic peak.

TOPROTON calculated the proton's Mott and Rosenbluth cross sections of the proton, the magnetic correction term and the electric and magnetic form factors of the proton based on de Vries' b' fit.

TOPDEUTR calculated the Mott cross section of the deuteron and the magnetic correction term which includes within it the relativistic correction to the wave functions.

TOPRADCR

```
      REAL M
      REAL LAMBDA
      DIMENSION PRES(8),DELT(8),ROH(8), HT(8), THW(8),B1(8),W(8),
     1          PRESH(8),PRESD(8),EELAF(8)
      DATA W(1)/ 938.25/, W(2)/ 938.25/, W(3)/938.25/, W(4)/ 938.25/
     1,W(5)/1875.5/,W(6)/1875.5/,W(7)/1875.5/, W(8)/1875.5/
      DATA B1(1)/1.0/,B1(2)/1.0/,B1(3)/1.0/,B1(4)/ 1./,B1(5)/2./, B1(6)/
     1 2./,B1(7)/2./,B1(8)/2.0/
      READ(5,301) PRES(1),PRES(2),PRES(3),PRES(4)
      WRITE(6,402)PRES(1),PRES(2),PRES(3),PRES(4)
  301 FORMAT(4F10.2)
  402 FORMAT(' HYDROGEN PRESSURE=', 4(F10.2,4X))
      READ(5,301) PRES(5), PRES(6),PRES(7),PRES(8)
      WRITE(6,302)PRES(5), PRES(6),PRES(7),PRES(8)
  302 FORMAT(' DEUTERIUM PRESSURES= ', 4(F10.2,4X))
      READ(5,303) EELAH  ,ATHETA ,DELT(1),DELT(2),DELT(3),DELT(4)
      WRITE(6,304) EELAH ,ATHETA ,DELT(1),DELT(2),DELT(3),DELT(4)
  303 FORMAT(6F10.3)
  304 FORMAT(' EHFI=',F10.2,'THETA =',F10.1,'HYDRO DELES =',4(F10.2,4X))
      READ(5,303) EELAD,   ATHETA,DELT(5),DELT(6),DELT(7),DELT(8)
      WRITE(6,305) EELAD,  ATHETA,DELT(5),DELT(6),DELT(7),DELT(8)
  305 FORMAT(' EDFI =',F10.2,'THETA =',F10.1,'DEUTR DELES =',4(F10.2,4X)
     1)
C NOW CALCULATE DENSITIES OF GAS
      REAL*4 MD,MH,M
      MH=0.0044447
      MD=0.00888272
      DATA BP /-0.189409E-3/, CP/0.129896E-7/,R/73.5915/,T/77.35/
      DO 306  I=1,4
      PRESH(I) = PRES(I) + 14.7
      ROH(I) = 27.675*(PRESH(I)*MH)  / (R*T*(1. +BP* PRESH(I) + CP *
     1PRESH(I)*PRESH(I)))
      WRITE(6,307) PRES(I) , ROH(I)
  307 FORMAT('PRESHG= ',F10.3, 5X, 'DENSITY = ' ,2X,F10.8)
  306 CONTINUE
       DO 308 I=5,8
      PRESD(I)   = PRES(I) +14.7
      ROH(I) = 27.675*PRESD(I) *MD/  (R*T*(1. +BP*PRESD(I)  +CP*PRESD(I)
     1*PRESD(I)))
      WRITE(6,309) PRES(I),  ROH(I)
  309 FORMAT('PRESD  = ',2X, F10.3,5X,'DENSITY = ' , 2X, F10.8)
```

```
  308 CONTINUE
C NOW OBTAIN INPUTS FOR RADIATION CORRECTIONS
      DO 310 I=1,4
      HT(I)  =ROH(I)* 5.08
C 5.08 IS THE 2 INCH TARGET EXPRESSED IN CM
      THW(I)   = HT(I)   / 1.007825
  310 CONTINUE
      DO 311 I=5,8
      HT(I)   = ROH(I) *5.08
      THW(I)   = HT(I) / 2.014102
  311 CONTINUE
      RHOW = 7.87
C     DENSITY OF STEEL WINDOWS   = RHOW
      XWIN   =  0.00254
C XWIN = WINDOW  THICKNESS
      TW = 2.0 * RHOW * XWIN
      Z1   = 1.0
      ZETA1 = 0.8
      AN2 =1.0
      Z2 = 26.
      A2 = 55.847
      ZETA2 = 0.8
      AK = 0.37
      EXCITE = 0.0
      EELAF(1) = EELAH
      EELAF(2) = EELAH
      EELAF(3) = EELAH
      EELAF(4) = EELAH
      EELAF(5) = EELAD
      EELAF(6) = EELAD
      EELAF(7) = EELAD
      EELAF(8) = EELAD
      DO 312 I=1,8
      AN1 = THW(I) * 55.847 / TW
      T = TW + HT(I)
      RHO  = (TW + HT(I)) / 5.0800
      EELAS = EELAF(I)
      M =W(I)
      A1 = B1(I)
      DELE = DELT(I)
      PRINT 100

      PRINT 101,Z1,Z2,A1,A2,ZETA1,ZETA2
      PRINT 201, AN1,AN2
      PRINT 102,AK,RHO,M
      PRINT 103,T,ATHETA,EXCITE, EELAS, DELE
```

```
201   FORMAT  (2X,28HNO. OF ATOMS OF ELEMENT 1 =    ,F10.5,2X,          00000910
     128HNO. OF ATOMS OF ELEMENT 2 =    ,F10.5)                         00000920
C     M = MASS OF NUCLEUS IN MEV                                        00000930
C     T = NORMAL TARGET THICKNESS IN GM/CM2                             00000940
C     AN1,2 = NO. OF ATOMS PER MOLECULE OF ELEMENT 1,2                  00000950
C     Z1,2  A1,2 = ATOMIC NO. , WT. OF ELEMENT 1,2                      00000960
                                                                        00000970
C     ZETA1,2 = WHEELER LAMB FACTOR                                     00000980
C     AK = 0.37 FOR LANDAU  0.3 FOR WILLIAMS THEORY                     00000990
C     RHO = DENSITY IN GM/CM2                                           00001000
C     ATHETA = SCATTERING ANGLE IN DEGREES                              00001010
C     EXCITE = NUCLEAR EXCITATION ENERGY IN MEV                         00001020
C     DELE = ENERGY INTERVAL OF INTEGRATION = FITLIN DEL                00001030
      THETA = ATHETA/57.2958                                            00001040
       TH = T                                                           00001050
C     TH = EFFECTIVE TARGET THICKNESS IN GM/CM2 FOR TRANSMISSION MODE   00001060
C     XO = RADIATION LENGTH IN GM/CM2                                   00001070
      XO = RADLN(AN1,Z1,A1,ZETA1,AN2,Z2,A2,ZETA2)                       00001080
      X = TH/2                                                          00001090
C     EL = RADIATION LOSS PASSING THROUGH HALF TARGET THICKNESS         00001100
      WD = W1(X,AN1,Z1,A1,AN2,Z2,A2)                                    00001110
      EL = ELOSS (X, RHO, WD, AK)                                       00001120
C     EFP = ENERGY ELASTIC + ENERGY LOSS FOR HALF TARGET THICKNESS      00001130
C     ENERGY AFTER ELASTIC SCATTER                                      00001140
      EFP = EELAS + EL                                                  00001150
C     EOP = ENERGY PRIOR TO SCATTER                                     00001160
      EOP = EFP/(1.-2.*EFP/M*SIN(THETA/2.)**2)                          00001170
C     EO = INCIDENT ENERGY                                              00001180
      EO = EOP + EL                                                     00001190
C     EF = FINAL ELECTRON ENERGY                                        00001200
      EF = (EOP-EXCITE-EXCITE**2/2./M)/(1.+2.*EOP/M*SIN(THETA/2.)**2)   00001210
     1 -EL                                                              00001220
C     CALCULATE BREMSTRAHLUNG CORRECTION                                00001230
C     XE = MEAN AVERAGE ENERGY GOING THROUGH TARGET                     00001240
      XE = SQRT(EO*EF)                                                  00001250
      BKB = AKB(XE,DELE,XO,TH)                                          00001260
C*****CALCULATE IONIZATION CORRECTION                                   00001270
      ALAM = LAMBDA(DELE,AN1,Z1,A1,AN2,Z2,A2,TH)                        00001280
      OMEG = OMEGA(ALAM)                                                00001290
      AIK = AKI(OMEG)                                                   00001300
C     CALCULATE 4-Q**2 AT CENTER OF TARGET                              00001310
C     EFPP = ENERGY AFTER SCATTER                                       00001320
      EFPP= (EOP-EXCITE -EXCITE**2/(2.*M))/(1.+2.*EOP/M*SIN(THETA/2.)**200001330
     1)                                                                 00001340
      Q42 = QSQ(EOP,EFPP,THETA)                                         00001350
      Q4 = SQRT(Q42)/197.32                                             00001360
```

```
      Q32 = QSQ3(Q42,M,EXCITE)
      Q3 = SQRT(Q32)/197.32
C     CALCULATE MOST PROBABLE ENERGY LOSS AND W1
      WID = W1(TH,AN1,Z1,A1,AN2,Z2,A2)
      ELOS = ELOSS(TH,RHO,WID,AK)
C     CALCULATE SCHWINGER CORRECTION FOR ELASTIC SCATTER
      SC = AKS (EELAS,DELE,Q42,THETA)
C     CALCULATE SCHWINGER CORRECTION FOR INELASTIC SCATTER
      SCIN = AKSIN(EOP,EFPP,DELE,Q42,THETA)
      CORR = AIK*BKB*SCIN
      FKB=1.0/(BKB*AIK)
      FKS=1.0/SCIN
      PRINT 104
      PRINT 108,EFP
  108 FORMAT(2X,31HENERGY AFTER ELASTIC SCATTER =    , F10.5 )
      PRINT 105, E0,EF,EOP,EFPP,Q4,Q3,TH,X0,ELOS,WID,ALAM,OMEG
      PRINT 106
      PRINT 107,AIK,BKB,SC,SCIN,CORR,FKS,FKB
C     INPUT
   10 FORMAT(8F10.5)
   11 FORMAT (2F10.5,F20.10)
   20 FORMAT(5F10.5)
C     OUTPUT


C     INPUT PARAMETERS
  100 FORMAT (20X,15HINPUT PARAMETERS      )
  101 FORMAT  (//,4X,16H Z OF ELEMENT 1=     , F10.5,4X,16HZ OF ELEMENT 2
     1 =    , F10.5,/,4X,16HA OF ELEMENT 1 =      ,F10.5,4X,16HA OF ELEMEN
     2T 2 =    ,F10.5,/,2X,19HZETA OF ELEMENT 1 =  ,F10.5,2X, 19HZETA OF
     3ELEMENT 2 =     , F10.5,/)
  102 FORMAT (6X,14HIONIZATION K = , F10.5, 2X, 18HDENSITY (GM/CM2) =
     1, F10.5 ,/,14X,6HMASS =  , F20.10,//)
  103 FORMAT (  5X,25HNORMAL TARGET THICKNESS =    ,F10.5,2X,
     18H(GM/CM2)    ,/,12X, 18HSCATTERING ANGLE =     ,F10.5,2X,7HDEGREES
     2  ,/,11X,19HEXCITATION ENERGY =    ,  F10.5,2X,3HMEV,/9X,21HELASTIC
     3 PEAK ENERGY =        , F10.5,2X,3HMEV,/,30HINTEGRATION INTERVAL(DELT
     4AE)=          ,F10.5,2X,3HMEV         )
C     OUTPUT PARAMETERS
  104 FORMAT (20X,  17HOUTPUT PARAMTERS,/,10X,19HALL ENERGIES IN MEV
     1    ,//)
  105 FORMAT  (13X,17HINCIDENT ENERGY =   ,F10.5,16X,14HFINAL ENERGY =   ,
     2F10.5,/,5X,25HENERGY PRIOR TO SCATTER = , F10.5,8X,22HENERGY AFTER
     3 SCATTER =     ,F10.5    ,/,3X,27H4-MOMENTUM TRANSFER (F-1) =
     4, F10.5,3X,27H3-MOMENTUM TRANSFER (F-1) =      ,F10.5,/,5X,
     5  37HEFFECTIVE TARGET THICKNESS (GM/CM2) =     ,F10.5, /,
```

```
     63X,27HRADIATION LENGTH (GM/CM2) =    ,F10.5,2X,33HMOST PROBABLE ENE
     7RGY LOSS(MEV) =     ,F10.5,1X,/,1X,
     839HW1 (3.98W1L OR 3.9W1W = ION. WIDTH ) =    ,F10.5,/,16X,15HLANDAU
     9  LAMDA =  ,F10.5 ,16X, 14HLANDAU OMEGA =  ,F10.5)
 106  FORMAT  (//, 1X,18HCORRECTION FACTORS,/, 1X,10HIONIZATION,7X,
     2 14HBREMSSTRAHLUNG   ,6X, 14HSCHWINGER ELAS, 6X,14HSCHWINGER INEL
     3     ,15X, 5HTOTAL,6X,3HFKS,19X,3HFKB)
 107  FORMAT ( 1X,F10.5,10X,F10.5, 10X,F10.5,10X,F10.5,10X,F10.5,7X,F8.6
     1,14X,F8.6,///)
      WRITE(6,500) HT(I), THW(I),TW
  500 FORMAT( 3(E20.6))
  312  CONTINUE
      END
      REAL FUNCTION AKSIN(E1,E2,DELE,QSQ,THETA)
C     SCHWINGER INELASTIC CORRECTION
C     MAXIMON, MIT SUMMER STUDIES REPORT P.249
      PI = 3.1415927
      ALPHA = 1./137.0388
      ALPHPI = 2.*ALPHA/PI
      EMASS = 0.510976
      EM2 = EMASS**2
      X = SQRT(E1*E2)/DELE
      DELS = ALPHPI*ALOG(X)*(ALOG(QSQ/EM2)-1.)
      FACTOR = 1. + ALPHPI*(13./12.*(ALOG(QSQ/EM2)-1.) -17./36.-.5*(
     1PI**2/6.-SPENCE(COS(THETA/2.)**2))-.25*ALOG(E1/E2)**2)
      AKSIN = EXP(-DELS)*FACTOR
      RETURN
      END
      REAL FUNCTION AKS(E,DELE,QSQ,THETA)
C     SCHWINGER CORRECTION FOR ELASTIC SCATTER
C     MAXIMON, MIT SUMMER STUDIES REPORT, P.245
      PI = 3.1415927
      ALPHA = 1./137.0388
      ALPHPI '= 2.*ALPHA/PI
      EMASS = 0.510976
      EM2 = EMASS**2
      DELS = ALPHPI*ALOG(E/DELE)*(ALOG(QSQ/EM2)-1.)
      FACTOR = 1. + ALPHPI*(13./12.*(ALOG(QSQ/EM2)-1.)-17./36.-
     1.5*(PI**2/6. - SPENCE(COS(THETA/2.)**2)))
      AKS = EXP(-DELS)*FACTOR
      RETURN
      END
      REAL FUNCTION AKB(E.DELE,X0,T)
C     BREMSSTRAHLUNG CORRECTION

C     BETHE AND ASHKIN, IN SEGRE, EXP NUC PHYS VOL  1
```

```
      AKB = EXP((T/(X0*.6931472))*ALOG(DELE/E))                         00002290
      RETURN                                                            00002300
      END                                                               00002310
      REAL FUNCTION LAMBDA(DELE,AN1,Z1,A1,AN2,Z2,A2,T)                  00002320
C*****LANDAU LAMBDA APPROXIMATION BERGSTROM MIT REPORT EQTN 11          00002330
      XI = 0.154*(AN1*Z1+AN2*Z2)/(AN1*A1+AN2*A2)*T                      00002340
      LAMBDA = DELE/XI - 0.05                                           00002350
      RETURN                                                            00002360
      END                                                               00002370
      REAL FUNCTION OMEGA(ALAM)                                         00002380
C     OMEGA APPROXIMATION                                               00002390
C     BORSCH-SUPAN, JOURNAL OF RESEARCH, NBS, 65B,1961, EQTN 10         00002400
      OMEGA = ALAM*(1.-(ALOG(ALAM)-0.42228)/(ALAM+1.))                  00002410
      RETURN                                                            00002420
      END                                                               00002430
      REAL FUNCTION AKI(OMEG)                                           00002440
C     LANDAU CORRECTION                                                 00002450
      AKI = 1.-1./OMEG                                                  00002460
      RETURN                                                            00002470
      END                                                               00002480
      REAL FUNCTION RADLN(AN1,Z1,A1,ZETA1,AN2,Z2,A2,ZETA2)              00002490
C     RADIATION LENGTH                                                  00002500
                                                                        00002510
C     MODIFICATION OF BUTCHER AND MESSEL NP 20(1960) P15,EQTN AFTER 7   00002520
      RE = 2.81777                                                      00002530
      ALPHA = 1./137.0388                                               00002540
      RADLN = 4.*RE**2*6.0225*.001*ALPHA                                00002550
      DENOM = AN1*A1+AN2*A2                                             00002560
      Z3 = ALOG(Z1)/3.                                                  00002570
      Z3 = EXP(Z3)                                                      00002580
      TNUM = AN1*Z1*(Z1+ZETA1)*(ALOG(183./Z3))                          00002590
      Z3 = ALOG(Z2)/3.                                                  00002600
      Z3 = EXP(Z3)                                                      00002610
      TNUM = TNUM + AN2*Z2*(Z2+ZETA2)*(ALOG(183./Z3))                   00002620
      RADLN = RADLN*TNUM/DENOM                                          00002630
      RADLN = 1./RADLN                                                  00002640
      RETURN                                                            00002650
      END                                                               00002660
      REAL FUNCTION QSQ(E1,E2,THETA)                                    00002670
C     QSQ = 4-MOMENTUM TRANSFER SQUARED IN MEV**2                       00002680
      QSQ = 4.*E1*E2*SIN(THETA/2.)**2                                   00002690
      RETURN                                                            00002700
      END                                                               00002710
      REAL FUNCTION QSQ3(QSQ,M,EXCITE)                                  00002720
      REAL M                                                            00002730
C     QSQ3 = 3-MOMENTUM TRANSFER SQUARED IN MEV**2                      00002740
```

```
      QSQ3 = ((QSQ/2./M) + EXCITE + EXCITE**2/(2.*M))**2 + QSQ
      RETURN
      END
      REAL FUNCTION ELOSS(X,RHO,W1,AK)
C     MOST PROBABLE ENERGY LOSS
C     BETHE AND ASHKIN IN SEGRE, EXP NUC PHYS VOL 1
      ELOSS = W1
      Y = X/RHO
      FACTOR = ALOG(Y) + 18.057448 - AK
      ELOSS = ELOSS*FACTOR
      RETURN
      END
      REAL FUNCTION W1(X,AN1,Z1,A1,AN2,Z2,A2)
      TUPI = 6.28319
      RE = 2.81777
      HBC = 197.32
      ALPHA = 1./137.0388
      AVOG = 0.0060225
      ZOVA = (AN1*Z1+AN2*Z2)/(AN1*A1 +AN2*A2)
      W1 = (TUPI*ALPHA*RE*HBC)*AVOG*X*ZOVA
      RETURN
      END
      REAL FUNCTION FTHICK(T,THETA)
      FTHICK = T/COS(THETA/2.)
C     FTHICK = EFFECTIVE TARGET THICKNESS
      RETURN
      END
      REAL FUNCTION SPENCE(X)
C*****
C*****
C*****
C*****THIS ROUTINE EVALUATES THE SPENCE FUNCTION FOR THE VARIABLE X
C*****FOR X BETWEEN 0. AND 1.  AN INTERPOLATION OF A STORED TABLE OF
C*****VALUES OF THE FUNCTION IS USED.
C*****FOR X OUTSIDE THIS RANGE , THE FUNCTION IS DETERMINED  USING
C*****A SET OF TRANSFORMATION EQUATIONS.
C*****AN INTERPOLATION ROUTINE IS REQUIRED  'POL'
C*****
C*****
      REAL L2,M2,N2
      DIMENSION L2(50), M2(46), N2(9)
      EQUIVALENCE (L2(50), M2(1)  )
      EQUIVALENCE (M2(46), N2(1)  )
      DATA L2/     .000000   ,.010025  ,.020101  ,.030228  ,.040407   ,
     1             .050639   ,.060925  ,.071265  ,.081660  ,.092110   ,
```

```
     2              .102618   ,.113183  ,.123806  ,.134489  ,.145231   , 00003200
     3              .156035   ,.166901  ,.177830  ,.188822  ,.199880   , 00003210
     4              .211004   ,.222195  ,.233454  ,.244782  ,.256182   , 00003220
     5              .267653   ,.279197  ,.290815  ,.302509  ,.314280   , 00003230
     6              .326130   ,.338059  ,.350070  ,.362163  ,.374342   , 00003240
     7              .386606   ,.398958  ,.411400  ,.423934  ,.436561   , 00003250
     8              .449283   ,.462103  ,.475022  ,.488043  ,.501168   , 00003260
     9              .514399   ,.527739  ,.541191  ,.554756  ,.568438    /00003270
      DATA M2 /     .568438   ,                                          00003280
     1              .582241   ,.596165  ,.610216  ,.624396  ,.638709   , 00003290
     2              .653158   ,.667747  ,.682480  ,.697361  ,.712395   , 00003300
     3              .727586   ,.742940  ,.758460  ,.774154  ,.790026   , 00003310
     4              .806083   ,.822330  ,.838776  ,.855427  ,.872292   , 00003320
     5              .889378   ,.906694  ,.924251  ,.942058  ,.960127   , 00003330
     6              .978469   ,.997099  ,1.016030 ,1.035278 ,1.05486   , 00003340
     7              1.074795  ,1.095103 ,1.115808 ,1.136936 ,1.158516  , 00003350
     8              1.180581  ,1.203168 ,1.226320 ,1.250087 ,1.274529  , 00003360
     9              1.299715  ,1.325729 ,1.352675 ,1.380685 ,1.409928  / 00003370
      DATA N2 /     1.409928  ,                                          00003380
     1              1.440634  ,1.473126 ,1.507899 ,1.545800 ,1.588625  , 00003390
     2              1.644934  ,1.701243 ,1.757552                      / 00003400
      IF( ( X .GE. 0. ) .AND. (X .LE. 1.) ) GO TO 1                      00003410
      IF( X .GT. 1. ) GO TO 2                                            00003420
      IF( ( X .GE.(-1.)).AND. (X .LT. 0. ) ) GO TO 3                     00003430
      IF ( X .LT.(-1.)) GO TO 4                                          00003440
      PRINT 5, X                                                         00003450
 5    FORMAT( /// 30H  ERROR SPENCE FUNCTION X=        ,   F15.5 , //// ) 00003460
      RETURN                                                             00003470
 1    SPENCE = POL( X, L2,0.,.01,103   )                                 00003480
      RETURN                                                             00003490
 2    SPENCE = 3.2898681E0-ALOG(X) **2 / 2. - POL(1./X,L2,0.,.01,103    )00003500
      RETURN                                                             00003510
 3    SPENCE = POL( X**2,L2,0.,.01, 103) /2. -                           00003520
     1   POL( ABS(X), L2,0.,.01,103    )                                 00003530
      RETURN                                                             00003540
 4    SPENCE = -1.6449341E0 + POL(1. /(1.-X) ,L2, 0., .01, 103 )  -      00003550
     1     ALOG( 1.-X) * ALOG( X**2 / (1.-X) ) /2.                       00003560
      RETURN                                                             00003570
      END                                                                00003580
      REAL FUNCTION POL( X,FX,XL,DX,N   )                                00003590
C*****                                                                   00003600
C*****                                                                   00003610
C*****THIS IS A LINEAR INTERPOLATION ROUTINE BASED ON A TAYLOR'S         00003620
C*****EXPANSION TO SECOND DIFFERENCES                                    00003630
C*****X - INDEPENDENT VARIABLE                                           00003640
C*****FX- TABLE OF DEPENDENT VARIABLE Y=F(X) FOR EQUALLY SPACED          00003650
C*****VALUES OF X                                                        00003660
```

```
C*****XL-  VALUE OF X FOR FIRST ENTRY IN TABLE FOR Y                    00003670
C*****DX-  INDEPENDENT VARIABLE SPACING                                 00003680
C***** N - NUMBER OF TABLE ENTRIES                                      00003690
C*****                                                                  00003700
C*****                                                                  00003710
      DIMENSION FX(1)                                                   00003720
      IF( X .LT. XL ) PRINT 1, X, XL                                    00003730
      K = ( X-XL )/DX                                                   00003740
      I = K + 1                                                         00003750
      IF( I .GT. (N-2) ) PRINT 2,I,N,X,XL,DX                            00003760
      XI = XL + DX*FLOAT(K)                                             00003770
      P = (X-XI) / DX                                                   00003780
      POL = ( (P-1.)*(P-2.)/2. ) * FX(I) +P * (2.-P) * FX(I+1)    +     00003790
     1     ( P * (P-1.)/2. ) * FX(I+2)                                  00003800
      RETURN                                                            00003810
 1    FORMAT ( /// 35H ERROR - INTERPOLATION ROUTINE X =    F15.5,      00003820
     1   5H XL =  F15.5 //        )                                     00003830
 2    FORMAT( ///  35H ERROR - INTERPOLATION ROUTINE I=    I4,          00003840
     1    3H N=  I4,   3H X=  F15.5,3HXL= F15.5, 3HDX= F15.5  ///     )00003850
      END                                                               00003860
```

TOP5FORM

```
      DIMENSION N(100),M(100),T(100),H(100),L(100),E(100),W(100),X(100)
      DIMENSION NN(100),MM(100),TT(100),HH(100),LL(100),EE(100),WW(100)
      DIMENSION XX(100),COUNTU(100),COUNTL(100),CNTVU(100),CNTVL(100)
      DIMENSION TNN(100),URATE(100),RATEL(100),TNU(100),TNL(100),C(100)
      DIMENSION TNNP(100)
      DIMENSION DIFF(100)
      DIMENSION PEAK(100)
C  THIS PROGRAM CALCULATES THE CROSS SECTION FOR EITHER HYDROGEN OR
C  DEUTERIUM, WHICHEVER IS IN THE GAS TARGET. THIS IS ONLY FOR GAS TARGT
      REAL*4  NUMER, NA, NCAP
C  NA (AVOGADRO,S NUMBER) NCAP (THE POWER OF THE CAPACITOR IN FARADS)
      DATA  EC/1.6E-19/,NA/6.023E23/,NCAP/1.0E-6/
      READ(5,99) FKS,FKB,        RHO,TH,A,PSI
C  FKS (SCHWINGER CORRECTION E.G. 1.05), FKB(BETHE CORRECTION E.G. 1.03)
C BETHE CORRECTION IS ACTUALLY THE PRODUCT OF THE BREMSSTRAHLUNG AND
C THE IONIZATION CORRECTIONS OF TOPRADCR
C                                  RHO (TARGET DENSITY IN GM/CM3),
C  TH (TARGET THICKNESS IN CM), A ( MASS OF MOLECULE IN AMU E.G. 16.02)
C  PSI (ANGLE OF THE TARGET IN DEGREES)
      WRITE(6,401) NA
  401 FORMAT(1H0,'FKS           FKB         RHO          TH         MOL. MASS  ANGL
     1E(PSI)    NA=',E16.6)
      WRITE(6,99) FKS,FKB,RHO,TH,A,PSI
   99 FORMAT(6F10.6)
      NUMER=(EC*FKS*FKB)/(2.0*0.0034877*NCAP)
      DENOM1=(RHO*TH*NA*1.831E-3)
      DENOM2=A*COS(PSI*6.28318/360.0)
      DENOM=DENOM1/DENOM2
      WRITE(6,120) DENOM1,DENOM2,DENOM
  120 FORMAT(3E16.6)
      CONSTA =NUMER/(0.001*DENOM)
      WRITE(6,117) DENOM,NUMER
  117 FORMAT(2E16.6)
      READ(5,103) SEMU, NBACKG, CBKG, VBKG, JAY
      WRITE(6,402) EC
  402 FORMAT(1H0,'     SEMU          NBACKG CBKG      VBKG          JAY
     1            EC=',E16.6)
      WRITE(6,103) SEMU,NBACKG, CBKG, VBKG ,JAY
  103 FORMAT(F10.6,I10,2F10.2,I10)
C  THE CONSTANT 0.001 ACCOUNTS FOR THE FACT THAT VOLTAGE IS GIVEN IN MV
C  SEMU  (EFFICIENCY OF THE SEM WITH THE UPPER TARGET MATERIAL EG 0.03)
      K=0
  600 READ(5,650,END=800)NUFIVE,NUBACK,UTIME,UEMACH,NUVOLT,UESET,UCAPAC,
     1 INTU,UMETER
      UINT=INTU/100.0000
```

```
      IF(UMETER.NE.0.0) UMET =UMETER                                    00000460
      IF(UINT.NE.0.0) WIU=UINT                                          00000470
  650 FORMAT(29X,1I6,45X,/I7,1X,F6.1,1X,F6.2,1X,I6,1X,F6.2,1X,F6.2,2X,  00000480
     1 I5,2X,F10.2)                                                     00000490
      NC=K+1                                                            00000500
      WRITE(6,301) NC                                                   00000510
  301 FORMAT(1H0,'NUFIVE   NUBACK      UTIME     UEMACH  NUVOLT UESET   00000520
     1UCAPAC  . UINT      UMETER           K=',I3)                      00000530
  675 WRITE(6,690) NUFIVE,NUBACK, UTIME,UEMACH,NUVOLT,UESET,UCAPAC,UINT 00000540
     1  ,UMET                                                           00000550
  690 FORMAT(1H0,I6,1X,I6,2F10.2,I7,4F10.4)                             00000560
      K=K+1                                                             00000570
      N(K)=NUFIVE                                                       00000580
      M(K)=NUBACH                                                       00000590
      T(K)=UTIME                                                        00000600
      H(K)=UEMACH                                                       00000610
      L(K)=NUVOLT                                                       00000620
      E(K)=UESET                                                        00000630
      W(K)=UCAPAC                                                       00000640
      X(K)=WIU                                                          00000650
      C(K)=UMET                                                         00000660
      WRITE(6,302) NBACKG                                               00000670
  302 FORMAT(1H0,'NUVOLT   WIU       UMET                               00000680
     1                                  NBACKG='I4)                     00000690
      WRITE(6,779) L(K),X(K),C(K)                                       00000700
  779 FORMAT(I6,1X,2F10.4)                                              00000710
      GO TO 600                                                         00000720
C     CALCULATE THE INTEGRAL                                            00000730
  800 LIM=K-1                                                           00000740
      SUM=0.0                                                           00000750
      LIMIT=LIM +1                                                      00000760
      DO 550 I=1,LIMIT                                                  00000770
      URATE(I)=N(I)/T(I)                                                00000780
      COUNTU(I)= N(I)/(1-.00097*URATE(I))                               00000790
      CNTVU(I)=COUNTU(I)*C(I)/X(I)                                      00000800
      BKG=(NBACKG*SEMU)/(CBKG*VBKG*C(I)/30.00)                          00000810
      TNU(I)=(CNTVU(I)*SEMU)/ (W(I)*L(I)*C(I)/30.00)                    00000820
      TNN(I)=TNU(I)-BKG                                                 00000830
      WRITE(6,303) I                                                    00000840
  303 FORMAT(1H0,'COUNTU             CNTVU              ENERGY       TNU 00000850
     1          BKG      I=',I3)                                        00000860
      WRITE(6,201) COUNTU(I),CNTVU(I),E(I),TNU(I),BKG                   00000870
  201 FORMAT(1H0,5F15.4)                                                00000880
      WRITE(6,304) LIMIT                                                00000890
  304 FORMAT(1H0,'URATE       NUVOLT         TNN    LIMIT=',I4)         00000900
      WRITE(6,70) URATE(I),L(I),TNN(I)                                  00000910
   70 FORMAT(F10.4,1X,I6,1X,1F16.4)                                     00000920
      PEAK(I)  = CNTVU(I) - NBACKG                                      00000930
```

```
      WRITE(6,963) PEAK(I),E(I)
  963 FORMAT(5X,'PEAK = ',F10.2,2X,'ENERGY =',F10.2)
  550 CONTINUE
      DO 660 J=1,LIM
      KK=5
      TMP=(TNN(J)+TNN(J+1))*(E(J)-E(J+1))/(E(J)*(1.0+0.0039*(KK-5)))
      WRITE(6,305) J
  305 FORMAT(1HO,'SUM                    TMP                    CONSTA
     1  J=',I4)
      WRITE(6,202) SUM,TMP,CONSTA
  202 FORMAT(3E16.6)
      SUM= SUM + TMP
  660 CONTINUE
      CROSS= SUM * CONSTA
      WRITE(6,94) CROSS
   94 FORMAT(1HO,'CROSS SECTION =', E16.6)
      CNTSUM=0.0
      DIFF(I) = 0.0
      PARSUM = 0.0
      NISUM =0.0
      DO 662 I=1, LIMIT
      NISUM = N(I) + NISUM
  662 CONTINUE
      DO 562  I=1,LIMIT
      PARSUM = CNTVU(I) - NBACKG
      CNTSUM=CNTSUM+PARSUM
      WRITE(6,563) CNTSUM , NISUM
  563 FORMAT(1HO,'SUM OF HYDROGENIC COUNTS =',F10.2,5X,'TOTAL COUNTS =',
     1I10)
  562 CONTINUE
C   STATISTICAL PERCENTAGE HERE INCLUDES BACKGROUND EFFECT
        A =NBACKG/ FLOAT(JAY)
        B = LIMIT * LIMIT
      BB = A*B
       D = FLOAT(NISUM) + BB
      F  = FLOAT(LIMIT) * FLOAT(NBACKG)
      EQ= FLOAT(NISUM) -F
      G =EQ*EQ
      Z  = D/G
      WRITE(6,927) A,B,BB,D,F,EQ,G, Z
  927 FORMAT(8E15.5)
      STAT=1.*(NISUM + ((LIMIT)**2)*NBACKG/JAY  ) / (NISUM-(LIMIT)*
     1NBACKG)**2
      STATP = 100.0 * SQRT(Z)
      WRITE(6,72) STATP
   72 FORMAT(1HO, 'STATISTICAL PERCENTAGE DUE TO # OF COUNTS=' F10.5)
      STOP
      END
```

```
      REAL*4 MRHO, MC2,MOTT,MOTTM ,MOTTRC ,MU ,MRHO2,KPM
      DATA  MC2/ 938.19995/,EC/1.60210E-19/,EPSIL  /8.8543E-12/
   99 READ(5,100,END=999) ENERGY,THETA
  100 FORMAT(2F10.5)
C  THIS PROGRAM  CALCULATES THE MOTT,MOTT PLUS RECOIL(MOTTRC) FOR PROTON
C  MOTT SCATTERING (ELECTRON HAS SPIN AND A DIRAC MAGNETIC MOMENT. THE
C  NUCLEUS HAS NEITHER SPIN NOR MAGNETIC MOMENT , HOFSTADTER P221,
C  EC= ELECTRON CHARGE
C  ELECTRON SPEED IS ASSUMED =C.
C  EPSILON= PERMITTIVITY OF FREE SPACE (IN UNITS OF(COULOMB)**2*(SEC)**2
C *(METERS)**-3*(KG)**-1  (RICHTMYER,K,C  COVER)
C MOTTM IS IN MKS UNITS
      A=(EC**2/(ENERGY**2))
         B= (COS(THETA*6.28318/(2.0*360.))) **2
      C=COS(THETA *6.28318/(2. *360.))  **2
      D=SIN(THETA*6.28318/(2.0*360.))
      E  =D**2
      Y =E**2
      F=    ((3.14159*EPSIL  *4)**2) *4
      MOTTM    =(  (A*B)/(Y*F))*EC**2
      WRITE(6,110) A,B,C,D,E,F
  110 FORMAT(E15.6,F10.6,F10.6,F10.6,F10.6,E15.6,/)
C     ENERGY = TOTAL ENERGY (INCLUDING REST ENERGY)
C     TO CONVERT  MOTT  TO   CM**2 AND MEV UNITS MODIFY IT AS FOLLOWS:
      MOTT = MOTTM*10000*(6.242E12)**2
C 10000CM2 =1METER2,  1JOULE= 6.242E12 MEV, MOTT IN  CM2 , ENERGY IN MEV
C  THETA IN DEGREES
C  NOW CALCULATE THE ENERGY OF THE RECOILING ELECTRON IN A PROTON
C  COLLISION
C  HOFSTADTER  PAGE 227  NUCLEAR AND NUCLEON STRUCTURE ( ELASTIC
C  SCATTERING)
      ENUC =((ENERGY )**2/MC2)*(1-COS(THETA*6.283180/360.))/  (1+(ENERGY/
     1MC2)*(1 -COS(THETA*6.283180/360.)))
      ENELAS = ENERGY-ENUC
C  NOW DO MOTT WITH RECOIL  CALL THIS MOTTRC  HOFSTADTER P 231 =SIGMA NS
      G =(2.0*ENERGY)/MC2
      GG=G*E
      H =1. + GG
      MOTTRC  =MOTT/H
C  THIS PROGRAM CALCULATES  THE  QFOUR   AND  ROSENBLUTH CROSS SECTION
C  OF A PROTON
C NOW CALCULATE  THE FOUR MOMENTUM  TRANSFER   Q4   FROM  HOFSTADTER
C  HIGH ENERGY ELECTRON SCATTERING TABLES  PAGE 6
```

```
C  FIRST GET THE SPEED OF LIGHT TIMES PLANCK'S CONSTANT (HBARC IN MEV-
C  FERMI)
      HBARC=(6.5819E-22)*( 2.997925E10)* (1.0E13)
      AA=  2.0*ENERGY/HBARC
      AB= 1.0 +2.0*ENERGY*E/MC2
      AC= SQRT(AB)
      Q4=AA*D/AC
      WRITE(6,401) AA,AB,AC
  401 FORMAT(3F15.6)
C     THE APPROXIMATION  MASS(ELECTRON) GOES TO  ZERO   (MUIRHEAD P514)
C     IS  USED IN THE ABOVE  DERIVATION
C     Q4 IN UNITS OF  FERMI'S -1
C THIS PROGRAM CALCULATES THE  PROTON AND NEUTRON  ELECTRIC AND MAGNETIC
C FORM FACTORS:  DE VRIES  PHYS REV  134  #4B
C FORM FACTORS  USING  DE VRIES  B' MODEL  ( BROOKS & SESSLER  P13 )
      DATA  SE1/2.628/,SE2/-1.853/,SM1/4.193/,SM2/-3.435/, VE1/1.191/,
     1VM1/1.064/, MRHO2/8.463/
C     MRO2 IS IN UNITS OF  F-2
      QSQR = Q4*Q4
C  MRHO IS DE VRIES  SYMBOL FOR  MASS OF RHO MESON. MC2 =PROTON MASS
C  TIMES THE SPEED OF LIGHT SQUARED
      GES = 0.50*(SE1/(1+QSQR/15.6) + SE2/(1+QSQR/26.6) +(1-SE1 -SE2))
      GEV = 0.50*(VE1/(1+QSQR/MRHO2) + (1-VE1))
      GMS = 0.44*(SM1/(1+QSQR/15.6) + SM2/(1+QSQR/26.6) +(1-SM1 -SM2))
      GMV = 2.353*(VM1/(1+QSQR/MRHO2) + (1-VM1)    )
      GEP = GES + GEV
      GMP = GMS + GMV
      GEN = GES - GEV
      GMN = GMS - GMV
      WRITE(6,101)  GEP, GMP , GEN , GMN  , QSQR
  101 FORMAT(5X,'DE VRIES B PRIME FORM FACTORS:'//,6X,'GEP=',2X,F8.6,
     1 6X,'GMP=',2X,F9.6,6X,'GEN=',2X,F9.6,6X,'GMN=',2X,F9.6,6X,  /,2X,/
     2,2X,'4-MOMENTUM TRANSFER  TO PROTON SQUARED =',2X,F10.6,2X,'F-2')
C    NOW DO THE ROSENBLUTH  CROSS SECTION FOR A PROTON  (ROSENE): FROM
C     MUIRHEAD  P514 TO 518   AND  KALLEN  P225
C  NOTE THAT (HQ/2(MC)) SQUARED=((HBARC*Q4)/(2*MC2)) SQUARED
      TAU= (  (HBARC*Q4)/(2*MC2))**2
C     ROSENE  USES  DE VRIES  FORM FACTORS
      ROSENE =  MOTTRC*    ( GEP*GEP/( 1+TAU)  +TAU*GMP*GMP/(1+TAU)
     1  + TAU*GMP*GMP*2*(TAN(THETA*6.28318/(2*360.)))**2 )
C    NOW ASSUME THAT  SCALING  HOLDS AND  COMPUTE ROSENBLUTH  CROSS
C  SECTION WITH SCALING, CALL IT ROSENS
C LET GMPS  BE GMP SCALED BY   GMPS =  MUP*GEP  ;  MUP = KAPPA +1 = 2.79
      GMPS = 2.7927*GEP
      ROSENS =  MOTTRC * (( GEP*GEP) * ( 1/(1+TAU)) + TAU*GMPS*GMPS/ (1
     1  +TAU) + TAU*GMPS*GMPS*2*( TAN (THETA*6.28318/ (2*360.)))**2 )
C     NOW CALCULATE  THE  ABSOLUTE  PROTON FORM FACTOR CALL  GPABSS
C     WHEN USING ROSENS SCALED AND  GPABSE WHEN USING ROSENE
```

```
      GPABSS=  ROSENS / MOTTRC                                          00000940
      GPABSE = ROSENE / MOTTRC                                          00000950
      WRITE(6,102)  ENERGY , THETA ,MC2                                 00000960
  102 FORMAT(5X,'INCIDENT ENERGY =',F10.4,2X,'MEV',6X,'THETA =',2X,F10.300000970
     1,2X,'DEGREES',6X,'MASS =',2X,F12.7,2X,'MEV',/)                    00000980
      WRITE(6,103)  MOTTRC                                              00000990
  103 FORMAT(5X,'MOTT CROSS SECTION (INCL RECOIL) FOR PROTON =',E15.6,2X00001000
     1,'CM2' ,/)                                                        00001010
      WRITE(6,104) ENELAS                                               00001020
  104 FORMAT('  ENERGY OF ELASTIC SCATTERING ELECTRON FROM PROTON =',2X,00001030
     1 F10.4,2X,'MEV',/)                                                00001040
      WRITE(6,105) Q4                                                   00001050
  105 FORMAT(5X  ,'FOUR MOMENTUM TRANSFER =',2X,F10.7,2X,'F-1',/)       00001060
      WRITE(6,106) HBARC, TAU,  ROSENE , ROSENS                         00001070
  106 FORMAT(5X,'HBARC =',E15.5 ,'MEV-FERMI',6X,'TAU =  ',F10.6, / ,    00001080
     1 5X,'ROSENBLUTH CROSS SECTION WITH DEVRIES FORM FACTORS =  ',E15.600001090
     2,'  CM2',/,5X,'ROSENBLUTH CROSS SECTION WITH SCALING LAWS = ',E15.00001100
     36,' CM2',/)                                                       00001110
      WRITE(6,107) GPABSE , GPABSS                                      00001120
  107 FORMAT(5X,'ROSENE ABSOLUTE  FORM FACTOR SQUARED =  ',F10.6, /,5X, 00001130
     1'ROSENS ABSOLUTE FORM FACTOR SQUARED =',F10.6 ,//)                00001140
      WRITE(6,108) MOTTM,MOTT                                           00001150
  108 FORMAT(2E15.6)                                                    00001160
      WRITE(6,109)GES,GEV,GMS,GMV                                       00001170
  109 FORMAT(4F10.6)                                                    00001180
      WRITE(6,210) G,H,GG                                               00001190
  210 FORMAT(3F15.5)                                                    00001200
      MU = 2.79                                                         00001210
      X  =  ( TAN(THETA*6.28318   / (  360. * 2.   )))**2               00001220
       CP = TAU * MU * MU * ( 1. + 2. * ( 1. + TAU ) * X  )             00001230
       KPM  = ( 1. + TAU ) / ( 1. + CP )                                00001240
      WRITE(6,220) KPM,CP                                               00001250
  220 FORMAT(5X, ' MAGNETIC CORRECTION TERM = ', F10.6,2X,//, 'THIS MAGN00001260
     1ETIC CORRECTION IS OBTAINED BY USING THE  SCALING GM = MU*GE','CP=00001270
     1 ', F10.6)                                                        00001280
      WRITE(6,901)                                                      00001290
  901 FORMAT(//,5X,'**************************************************')00001300
      GO TO 99                                                          00001310
  999 CONTINUE                                                          00001320
      STOP                                                              00001330
      END                                                               00001340
```

TOPDEUTR

```
      REAL*4 MRHO, MC2,MOTT,MOTTM ,MOTTRD ,MUP,MRHO2,KDM                00000030
      REAL*4 MC2PRO, MUDEU                                              00000040
      DATA  MC2PRO/  938.19995/                                         00000050
      DATA  MC2/1875.5    /,EC/1.60210E-19/,EPSIL  /8.8543E-12/         00000060
   99 READ(5,100,END=999) ENERGY,THETA                                  00000070
  100 FORMAT(2F10.5)                                                    00000080
C  THIS PROGRAM  CALCULATES THE MOTT,MOTT PLUS RECOIL(MOTTRC) FOR THE   00000090
C  DEUTERON                                                             00000100
C  MOTT SCATTERING (ELECTRON HAS SPIN AND A DIRAC MAGNETIC MOMENT. THE  00000110
C  NUCLEUS HAS NEITHER SPIN NOR MAGNETIC MOMENT , HOFSTADTER P221, THE  00000120
C  EC= ELECTRON CHARGE                                                  00000130
C  ELECTRON SPEED IS ASSUMED =C.                                        00000140
C  EPSILON= PERMITTIVITY OF FREE SPACE (IN UNITS OF(COULOMB)**2*(SEC)**200000150
C *(METERS)**-3*(KG)**-1  (RICHTMYER,K,C  COVER)                        00000160
C MOTTM IS IN MKS UNITS                                                 00000170
      A=(EC**2/(ENERGY**2))                                             00000180
         B= (COS(THETA*6.28318/(2.0*360.))) **2                         00000190
      C=COS(THETA *6.28318/(2. *360.))  **2                             00000200
      D=SIN(THETA*6.28318/(2.0*360.))                                   00000210
      E  =D**2                                                          00000220
      Y =E**2                                                           00000230
      F=    ((3.14159*EPSIL   *4)**2) *4                                00000240
      MOTTM    =(  (A*B)/(Y*F) )*EC**2                                  00000250
      WRITE(6,110) A,B,C,D,E,F                                          00000260
  110 FORMAT(E15.6,F10.6,F10.6,F10.6,E15.6,/)                           00000270
C     ENERGY = TOTAL ENERGY (INCLUDING REST ENERGY)                     00000280
C     TO CONVERT  MOTT  TO   CM**2 AND MEV UNITS MODIFY IT AS FOLLOWS:  00000290
      MOTT = MOTTM*10000*(6.242E12)**2                                  00000300
C 10000CM2 =1METER2,  1JOULE= 6.242E12 MEV, MOTT IN  CM2 , ENERGY IN MEV00000310
C  THETA IN DEGREES                                                     00000320
C  NOW CALCULATE THE ENERGY OF THE RECOILING ELECTRON IN A DEUTERON     00000330
C  COLLISION                                                            00000340
C  HOFSTADTER  PAGE 227  NUCLEAR AND NUCLEON STRUCTURE ( ELASTIC SCATT.)00000350
      ENUC =((ENERGY)**2/MC2)*(1-COS(THETA*6.283180/360.))/  (1+(ENERGY/00000360
     1MC2)*(1 -COS(THETA*6.283180/360.)))                               00000370
      ENELAS = ENERGY-ENUC                                              00000380
C  NOW DO MOTT WITH RECOIL  CALL THIS MOTTRC  HOFSTADTER P 231 =SIGMA NS00000390
      G =(2.0*ENERGY)/MC2                                               00000400
      GG=G*E                                                            00000410
      H =1. + GG                                                        00000420
      MOTTRD  =MOTT/H                                                   00000430
C NOW CALCULATE  THE FOUR MOMENTUM  TRANSFER   Q4   FROM  HOFSTADTER    00000440
C  HIGH ENERGY ELECTRON SCATTERING TABLES  PAGE 6                       00000450
```

```
C  FIRST GET THE SPEED OF LIGHT TIMES PLANCK'S CONSTANT(HBARC IN MEV-F.)
      HBARC=(6.5819E-22)*( 2.997925E10)* (1.0E13)
      AA=  2.0*ENERGY/HBARC
      AB= 1.0 +2.0*ENERGY*E/MC2
      AC= SQRT(AB)
      Q4=AA*D/AC
      WRITE(6,401) AA,AB,AC
 401  FORMAT(3F15.6)
C     THE APPROXIMATION  MASS(ELECTRON) GOES TO  ZERO   (MUIRHEAD P514)
C     IS  USED IN THE ABOVE  DERIVATION
C     Q4 IN UNITS OF  FERMI'S -1
      QSQR = Q4*Q4
      ETA= (  (HBARC*Q4)/(2*MC2))**2
      TAU= (  (HBARC*Q4)/(2*MC2PRO))**2
      WRITE(6,102)  ENERGY , THETA ,MC2
 102  FORMAT(5X,'INCIDENT ENERGY =',F10.4,2X,'MEV',6X,'THETA =',2X,F10.3
     1,2X,'DEGREES',6X,'MASS =',2X,F12.7,2X,'MEV',/)
      WRITE(6,201)  MOTTRD,QSQR,Q4
 201  FORMAT(5X,  'MOTT CROSS SECTION (INCL RECOIL)  FOR DEUTERON  =',
     1  E16.7,2X,  'CM2',//, 5X, 'FOUR MOMENTUM TRANSFER TO THE DEUTERON
     2 SQUARED  =',2X,  F12.6,2X, ' F-2', //,5X,   'FOUR MOMENTUM TRANSF
     3ERED TO THE DEUTERON  =', E12.6,2X,  'F-1',//)
      WRITE(6,206) HBARC,ETA ,TAU
 206  FORMAT(5X,  'HBARC ='  E15.5, 'MEV-FERMI',  6X,  'ETA  = ',F10.6
     1  ,6X,'TAU=',F10.6)
      WRITE(6,104) ENELAS
 104  FORMAT('ENERGY OF ELASTIC SCATTERING ELECTRON FROM DEUTERON =',2X,
     1 F10.4,2X,'MEV',/)
      WRITE(6,108) MOTTM,MOTT
 108  FORMAT(2E15.6)
      TAU = ( ( HBARC* Q4 )/  (2. * MC2PRO))**2
      MUDEU  =  0.857393
      X  = (TAN(6.28318*THETA  / (360.0 *2. )))**2
      CD= (2./3.)*TAU*MUDEU*MUDEU*(1.+     2. *( 1. + ETA )*X) *(1.+ETA)
      WRITE(6,301) CD
 301  FORMAT(5X,'CD =', E16.6)
      KDM  = ( 1. / (1. + CD))  * (1./ (1. - TAU/ 2.)**2)
      WRITE(6,300) KDM
 300  FORMAT(5X,'MAGNETIC CORRECTION TERM =  ', F10.6,2X,//,  ' THIS
     1 MAGNETIC CORRECTION TERM USES THE SCALING G1  = MUDEU * GO * MD/
     2MP  -  THIS HAS THE RELATIVISTIC CORRECTIONS PER ',//,'SCHUMACKER
     3ON PAGE3')
      WRITE(6,901)
 901  FORMAT(//,5X,'**************************************************')
      GO TO 99
 999  CONTINUE
      STOP
      END
```

BIBLIOGRAPHY

1. Mader, T.W., Naval Postgraduate School Thesis, (June 1971).

2. Stewart, J.W., Ph.D. Thesis, Naval Postgraduate School, (June 1970).

3. Drickey, D.J. and Hand, L.N., Phys. Rev. Ltrs. 9, 521 (1962).

4. Krohn, V.E. and Ringo, G.R., Phys. Rev. 148, 1303 (1966).

5. Mott, N.F., Proc. Roy. Soc. (London), A124, 425 (1929).

6. Hofstadter, R., Nuclear and Nucleon Structure, W.A. Benjamin, N.Y. (1963).

7. Sachs, R.G., Phys. Rev. 126, 2256 (1963).

8. Ernst, F.J., Sachs, R.G., and Wali, K.C., Phys. Rev. 119, 1105 (1960).

9. Källen, G., Elementary Particle Physics, Addison Wesley, Reading, Ma. (1964).

10. deVries, C., Hofstadter, R., Johansson, A., and Herman,R., Phys. Rev. 134, B848 (1964).

11. Bumiller, F., Croissiaux, M., Dally, E., and Hofstadter,R., Phys. Rev. 124, 1623 (1961).

12. Chen, K.W., Cone, A.A., Dunning, J.R. Jr., Frank, S.G.F., Ramsey, N.F., Walker, J.K., and Wilson, R., Phys. Rev. Ltrs. 11, 561 (1963).

13. Janrus, V.Z., Phys. Rev. 102, 1586 (1956).

14. Lomon, E.L., private communication.

15. Lomon, E.L., and Feshbach, H., Annals of Physics 48, 94-172 (1968).

16. Havens, W.W. Jr., Rabi, I.I., and Rainwater, L.J., Phys. Rev. 72, 634 (1947).

17. Fermi, E., and Marshall, L., Phys. Rev. 72, 279 (1948).

18. Hughes, D.J., Harvey, L.A., Goldberg, M.D., and Stafne, M.J., Phys. Rev. 90, 497 (1953).

19. Hand, L.N., Miller, D.G., and Wilson, R., Rev. Mod. Phys. 35, 335 (1963).

20. Casper, B.M. and Gross, F., Phys. Rev. 155, 1607 (1967).

21. Bumiller, F.A., Buskirk, F.R., Stewart, J.W., and Dally, E.B., Phys. Rev. Ltrs. 25, 1774 (1970).

22. Hofstadter, R. and McAllister, R.W., Phys. Rev. 98, 217 (1955).

23. Pauli, W., Rev. Mod. Phys. 13, 203 (1941).

24. Foldy, L.L., Phys. Rev. 87, 688 (1952).

25. Hofstadter, R., Bumiller, F., and Croissiaux, M., Phys. Rev. Ltrs. 5, 263 (1960).

26. Rosenbluth, M.N., Phys. Rev. 79, 615 (1950).

27. Foldy, L.L., Phys. Rev. 83, 688 (1951).

28. Foldy, L.L., Rev. Mod. Phys. 30, 471 (1958).

29. Hammermesh, Ringo, and Wattenberg, Phys.Rev. 85, 483(L) (1952), quoted in Reference 59.

30. Crouch, Krohn, and Ringo, Phys. Rev. 102, 1321 (1956), quoted in Reference 59.

31. Yennie, D.R., Levy, M.M., and Ravenhall, D.G., Rev. Mod. Phys. 29, 144 (1957).

32. Schiff, L.I., Rev. Mod. Phys. 30, 462 (1958).

33. Foldy, L.L. and Wouthuysen, S.A., Phys. Rev. 78, 29 (1950).

34. Yearian, M.R. and Hofstadter, R., Phys. Rev. 110, 552 (1958).

35. Hofstadter, R., Bumiller, F., and Yearian, M.R., Rev. Mod. Phys. 30, 482 (1958).

36. Muirhead, H., The Physics of Elementary Particles, Pergamon, N.Y., N.Y. (1965).

37. Drell, S.D. and Zachariasen, F., Electromagnetic Structure of Nucleons, Oxford University Press (1961).

38. Chew, Karplus, Gasiorowicz, and Zachariasen, Phys. Rev. 110, 265 (1958).

39. Nambu, Y., Phys. Rev. 106, 1366 (1957).

40. Clementel, E. and Villi, C., Nuovo Cimento 4, 1207 (1956).

41. Lehman, P., Taylor, R., and Wilson, R., Phys. Rev. 126, 1183 (1962).

42. Wilson, R. and Schumacher, C.R., Proceedings 1971 International Symposium on Electron and Photon Interactions at High Energies, Ed. N.B. Nistry, Cornell University (1972).

43. Meyerhof, W.E., Elements of Nuclear Physics, McGraw-Hill, N.Y., N.Y. (1967).

44. Schumacher, C.R. and Bethe, H.A., Nucleon Electromagnetic Structure (to be published).

45. Arya, A.P., Fundamentals of Nuclear Physics, Allyn and Bacon, Boston, Ma. (1966).

46. Enge, H.A., Introduction to Nuclear Physics, Addison-Wesley, Reading, Ma. (1966).

47. Glaser, V. and Jaksic, B., Nuovo Cimento 5, 1197 (1957).

48. Dubovik, V.M. and Cheshkov, A.A., JETP 24, 111 (1967).

49. Elias, J.E., et al., Phys. Rev. 177, 2075 (1969).

50. Gross, F., Phys. Rev. 142, 1025 (1966).

51. Chodorow, M., Ginzton, E.L., Hansen, W.W., Kyhl, R.L., Neal, R.B., and Panofsky, W.K.H., Rev. of Sci. Inst. 26, 134 (1955).

52. Barnett, M.T. and Cunneen, W.J., M.S. Thesis, Naval Postgraduate School (1966).

53. Oberdier, L.D., M.S. Thesis, Naval Postgraduate School (1967).

54. Schwinger, J., Phys. Rev. 76, 790 (1949).

55. Gordon, J.A., M.S. Thesis, Naval Postgraduate School (1970).

56. Tsai, Y.-S., Phys. Rev. 122, 1898 (1961).

57. Meister, N.T. and Yennie, D.R., Phys. Rev. 130, 1210 (1963).

58. Maximon, L.C., Medium Energy Nuclear Physics with Electron Linear Accelerators, MIT 1967 Summer Study, edited by W. Bertozzi and S. Kowalski, TID-24667, p. 249 and 242.

59. Bethe, H. and Heitler, W., Proc. Roy. Soc. (London), A146, 83 (1934).

60. Heitler, W., The Quantum Theory of Radiation, Oxford University Press, London (1954).

61. Bethe, H. and Ashkin, J., Experimental Nuclear Physics, Vol. I, edited by Segre John Wiley & Sons, Inc., N.Y., N.Y. (1953).

62. Butcher, J.C. and Messel, H., Nuc. Phys. 20, 15 (1969).

63. Landau, L., Soviet J. of Physics VIII, No. 4, 201 (1944).

64. Breuer, H., Nuc. Insts. and Meth. 33, 226 (1965).

65. Isabelle, D.B. and Bishop, G.R., Nuc. Phys. 45, 209 (1963).

66. Börsch-Supan, W., Journal of Research of the National Bureau of Standards 65B, 245 (1961).

67. Bergstrom, J., Medium Energy Nuclear Physics with Electron Linear Accelerators, MIT 1967 Summer Study, edited by W. Bertozzi and S. Kowalski, TID-24667, p. 253.

68. Buchanan, C., Ph.D. Thesis, Stanford University, unpublished (1966).

69. Michels, A. and Goudeket, M., Physica 8, 347 (1941); Physica 8, 353 (1941).

70. Condon, E.U. and Odishaw, H., Ed. Handbook of Physics, McGraw-Hill, N.Y., N.Y. (1958).

71. Savage, C.D., M.S. Thesis, Naval Postgraduate School, (1971).

72. Wilson, R., The Nucleon-Nucleon Interaction, Interscience Publishers, N.Y., N.Y. (1963).

INITIAL DISTRIBUTION LIST

		No. Copies
1.	Defense Documentation Center Cameron Station Alexandria, Virginia 22314	2
2.	Library, Code 0212 Naval Postgraduate School Monterey, California 93940	2
3.	Electron Linear Accelerator Naval Postgraduate School % Professor J.N. Dyer, Code 61Dy Dept. of Physics & Chemistry Monterey, California 93940	10
4.	Professor Earle Lomon Laboratory for Nuclear Science Mass. Inst. of Technology Cambridge, Mass. 02139	1
5.	Professor William Bertozzi Laboratory for Nuclear Science Mass. Inst. of Technology Cambridge, Mass. 02139	1
6.	Chairman, Dept. of Physics & Chemistry Naval Postgraduate School Monterey, California 93940	1
7.	CDR R.L. Topping Naval Weapons Laboratory Dahlgren, Virginia 22448	3

DOCUMENT CONTROL DATA - R & D

(Security classification of title, body of abstract and indexing annotation must be entered when the overall report is classified)

ORIGINATING ACTIVITY (Corporate author)
Naval Postgraduate School
Monterey, California 93940

2a. REPORT SECURITY CLASSIFICATION
Unclassified

2b. GROUP

REPORT TITLE
Elastic Electron-Deuteron Scattering Measurements and the Neuteron Charge Form Factor at Very Low Momentum Transfers

DESCRIPTIVE NOTES (Type of report and, inclusive dates)
Ph.D. Thesis, December 1972

AUTHOR(S) (First name, middle initial, last name)
Robert Leavy Topping

REPORT DATE	7a. TOTAL NO. OF PAGES	7b. NO. OF REFS
December 1972	155	72

a. CONTRACT OR GRANT NO.

b. PROJECT NO.

c.

d.

9a. ORIGINATOR'S REPORT NUMBER(S)

9b. OTHER REPORT NO(S) (Any other numbers that may be assigned this report)

0. DISTRIBUTION STATEMENT
Approved for public release; distribution unlimited.

1. SUPPLEMENTARY NOTES

12. SPONSORING MILITARY ACTIVITY
Naval Postgraduate School
Monterey, California 93940

3. ABSTRACT

Seventy-five measurements of the differential elastic electron-deuteron scattering cross section were made for values of q^2 ranging from 0.05 to 0.35 fm^{-2} at the NPS LINAC with electron scattering angles of 60° to 120°. The charge radius of the deuteron was determined to be $r_{E_d} = 1.9641 \pm 0.0074$ fm. Values of the neutron charge form factors were calculated using Lomon-Feshbach Models 1,5, and 15 and relativistic corrections to the deuteron wave functions. Lomon-Feshbach Model 15 gave $\frac{d}{dq^2} G_{E_n}(0) = 0.0200 \pm 0.0058$ fm^2, in closest agreement with the value of $\frac{d}{dq^2} G_{E_n}(0)$ determined by thermal neutron work. A Rosenbluth plot of the data at $q^2 = 0.2$ shows good agreement with theory

Unclassified
Security Classification

14 KEY WORDS	LINK A		LINK B		LINK C	
	ROLE	WT	ROLE	WT	ROLE	WT
Form Factors						
Neutron						
Deuteron						
LINAC						

Unclassified
Security Classification

141806

Thesis
T729 Topping
c.1 Elastic electron-deuteron scattering measurements and the neutron charge form factor at very low momentum transfers.